AD NUMBER

AD879661

LIMITATION CHANGES

TO:

Approved for public release; distribution is unlimited.

FROM:

Distribution authorized to U.S. Gov't. agencies and their contractors; Critical Technology; JAN 1971. Other requests shall be referred to Air Force Materials Laboratory, Attn: AFML/LN, Wright-Patterson AFB, OH 45433. This document contains export-controlled technical data.

AUTHORITY

AFML ltr, 7 Dec 1972

The following notice applies to any unclassified (including originally classified and now declassified) technical reports released to "qualified U.S. contractors" under the provisions of DoD Directive 5230.25, Withholding of Unclassified Technical Data From Public Disclosure.

NOTICE TO ACCOMPANY THE DISSEMINATION OF EXPORT-CONTROLLED TECHNICAL DATA

1. Export of information contained herein, which includes, in some circumstances, release to foreign nationals within the United States, without first obtaining approval or license from the Department of State for items controlled by the International Traffic in Arms Regulations (ITAR), or the Department of Commerce for items controlled by the Export Administration Regulations (EAR), may constitute a violation of law.

2. Under 22 U.S.C. 2778 the penalty for unlawful export of items or information controlled under the ITAR is up to ten years imprisonment, or a fine of $1,000,000, or both. Under 50 U.S.C., Appendix 2410, the penalty for unlawful export of items or information controlled under the EAR is a fine of up to $1,000,000, or five times the value of the exports, whichever is greater; or for an individual, imprisonment of up to 10 years, or a fine of up to $250,000, or both.

3. In accordance with your certification that establishes you as a "qualified U.S. Contractor", unauthorized dissemination of this information is prohibited and may result in disqualification as a qualified U.S. contractor, and may be considered in determining your eligibility for future contracts with the Department of Defense.

4. The U.S. Government assumes no liability for direct patent infringement, or contributory patent infringement or misuse of technical data.

5. The U.S. Government does not warrant the adequacy, accuracy, currency, or completeness of the technical data.

6. The U.S. Government assumes no liability for loss, damage, or injury resulting from manufacture or use for any purpose of any product, article, system, or material involving reliance upon any or all technical data furnished in response to the request for technical data.

7. If the technical data furnished by the Government will be used for commercial manufacturing or other profit potential, a license for such use may be necessary. Any payments made in support of the request for data do not include or involve any license rights.

8. A copy of this notice shall be provided with any partial or complete reproduction of these data that are provided to qualified U.S. contractors.

DESTRUCTION NOTICE

For classified documents, follow the procedure in DoD 5220.22-M, National Industrial Security Program, Operating Manual, Chapter 5, Section 7, or DoD 5200.1-R, Information Security Program Regulation, Chapter 6, Section 7. For unclassified, limited documents, destroy by any method that will prevent disclosure of contents or reconstruction of the document.

AFML-TR-66-310
PART V
VOLUME III

INTEGRATED RESEARCH ON CARBON COMPOSITE MATERIALS

VOLUME III
STRUCTURAL COMPONENT DEVELOPMENT

UNION CARBIDE CORPORATION
CARBON PRODUCTS DIVISION
-IN ASSOCIATION WITH-
CASE WESTERN RESERVE UNIVERSITY
BELL AEROSPACE COMPANY, DIVISION OF TEXTRON

PROGRAM SUPERVISORS
H.F. VOLK
H.R. NARA
D.P. HANLEY

TECHNICAL REPORT AFML-TR-66-310, PART V, VOLUME III

JANUARY 1971

AIR FORCE MATERIALS LABORATORY
AIR FORCE SYSTEMS COMMAND
WRIGHT-PATTERSON AIR FORCE BASE, OHIO

DISCLAIMER NOTICE

THIS DOCUMENT IS THE BEST QUALITY AVAILABLE.

COPY FURNISHED CONTAINED A SIGNIFICANT NUMBER OF PAGES WHICH DO NOT REPRODUCE LEGIBLY.

NOTICES

When Government drawings, specifications, or other data are used for any purpose other than in connection with a definitely related Government procurement operation, the United States Government thereby incurs no responsibility nor any obligation whatsoever; and the fact that the Government may have formulated, furnished, or in any way supplied the said drawings, specifications or other data, is not to be regarded by implication or otherwise as in any manner licensing the holder or any other person or corporation, or conveying any rights or permission to manufacture, use, or sell any patented invention that may in any way be related thereto.

This document is subject to special export controls and each transmittal to foreign Governments or foreign Nationals may be made only with prior approval of the Nonmetallic Materials Division, AFML/LN, Air Force Materials Laboratory, Wright-Patterson Air Force Base, Ohio 45433.

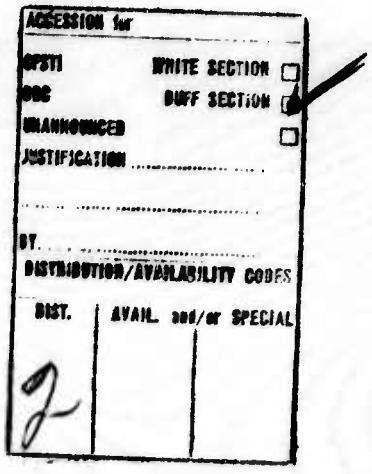

Copies of this report should not be returned unless return is required by security considerations, contractual obligations or notice on a specific document.

INTEGRATED RESEARCH ON CARBON COMPOSITE MATERIALS

Summary Technical Report

AFML-TR-66-310, Part V (see Part II Vol 2 AD 863663)

Volume III

Structural Component Development

Program Supervisors

H. F. Volk
H. R. Nara
D. P. Hanley

January 1971

FOREWORD

The work reported herein was performed under the sponsorship of the Advanced Research Projects Agency, Department of Defense, through Contract F33615-68-C-1077, ARPA Order No. 719, Program Code 7D10, with the Air Force Materials Laboratory, LN, Wright-Patterson Air Force Base, Ohio. Mr. H. S. Schwartz is the Air Force Program Manager.

This work is a continuation of the effort under Contract AF 33(615)-3110 which had covered the period May 17, 1965 to June 17, 1969, and which was reported in Parts I through IV of this series.

The prime contractor is Union Carbide Corporation, Carbon Products Division with Dr. H. F. Volk (Phone 216-433-8600) as program supervisor. The subcontractors are the Case Western Reserve University with Dr. H. R. Nara (Phone 216-368-4192) as program supervisor and Prof. T. P. Kicher as associate program supervisor and Bell Aerospace Company, a Division of Textron, with Mr. D. P. Hanley (Phone 716-297-1000) as program supervisor.

This is Part V of the report and covers work performed from July 1969 to September 1970. Part V is issued in three volumes. Volume I covers materials research; Volume II, structural mechanics; and Volume III, structural component development.

This report was submitted by the authors in September 1970.

This technical report has been reviewed and is approved.

A. M. Lovelace

A. M. Lovelace
Director
Air Force Materials Laboratory

ABSTRACT

The work presented in this volume is concerned with the performance prediction, testing, and post-test evaluation of a representative graphite-fiber, resin-matrix aircraft fuselage component. Additional material properties were determined and structural margins of safety defined by discrete element analysis. After seven response tests under various load combinations, the component was tested to destruction under combined bending and shear loads. Failure occurred at 110 percent of the target design load but below the failure load predicted from tests on flat panels. A weight saving of 27 percent over an aluminum structure of equivalent strength was demonstrated. The component was also three times stiffer than an aluminum structure of the same weight. Performance projections indicate that the same component built with presently available "Thornel" 50S fibers would offer a weight saving of 49 percent. Post-test evaluations included tensile and compression tests on curved skin panels, on stringers, and on stringer-skin combinations. Optical and electron microscopic examination of the fracture surfaces provided further insight into the failure mechanism.

BLANK PAGE

TABLE OF CONTENTS

LIST OF ILLUSTRATIONS

LIST OF ILLUSTRATIONS (Cont'd.)

LIST OF ILLUSTRATIONS (Cont'd.)

LIST OF TABLES

SECTION I

INTRODUCTION

The present program is a continuation of the work performed under Contract AF 33(615)-3110 (see References 1 through 6). This report covers the fifth (and final) year's work of a program which represented a novel approach designed to fulfill three different, but clearly interdependent, needs of the Department of Defense: a materials need, a structural design capability need, and a need for more scientists and engineers trained in applied materials problems and advanced design methods. The Carbon Products Division of Union Carbide Corporation, Case Western Reserve University, and Bell Aerospace Company have formed an Association to meet these needs.

The Association has formulated a broad program which includes the development of new materials, generation of advanced analyses and design methods, and education of graduate students. In brief, the major objectives are (1) to develop high modulus graphite fiber composites, (2) to extend the methods of structural mechanics, (3) to identify DOD applications toward which the program efforts should be directed, (4) to educate engineers capable of developing and using modern materials, and (5) to integrate materials research with the needs of the design by extending the technique of structural synthesis to include material variables.

The primary responsibilities of Union Carbide Corporation, Carbon Products Division, are the development and production of composite materials and the measurement of those mechanical and thermal properties needed for the structural design work within the Association. The technical program at Union Carbide consists of: (1) materials research, a research program to develop new, improved composites of high modulus graphite fibers in both resin and metal matrices; (2) materials fabrication, an applied research program to prepare materials for the joint research programs of the Association and to seek new ways of fabricating structural prototypes which better utilize the superior properties of composite materials; (3) properties evaluation, the measurement of the mechanical and thermal properties of certain composites to provide data for the joint research programs of the Association; and (4) failure criteria, a basic research program to determine experimentally adequate failure criteria for anisotropic materials under multiaxial stress states and to find ways of representing the failure surface which can be used by the designer in practical calculation.

The work at Case Western Reserve University has two major objectives. The first objective is to advance the basic structural mechanics technology required for rational design with

composite materials. Composite materials offer the structural design engineer the prospect of being able ultimately to carry on simultaneously the design of the structural configuration and the material. Achieving this capability will require fundamental advances in structural synthesis as well as a substantially improved understanding of the behavior of composite materials. The goals of the structural mechanics research program at Case are (1) the quantitative formulation and efficient solution of the structural synthesis problem, including material variables, for elementary, but representative components fabricated from composite materials; (2) experimental stress analysis studies and theoretical investigations in micromechanics with the objective of improving the measurement and calculation of stiffness properties and failure mode criteria for composite materials; and (3) the development of improved analysis methods for anisotropic, nonlinear, and nonconservative materials. The second objective of the work at Case Western Reserve University is to develop new or improved graphite fiber-resin composites through materials research. At present, the knowledge of fiber surface morphology and the relation between fiber surface characteristics and interfacial adhesion to the resin systems(s) is incomplete. A better understanding of these interfacial interactions will lead to improvements in presently used fiber resin composites and will ultimately permit the judicious selection of new resins and new fabrication methods, thus leading to a second generation of advanced composites.

The primary purposes of Bell Aerospace Company's participation in this program are to interject user requirements into the applied materials research efforts; to apply at the prototype design level, the advanced analytical procedures and improved understanding of material behavior which will result from the research; and to establish application-related property specifications for materials research activities. To attain these objectives, a six-part technical program is being performed by Bell: (1) application selection, the objective of which is to define representative configurations and environmental conditions which reflect DOD requirements; (2) recognition of failure modes, a task which involves the overall structural behavior such as elastic instability, deformation limits, and fracture and the material failure modes; (3) determination of the nature of and methods for the application of analytical tools needed to cope with the anisotropic, anelastic, and nonconservative material property behavior and the multiaxial stress distributions anticipated in structural configurations associated with the use of the subject materials; (4) structural synthesis, a task which involves the application of structural synthesis techniques at the practical level to define the most desirable material compositions within a particular class of composites; (5) study of creative design concepts which will be required because of the complex material behavior of composites; (6) testing to verify the value of analysis procedures used to design composite materials and the components made from composite materials.

Although this report of the Association's fifth year activities is the last report of the Association, the Case Western Reserve University will be continuing research on composite materials during the sixth year under sponsorship of the Advanced Research Projects Agency.

This report is divided into three volumes. Volume I covers the effort on materials research; Volume II covers the work on structural mechanics, analysis, and optimization; and Volume III covers the testing, stress analysis and evaluation of a representative subscale fuselage component. This division was made because particular projects might be of interest to a particular audience; this arrangement also made possible the reduction of the physical size of each volume. However, the following Summary (Section II) also contains a brief outline of the contents of the other two volumes.

SECTION II

SUMMARY

Volume III: Structural Component Development

Material properties for the fuselage component stress analysis were determined. Actual measurements and theoretical predictions, the latter supported by correlations with flat panel test results, were used to determine property values. A discrete element analysis of the fuselage component was completed to define structural margins of safety for nominal test conditions. Results were compared with the previous analysis, which was based on "Thornel" 40 construction.

After seven low-load response tests under various load combinations were performed, the graphite fiber composite fuselage component was tested to destruction under combined bending and shear loads. Failure occurred at 110 percent of the target design load requirement but below the failure load predicted from flat panel tests. A weight saving of 27 percent over an aluminum structure of equivalent load capacity was demonstrated. The composite component was also three times stiffer than an aluminum structure of the same weight. Strains, deflections, and stiffnesses generally agreed with the predictions, except for some very localized skin bending effects. The component behaved linearly on loading and unloading with no discernable hystereses.

A new analysis and performance projection showed that a fuselage component of the same design constructed with "Thornel" 50S fibers (rather than the experimentally treated "Thornel" 50 fibers actually used) would offer a weight saving of 49 percent over an equivalent load capacity aluminum construction.

As part of post-test evaluations of the fuselage component, test methods were developed to evaluate strengths and moduli of curved skin specimens and of stringers. Tension and compression tests were conducted on sections of the fuselage skin; the results verified predicted values. Tests on stringers remaining from the fuselage fabrication program yielded tensile strength values ranging from 50,500 to 54,500 psi. These strengths exceed the value of 45,000 psi used in the shell analysis program. The Young's moduli agreed well with previous sonic measurements on the same stringers. Photomicrographs of stringers tested to near failure in tension are also presented. Tensile tests on skin-stringer combination specimens cut from the component gave lower strength values than the stringers alone. This result is attributed to damage incurred by the specimens during the fuselage destruct test and also to unavoidable stress concentrations in the test fixture. Optical and scanning electron microscope investigation

of the fuselage fracture surface indicated that tensile failure initiated at or near stringer No. 1 and propagated circumferentially across the adjacent stringers on either side. Certain regions of high and low fiber pull-out were observed and are attributed to correspondingly high or low stresses in these regions during the test.

Contents of Volume I:

The work presented in Volume I is concerned with materials research on graphite fiber reinforced composites. Graphite fiber surfaces were characterized by gas phase and solution adsorption experiments and by Raman spectroscopy. The latter technique allows a differentiation between fibers of different origins and heat-treatment temperatures. The fabrication of "Thornel" fiber, polyamide-imide and polysulfone composites was investigated. Fabrication of polyamide-imide composites was very tedious, and evaluation was limited to determinations of torsion shear strength. Several plates of polysulfone matrix composites were fabricated; the evaluation of these plates is presented in Volume II of this report. "Thornel" fiber composites were also prepared by *in situ* polymerization of nylon. The epitaxial crystallization of nylon monomer on graphite fiber surfaces has been investigated. Graphite-fiber, nickel-matrix composites were further characterized at room and at elevated temperatures. Measurements of Young's moduli, tensile strength, thermal expansion, and thermal fatigue are presented.

Contents of Volume II:

The work presented in Volume II is concerned with the structural mechanics and synthesis of graphite-fiber reinforced composite materials. Optimization studies (minimum weight design) of stiffened cylinders similar to the fuselage component were carried out by two different techniques. The behavior of composite structural elements was investigated in plate buckling and post-buckling studies, buckling of stiffened plates with cut-outs, and application of shell theory to anisotropic cylinders. Micromechanics studies of fibrous composites included development of a photoelastic technique for analyzing frozen stresses, a discrete element microstress analysis of unidirectional fiber composites, an application of the theory of physically nonlinear elastic solids to composite materials, and an investigation of the multiple circular inclusion problem in plane elastostatics. Failure of composite structural elements was investigated through studies of the failure mechanism for off-axis composites, the fracture toughness of composites, the effect of fatigue and sustained loads on cross-plied composites, the notch sensitivity of cross-plied composites, and the effect of a variety of known intentionally interjected defects on the fracture strength. Further studies were concerned with multiaxial stress testing of composite cylinders. The effects of circular and square cut-outs in flat panels and in a stiffened panel, and methods of reinforcement of cut-outs were investigated and correlated with predictions based on discrete element analysis.

SECTION III

FUSELAGE COMPONENT TESTING

Selection of a fuselage section for the representative fiber composite component was described in Section IV of the First Annual Report (1). Section X of the Second Annual Report (2) described preliminary design of the fuselage section and development of analytical methods required for final design. Section IX of the Third Annual Report (3) described implementation of the advanced analysis methods and the material and structural element evaluations leading to the final design of the fuselage section. Final design and fabrication of the component were described in Sections III and V of the Fourth Annual Report (6), and the test plan was outlined in Section IX. This report section describes test preparations and results of the preliminary tests, the series of response tests, and the component destruct test.

The cylindrical component was four feet in length with a diameter tapered from 24 to 20 inches, stiffened by 31 hat-section stringers and 4 stabilizing rings. The shell skin consisted of a four-ply (90, 15, -15, 90°) combination wet wound/prepreg layup, and the molded longitudinal stringers employed four-ply (10, -10, -10, 10°) construction. Ring stiffeners were made of a light weight balsa-wood core reinforced with three-ply (0, ±45°) side panels and four-ply 0° inner ring caps. Material used was Union Carbide's "Thornel"* 50 yarn which had been experimentally treated to improve fiber/resin bonding and composite shear strength. The resin matrix system was Union Carbide's ERLA 2256/MDA. All bonded construction was utilized in attaching stringers and rings to the shell skin. The graphite composite structure weighed slightly over 16 lb. Fiberglass lay-ups with segmented aluminum rings were bonded to the component to permit attachment of the structure to the test stand.

A. Test Preparations
(S.L. Cross, Bell Aerospace)

The fuselage component was delivered to Bell on September 3, 1969 and was transported directly to the Instrumentation Laboratory. A visual inspection was completed by Bell and Union Carbide with no discrepancies noted. Strain gage location lay-out was started that evening.

---

*"Thornel" is a registered trademark of Union Carbide Corporation.

In view of the locally rough surface areas on the component skin, it was agreed that a very light sanding procedure would be used prior to gage bonding to remove the surface epoxy. This method was tried on one gage position and was found unsatisfactory due to thinness of the epoxy layer and the potential fiber damage. It was therefore decided to bond directly to the skin surface where possible and, in areas of considerable roughness, a filler material would be used to provide an acceptable bond surface. Strain gage instrumentation was completed on September 19 and the component was transported to the Static Test Laboratory. Protective coverings were taped over all gages.

A series of strain gage zero checks were planned to ensure proper test assembly counterbalance prior to structural testing. These gage checks were specified:

a. Zeroing all gages prior to shipment to the Static Test Laboratory.

b. Installing the large end-ring to the component and assembly to the back-stop support structure. Two gages from the top and two from the bottom of the component will be used to read out strain.

c. Installing the small diameter end-ring, load beam, and counter balance and read the four gages - all readings should be zero. If gages do not read zero, the counter balance will be adjusted until zero is achieved.

d. Installing load cells and cylinders for the response tests. Strain outputs should be zero. If not, provide final adjustment to the counter balance until zero is achieved.

This procedure provided assurance that no residual strain was imposed on the component due to test stand and hardware assembly.

B. Preliminary Tests
(S.L. Cross, L.H. Kocher, and D.P. Hanley, Bell Aerospace)

Prior to the planned response tests, check-out tests were conducted to verify proper operation of the test facility, set-up, and instrumentation. Figure 1 shows the component mounted to the steel frame back-stop and the A-frame loading structure. Three preliminary tests were conducted as summarized in Table I.

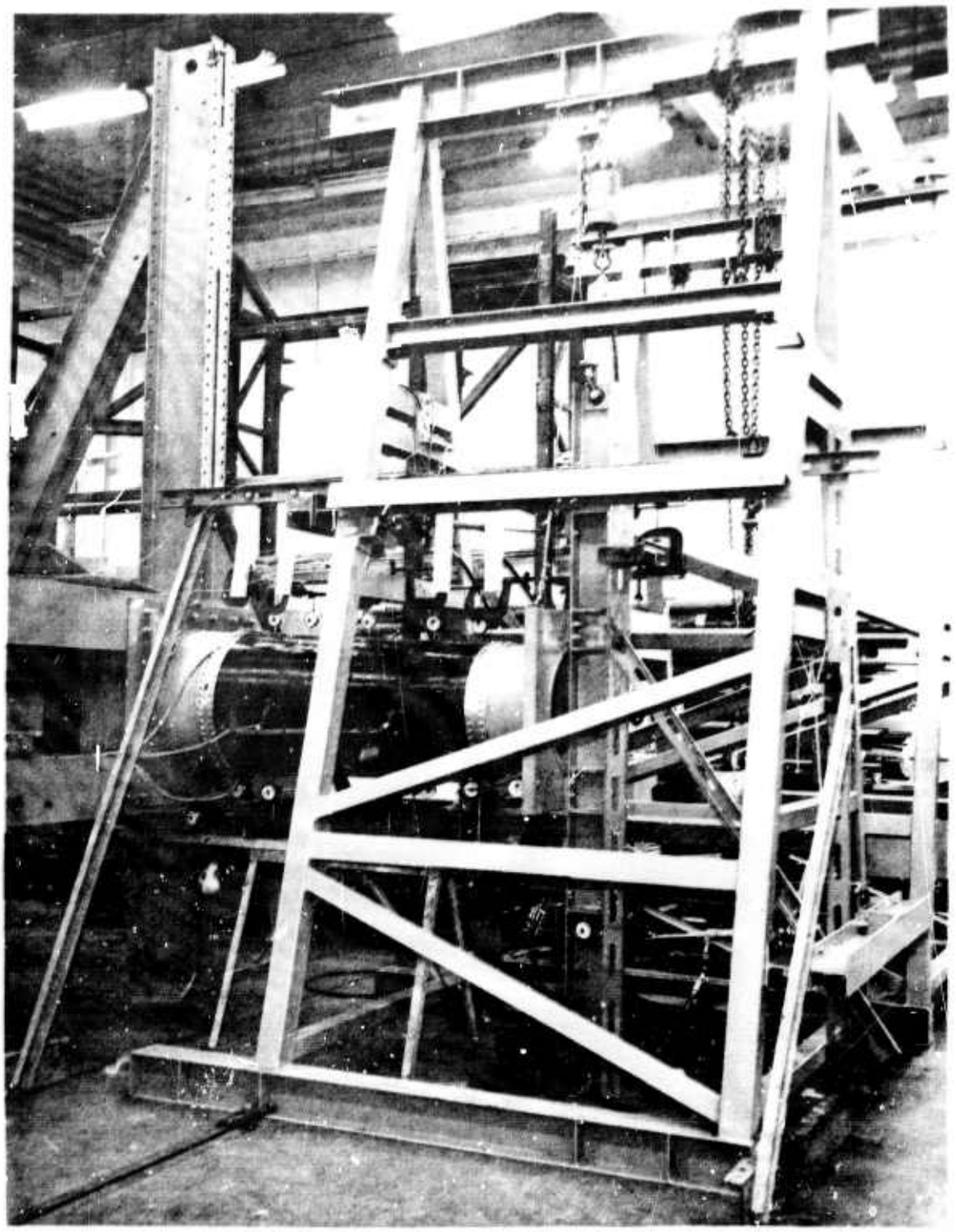

Figure 1. Fuselage Component in Test Stand.

P700068

TABLE I

PRELIMINARY TESTS ON FUSELAGE COMPONENT

Type of Loading	Load Level (lb/in.)	Percent of Predicted Ultimate
Pure Bending	450	17
Axial Compression	465	16
Pure Bending	300	12

Table II shows the updated loads for the response and destruct tests. The lb/in. load levels given in Table I were calculated as percentages of predicted ultimates corresponding to the allowable loads given in Table II. The latter values were established from material properties given in Section IV A.

The preliminary tests confirmed the proper performance of all test system hardware, including hydraulic cylinder load rate control, data recording system, load application sequence, and strain gage outputs.

For the first bending test, loads were applied in 1000-lb/cylinder increments up to 3000 lb/cylinder giving a maximum bending moment of 182,000 in-lb. The two F_1 load jacks shown in Table II were used. Resultant axial loading was 450 lb/in. of circumference in the small end at the top and bottom of the shell, at 17% of the predicted ultimate strength.

Deflection data indicated that most of the bending occurred in the composite test section and that the end attachments were quite rigid. Back-stop deflections at maximum load were 0.0035 in. corresponding to a one-minute rotation at the fixed end of the component. The load beam angular rotation was 17 minutes as indicated by a 0.15 in. horizontal deflection at the bottom of the load beam. Load-deflection curves and load-strain curves were all linear. A high degree of local skin bending was indicated by a pair of back-to-back gages in the vicinity of stringer No. 1 in the large end mid-bay. This behavior was observed throughout all of the component tests and is discussed further under the response tests. During unloading, all gages returned linearly indicating no permanent set of the structure or test fixture. At maximum load, the average longitudinal strain in the large end mid-bay was 384μ in./in. indicating an EI bending stiffness of 5.26×10^9 lb-in.^{2}. The predicted stiffness at this station was 5.27×10^9 lb-in.^{2}

TABLE II

UPDATED LOADS FOR FUSELAGE COMPONENT STRUCTURAL TEST

Allowable Loads (lb/in.)

	Tension	Bending	Compression	Shear
Ultimate	2610	2610	2910	414
Yield	2595	2595	2910	380
Limit	1740	1740	1940	280

Test Sequence Loads (lb)

Response Tests	F1	F2	F3	F4
1. Bending & Shear	2060	-	4450	-
2. Torsion	-	1520	-	-
3. Bending & Torsion	4780	956	-	-
4. Local Frame	-	-	-	80
Destruct Test				
5. Bending & Shear	10,850	-	8400	-

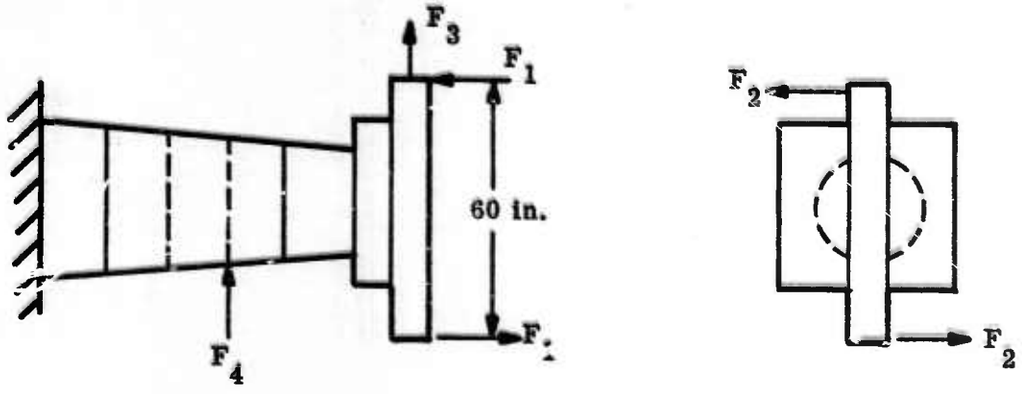

Loads for the axial check test were incrementally applied in six steps to a maximum of 15,000 lb/cylinder to give a total compressive load of 30,000 lb. Circumferential loading, assumed uniformly distributed at the small end, was 465 lb/in. or 16% of predicted ultimate strength. The maximum axial deflection was 0.147 inch. Again, all gages were linear throughout loading and unloading. Predicted and measured axial stiffnesses are shown in Figure 2. The average measured values were about 75% of theoretical.

Several anomalies were observed in the axial loading test: first, the same localized skin bending was observed as in the bending test, and secondly, the axial strain gage elements of the rosettes located on the sides of the component recorded only 20% of the axial strains measured along the top and bottom of the component. An explanation of the first anomaly has not yet been found. With regard to the second effect, it was thought that loads were not being properly diffused into the component, i.e., that line loads were "beaming down" the top and bottom of the structure. To investigate this possibility, analyses were made of test fixture deflections. Results indicated that the fixturing could not possibly deflect enough to account for such effects. Additional dial and strain gage instrumentation was subsequently employed to further study the problem.

Preliminary test 3 was performed similarly to the first checkout test; however, maximum jack load was only 2000 lb/cylinder or 300 lb/in. loading. Eight additional dial gages were added along the top and bottom of the component to obtain a more complete deflection profile and determine the amount of "ovalling" between ring frames. Positioning of the dial gages is shown in Figure 3, and the deflection profile at maximum load is shown in Figure 4. Figure 4 confirmed curve shapes obtained from the first preliminary test where there were considerably fewer data points. In this test a maximum difference of 0.005 in. deflection was noted between top and bottom of the component in the first and second bays thus indicating slight ovalling.

Strain response in preliminary test 3 appeared normal except for skin gages 29 and 30 as before. Considerable divergence between inside and outside strains was noted. Gage 29 (outside skin) recorded only 25% of the strain observed on gage 30 (inside skin). Predicted strain in this region was midway between the two recorded values. A potential failure region was therefore identified since gage 30 measured a value 37% higher than predicted. The component was subsequently inspected, with both Bewindow X-ray and ultrasonics; however, no local defects were found.

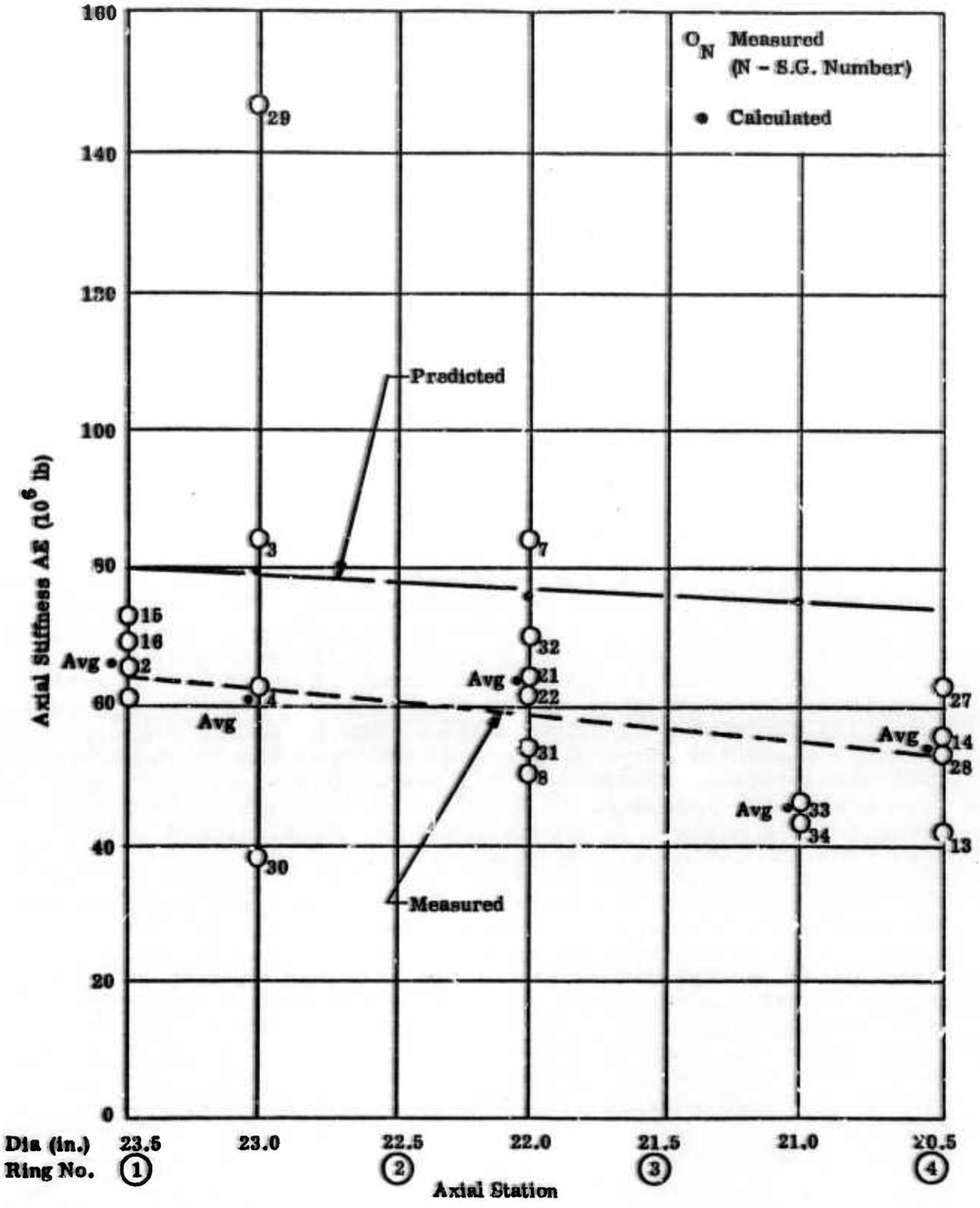

Figure 2. Axial Stiffnesses from Preliminary Test 2

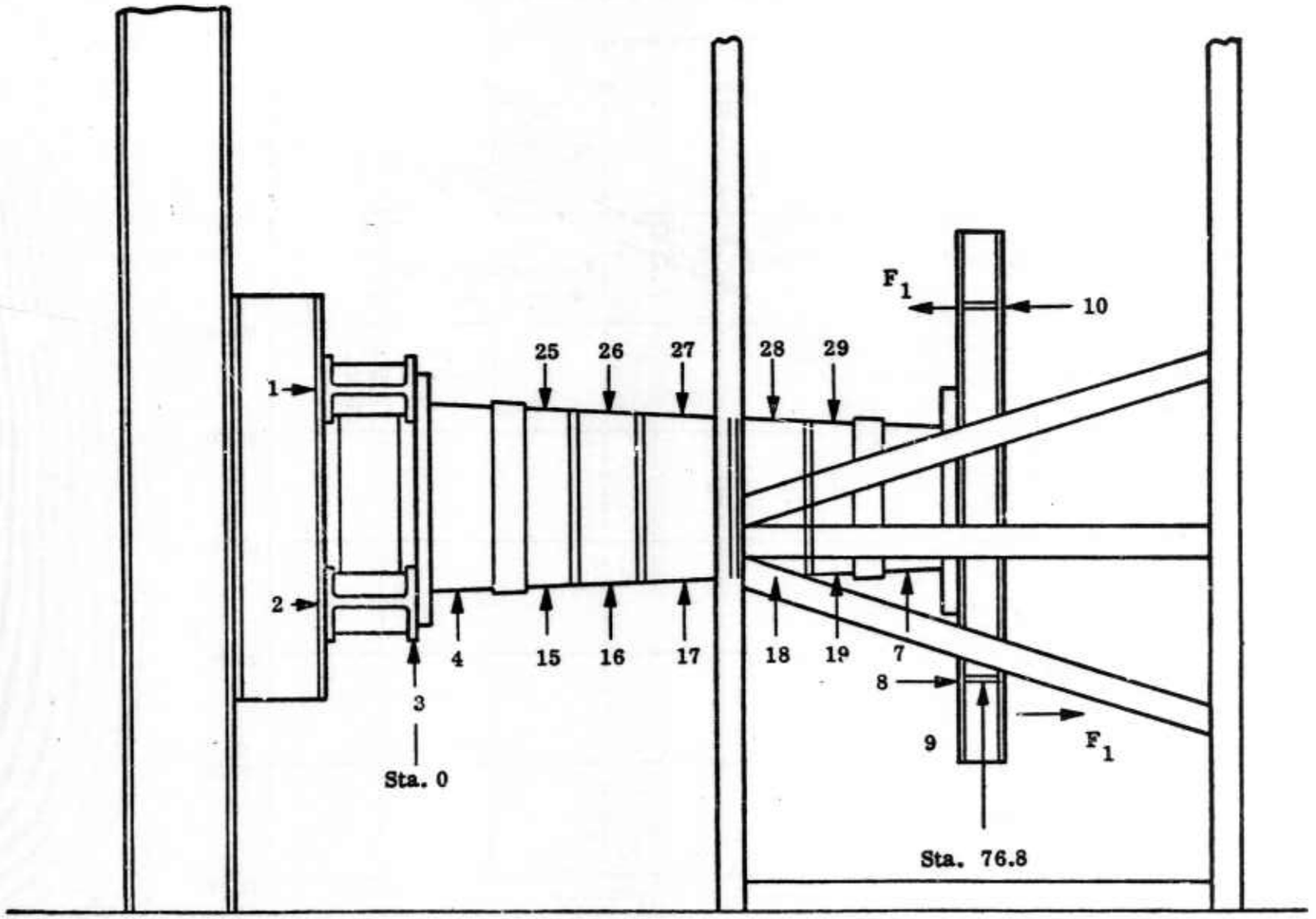

Figure 3. Dial Indicator Positions for Preliminary Test 3

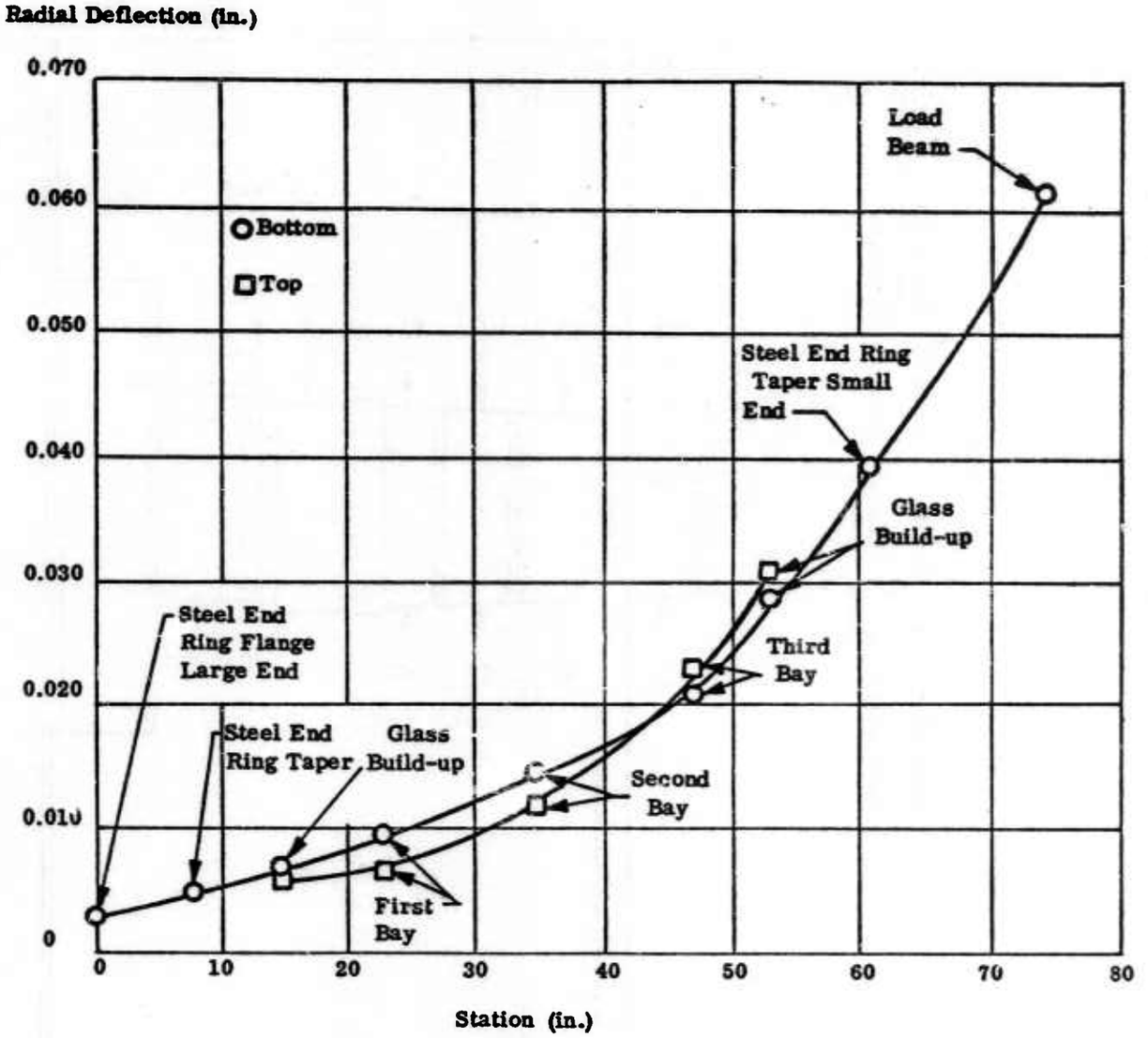

Figure 4. Radial Deflections from Preliminary Test 3

C. Response Tests
(S.L. Cross, L.H. Kocher, and D.P. Hanley, Bell Aerospace)

Response tests simulating four typical airframe fuselage loading conditions were performed to verify analytical predictions of structural behavior and to gain further insight for anticipating failure mode in the destruct test. The load levels were selected at one-half of the limit loads shown in Table II corresponding to one-third of ultimate allowables. Achieved loadings were very close to the desired values as seen in Table III.

TABLE III

RESPONSE TEST LOADINGS

Test No.	Type of Loading		Desired Load Level lb/in.	% Ult.	Actual Load Level (lb/in.) lb/in.	% Ult.
1	Bending and Shear	N_x	870	33.3	771	29.6
		N_{xy}	140	33.3	125	30.2
2	Torsion	N_{xy}	140	33.3	136	33.0
3	Bending and Torsion	N_x	870	33.3	895	34.3
		N_{xy}	140	33.3	85	21.0
4	Frame Load		80 lb	33.3	80 lb	33.3

1. Response Test 1

The predicted and actual load profiles for Response Test 1 (RT 1) are shown in Figure 5. Shear and bending loads are plotted versus load steps. The lower profile represents bending loads/cylinder (F_1) while the upper profile is the shear load (F_3). Actual loads are indicated within brackets. The desired maximum loads at load step 10 were not achieved due to high inside skin strain measured by gage 30 on the tension side (bottom) of the large end. Loading was terminated according to the test plan when a strain gage measured 1000μ in./in. This was the case on gage 30 at load step 9.

A typical plot of load level versus predicted and actual strains is shown in Figure 6 for strain gages 15 and 16 (15 on skin at top in large end mid-bay, 16 on stringer cap at top in

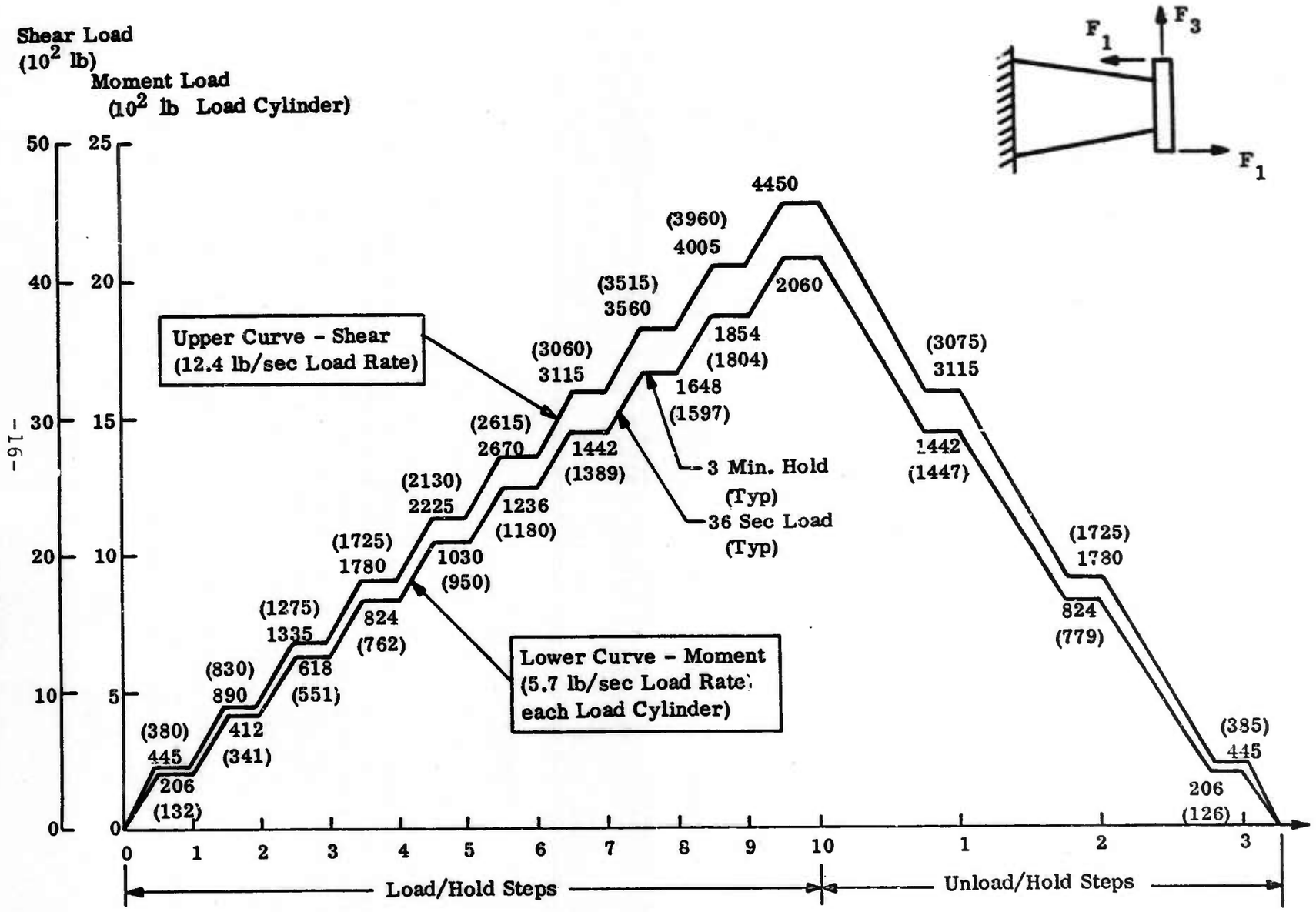

Figure 5. Response Test 1 Load Profile

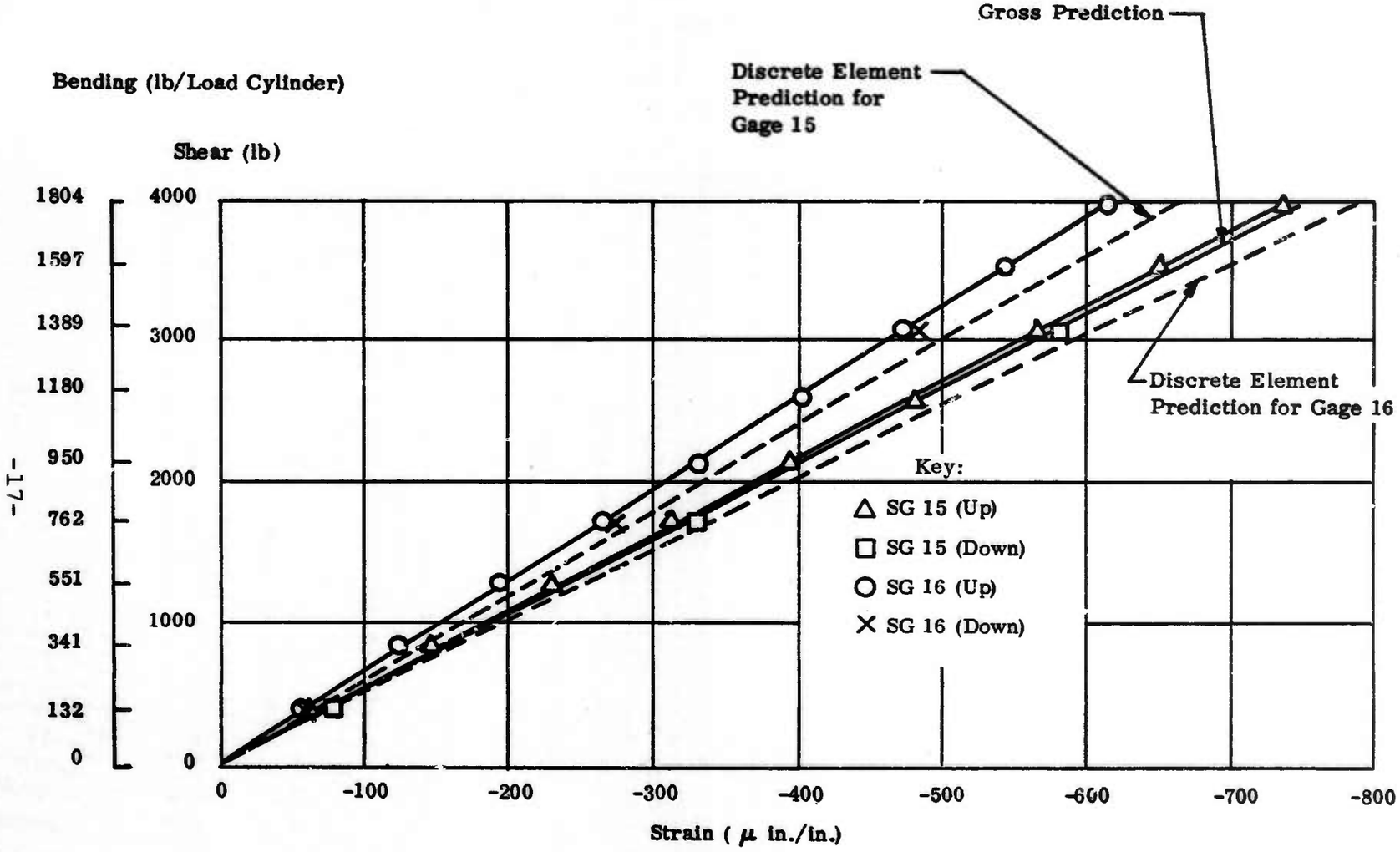

Figure 6. Typical Load-Strain Curves from Response Test 1

large end mid-bay). Discrete element and gross predictions are shown and agree quite well with actual values.

Strains recorded at maximum load (values in μin./in.) are shown within the ovals in Figure 7. The empty ovals indicate strain gages applied after this test. All axial gages along the top recorded compressive strain as expected while tension was observed along the bottom. In general, good load distribution was indicated in the structure as evidenced by nearly equal stringer and skin strains at a given station. Back-to-back skin gages 29 and 30 and 66 and 67 showed wide divergence in the mid-bay between ring frames 1 and 2 as commented on earlier.

Strains recorded by the skin rosettes showed a maximum value of 440μ in./in. on gage 57 which is one-half of the shear strain at that location. As expected, maximum shear occurred on the sides of the small end. Gages 41 and 47 in the center mid-bay showed about one-half of the expected values. For this reason, along with analyses of the test fixture hardware deflections, these readings were suspect and believed traceable either to the gages or their installation procedure (See Section VI A).

Measured and predicted flexural stiffnesses are shown in Figure 8. Stiffness measured from gages 29 and 67 are much higher than predicted while gages 30 and 66 are much lower. These were the back-to-back skin gages which showed severe local bending. Otherwise, measured stiffness of the structure was in excellent agreement with prediction, and results confirmed those obtained in the preliminary simple bending tests. Predicted tip deflection was 0.155 in. and 0.188 in. was measured, with backstop deflection taken into account.

2. Response Test 2

The fuselage component was subjected to torsion for RT 2 to a load level of 136 lb/in. (Table III). Load application was in 10 steps with load removal in 3 steps, similar to that for RT 1 (Figure 5). Maximum strains are shown in Figure 9. All gages behaved linearly and returned to their zeroes after test. Strains measured by the 45-degree rosette elements were all reasonably close (gages 42, 44, 48, 51, 54, and 57) and averaged 550μ in./in. In general the outside axial skin gages recorded low compressive strains and the axial stringer cap gages recorded mostly low tensile strains.

A maximum end rotation at the load beam of 27 minutes was predicted by the discrete element analysis, very close to the measured value of 24 minutes. Measured torsional stiffnesses as

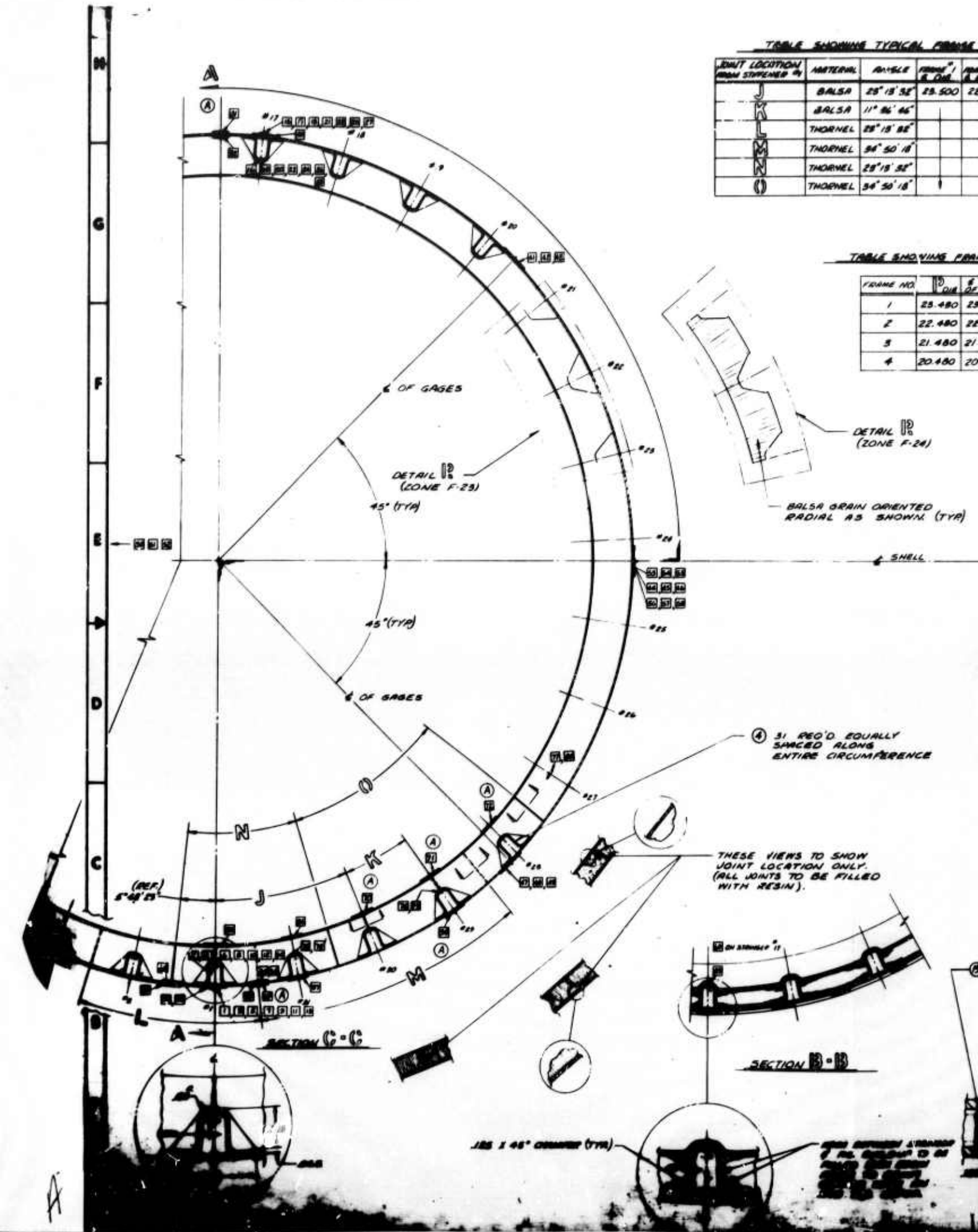
TABLE SHOWING TYPICAL FRAME
JOINT LOCATION FROM STIFFENER
MATERIAL
ANGLE
BALSA
25° 15' 52"
BALSA
11° 56' 46"
THORNEL
25° 15' 52"
THORNEL
34° 50' 18"
THORNEL
25° 15' 52"
THORNEL
34° 50' 18"
TABLE SHOWING FRA
FRAME NO.
1
25.480
2
22.480
3
21.480
4
20.480
DETAIL B
(ZONE F-24)
BALSA GRAIN ORIENTED RADIAL AS SHOWN (TYP)
℄ OF GAGES
DETAIL B
(ZONE F-23)
45° (TYP)
℄ SHELL
45°(TYP)
℄ OF GAGES
④ 31 REQ'D EQUALLY SPACED ALONG ENTIRE CIRCUMFERENCE
THESE VIEWS TO SHOW JOINT LOCATION ONLY. (ALL JOINTS TO BE FILLED WITH RESIN).
(REF.)
SECTION C-C
SECTION B-B
.125 X 45° CHAMFER (TYP)

AL FRAME CONSTRUCTION

	FRAME #1 ⌀ DIA	FRAME #2 ⌀ DIA	FRAME #3 ⌀ DIA	FRAME #4 ⌀ DIA	NO. REQ'D
	23.500	22.500	21.500	20.500	15
					1
					14
					1
					14
					1

OWING FRAME DIAMETERS

	DIA	⌀ DIA OF FRAME	DIA
	23.480	23.500	23.520
	22.480	22.500	22.520
	21.480	21.500	21.520
	20.480	20.500	20.520

24.1

TED
N. (TYP)

LL

ICE

VIEW C
(SEE SHEET #2)

-735
-805
-70
-615
-580
20
400
0
35
(ON STRINGER #6)
24.00 DIA.
(INSIDE SHELL)
23.500 DIA
2.70 (TYP)
610
70
575
605
1000
750
680
360
500
305
FRAME ASSY. #1
(TYP)
.70 (TYP)
6.00 (TYP)
SEE DETAIL D
(SHEET 4-02)
(REF)
END ATTACHMENT
FIXTURE NO. 1 (LARGE)
SHEET 1 OF 2
6.00

(P) SHOWING TYP. ROLL PIN INSTALLATION.

2.00
.040
.480

P

6

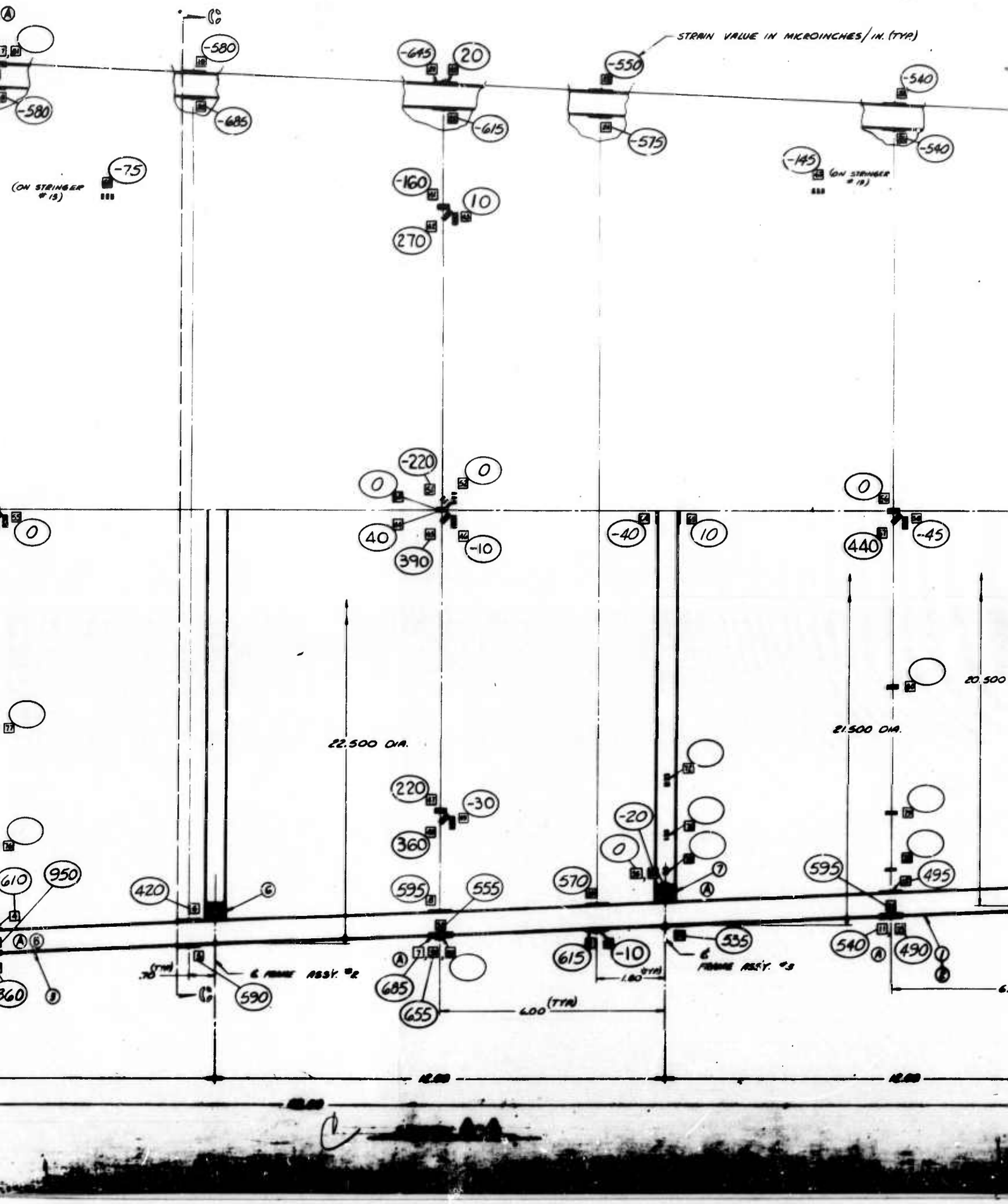
STRAIN VALUE IN MICROINCHES/IN. (TYP.)
-580
-580
-685
-645
20
-615
-550
-575
-540
-540
-145
(ON STRINGER #13)
-75
(ON STRINGER #13)
-160
10
270
-220
0
0
40
390
-10
0
-40
10
0
440
-45
22.500 DIA.
21.500 DIA.
20.500
220
-30
360
-20
0
610
950
420
595
555
570
595
495
615
-10
535
540
490
685
655
590
.75 (TYP)
1.80 (TYP)
4.00 (TYP)
6 FRAME ASSY. #2
6 FRAME ASSY. #3
360

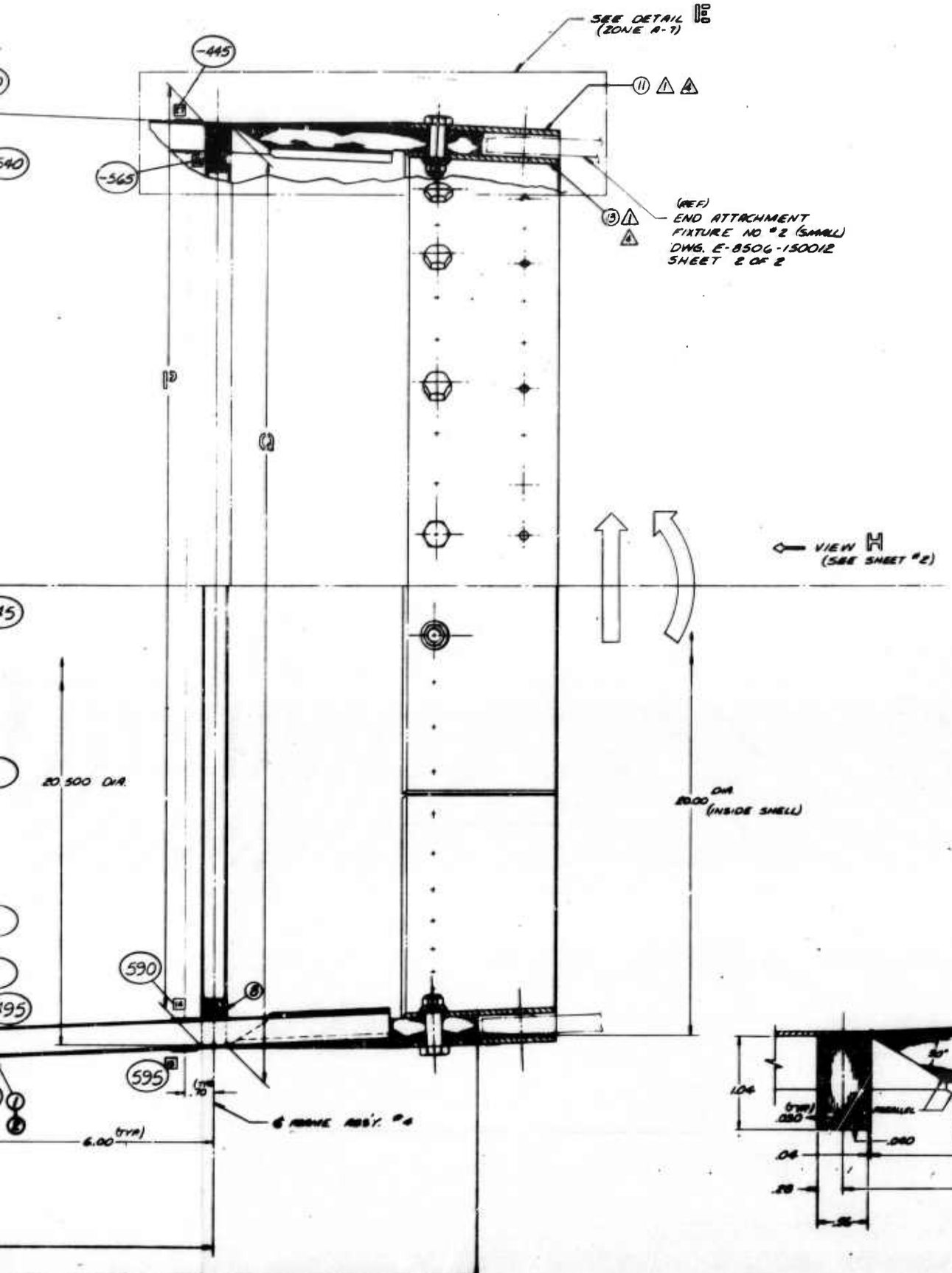

TABLE SHO
VARIOUS THI
FIBER ORIEN

ELEMENT	NUMBER OF LAMIN
SHELL	4
STRINGERS	4
FRAME (CAP)	4
FRAME (SIDE PANELS)	3

● 0° IS ALONG
■ 0° IS ALONG CIRCUMFERE

TABLE
INSTRUM
& AXIS

	GAGES	
	SG "1 THRU SG "28	
A	SG "29-34, 66-69, 81 & 82	
A	SG "35 THRU SG "37	C
	SG "38 THRU SG "40	C
	SG "41 THRU SG "58	B
B	SG "59 & SG "60	L
	SG "61 THRU SG "63	L
	SG "64, 65, 70, 71 & 72	C
	SG "75 THRU SG "80	L

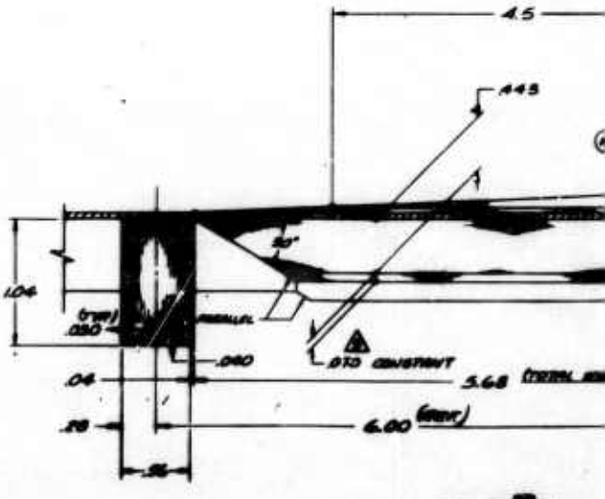

TABLE SHOWING
RIOUS THORNEL 50
R ORIENTATION

ENT	NUMBER OF LAYERS	AVERAGE FIBER ORIENTATION	
	4	90°, +15°, -15°, 90°	
RS	4	+10°, -10°, -10°, +10°	
(CAP)	4	0°	
SIDE S)	3	0°, +45°, -45°	

° IS ALONG SHELL
° IS ALONG SHELL
RCUMFERENTIAL DIRECTION

TABLE SHOWING
INSTRUMENTATION FUNCTION
& AXIS OF ORIENTATION

GES	ORIENTATION	GAGE FUNCTION
THRU 56 28	LONGITUDINAL	STRINGER BENDING
63-63, 81 & 82	LONGITUDINAL	SKIN BUCKLING
HRU 56 37	CIRCUMFERENTIAL	FRAME STRAINS
HRU 56 40	CIRCUMFERENTIAL	SKIN STRAINS
HRU 56 58	BIAXIAL PLUS SHEAR	SKIN STRAIN COMPONENTS
& 56 60	LONGITUDINAL	FIBERGLASS LOAD TRANSFER
THRU 56 63	LONGITUDINAL	STRINGER REPAIR EFFECTIVENESS
70, 71 & 72	CIRCUMFERENTIAL	RING BENDING
THRU 56 80	LONGITUDINAL	STRINGER STRAINS

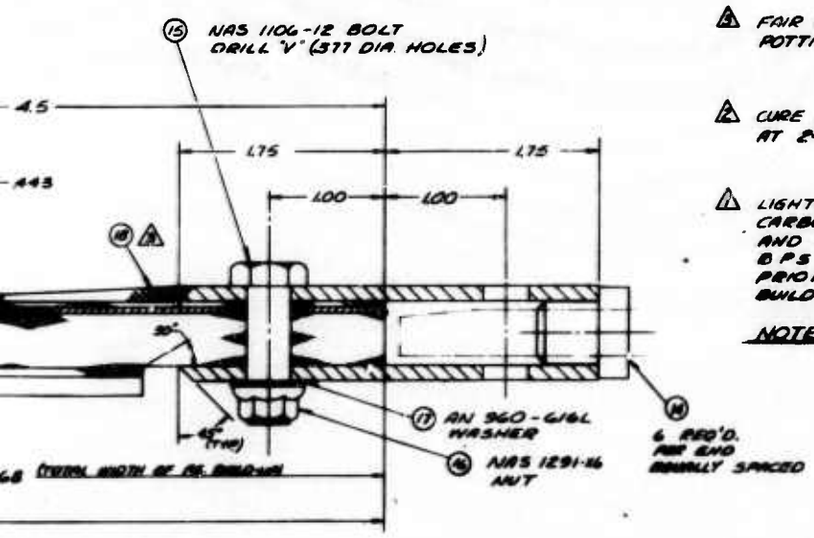

5 DRAPE .010 FIBERGLASS BUILD-UP PLIES - ONE LAYER AT A TIME.

6 BOND ON ALUM. PLATES WITH EC 2216.

8 FAIR WITH ROOM TEMPERATURE CURING POTTING COMPOUND AFTER ASSEMBLY.

12 CURE IN PLACE FOR 120 ± 5 MINUTES AT 245 ± 10°F AND 40 P.S.I.

11 LIGHTLY SAND (300 GRIT) AND DEGREASE CARBON LAMINATE WITH MEK. AND CLEAN AND ACID ETCH ALUMINUM PLATES PER BPS FW 4852, REV D, METHOD II PRIOR TO BONDING TO FIBERGLASS BUILDUP.

NOTES:

Figure 7. Maximu

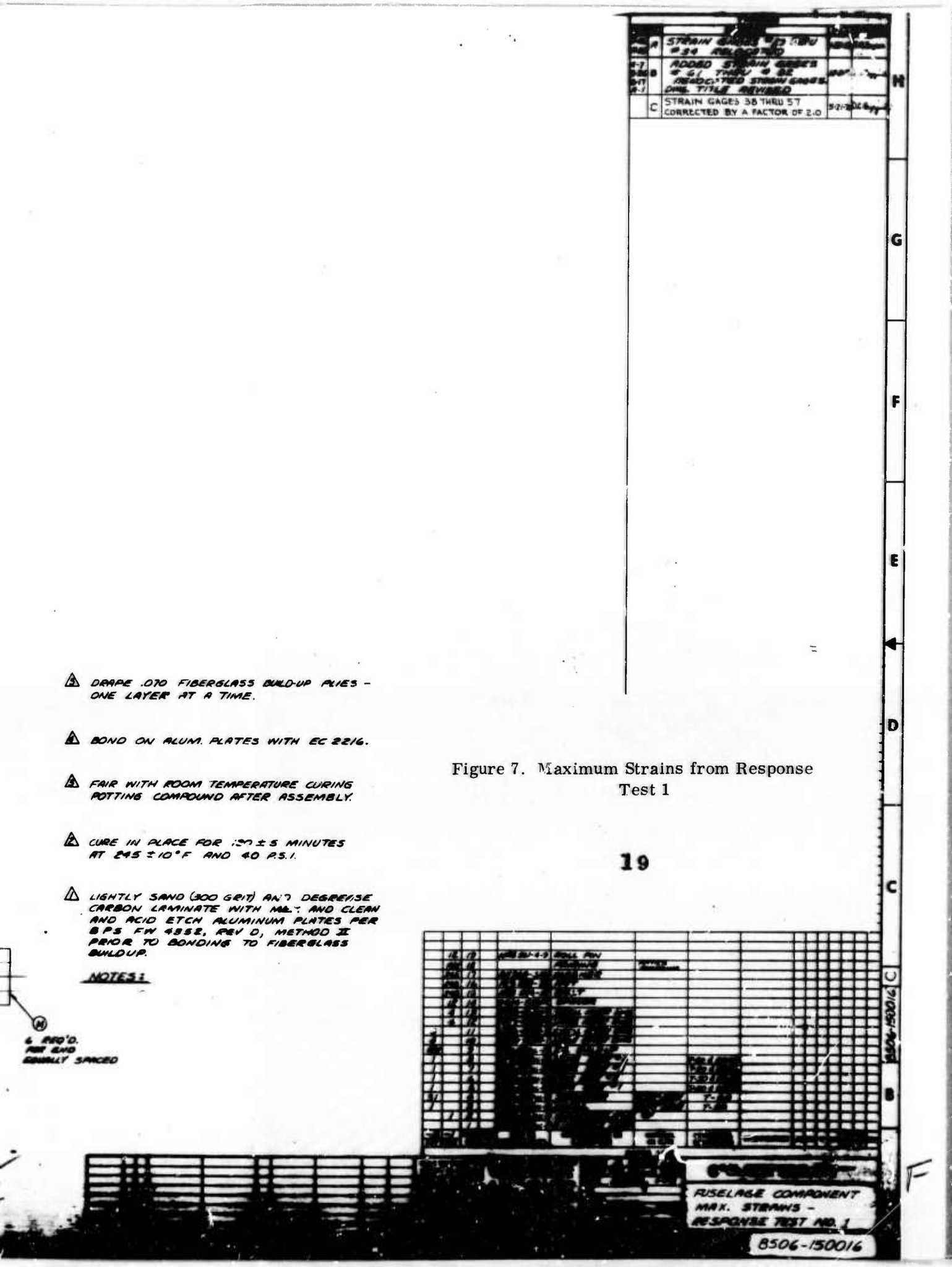

Figure 7. Maximum Strains from Response Test 1

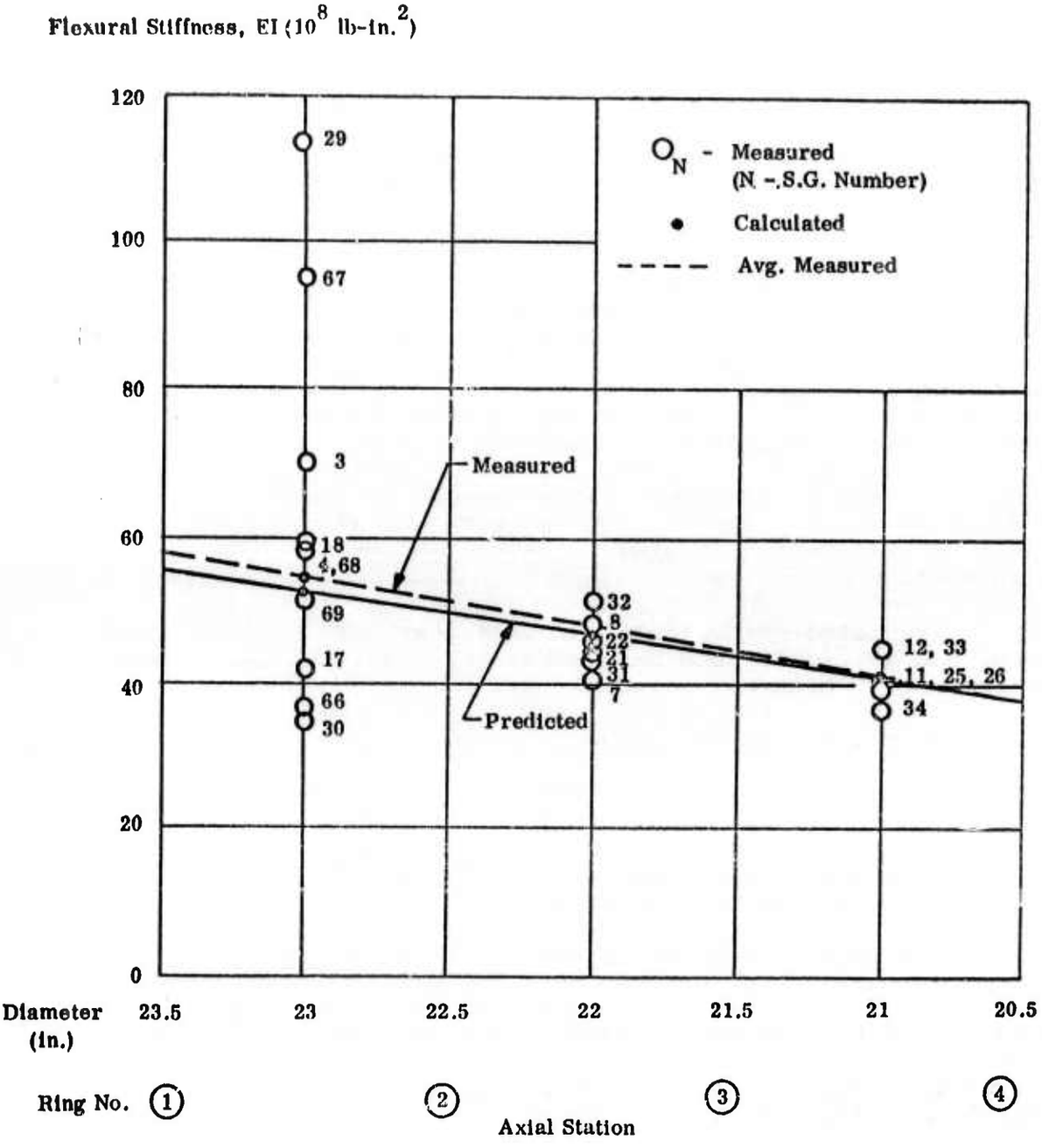

Figure 8. Flexural Stiffnesses from Response Test 1

shown in Figure 10 were 20 to 30 greater than predicted which is due to an unknown part of the torsion being carried by the stringers. Later in Section V A and shown on Figure 34, measured stiffness based on the 24 minute end rotation compared very well with predicted values.

3. Response Test 3

RT 3 was carried out under a combined bending and torsion load. Ten load increments were used in loading and three increments were used in unloading. The measured strains at maximum load are shown in Figure 11. These strains were generally as expected and conformed with results of RT 1 and 2. Maximum compressive strain was 735μ in./in., recorded by gage 17 on the skin along the top near the large diameter end. Maximum tensile strain was again recorded on gage 30, 1000μ in./in., at load step 10. Gage 29, on the skin exterior opposite gage 30, recorded only 250μ in./in. A similar bending effect was recorded on gages 66 and 67 between stringers 1 and 2 and adjacent to the region of gages 29 and 30. Gages 68 and 69, however, only an inch away from 29 and 30, did not "feel" the severe bending, nor did gages 3 and 4. Shear element gage strains resulting from the torsion load were fairly uniform on gages 45, 54, and 57, averaging 240μ in./in. Gage 51 read a much lower value because of its orientation dependency on the applied shear. Gages 41 and 47 recorded only one-half their expected strains. Again, the rosette readings were suspect.

Predicted deflections for this test were 0.060-in. tip movement and 17-minutes load beam rotation. Measured values were 0.084 in. and 14 minutes, respectively.

4. Response Test 4

For the final response test, an 80-lb concentrated load was applied in 10-lb increments to the bottom of the component at ring frame 3. A photograph of the 2 x 2-in. rubber-faced metal bearing pad is shown in Figure 12. A beam-fulcrum arrangement for loading is seen in the foreground.

The maximum recorded strain in this test was 120μ in./in. hoop compression in the skin near the point of load application at gage 37. Strains at maximum load are shown in Figure 13. Measured strains on frame 3 ranged from a maximum tensile value of 103μ in./in. on gage 35 just opposite the loading region to a maximum compressive strain of 63μ in./in. on gage 71, several stringers away from the loading point.

TABLE SHOWING TYPICAL FRAME CONSTRU

JOINT LOCATION FROM STIFFENER #1	MATERIAL	ANGLE	FRAME #1 O.D.	FRAME #2 O.D.	FRAME #3 O.D.
J	BALSA	28° 15' 32"	23.500	22.500	21.50
K	BALSA	11° 34' 46"	↓	↓	↓
L	THORNEL	28° 15' 32"	↓	↓	↓
M	THORNEL	34° 50' 18"	↓	↓	↓
N	THORNEL	28° 15' 32"	↓	↓	↓
O	THORNEL	34° 50' 18"	↓	↓	↓

TABLE SHOWING FRAME DIAME

FRAME NO.	I.D. DIA.	℄ DIA. OF FRAME	(C)
1	23.480	23.500	23.5
2	22.480	22.500	22.5
3.	21.480	21.500	21.5
4	20.480	20.500	20.5

DETAIL 12 (ZONE F-24)

DETAIL 12 (ZONE F-23)

45° (TYP)

℄ OF GAGES

BALSA GRAIN ORIENTED RADIAL AS SHOWN. (TYP)

℄ SHELL

45° (TYP)

℄ OF GAGES

(4) 31 REQ'D EQUALLY SPACED ALONG ENTIRE CIRCUMFERENCE

THESE VIEWS TO SHOW JOINT LOCATION ONLY. (ALL JOINTS TO BE FILLED WITH RESIN).

(REF.) 5°48'23"

SECTION ℄-℄

SECTION 13-13

.125 X 45° CHAMFER (TYP)

A

A820

S CONSTRUCTION

ground "2	ground "3	ground "4	NO. REQ'D.
22.500	21.500	20.500	15
			1
			14
			1
			14
			1

RAME DIAMETERS

& DIA OF FRAME	DIA
23.500	23.520
22.500	22.520
21.500	21.520
20.500	20.520

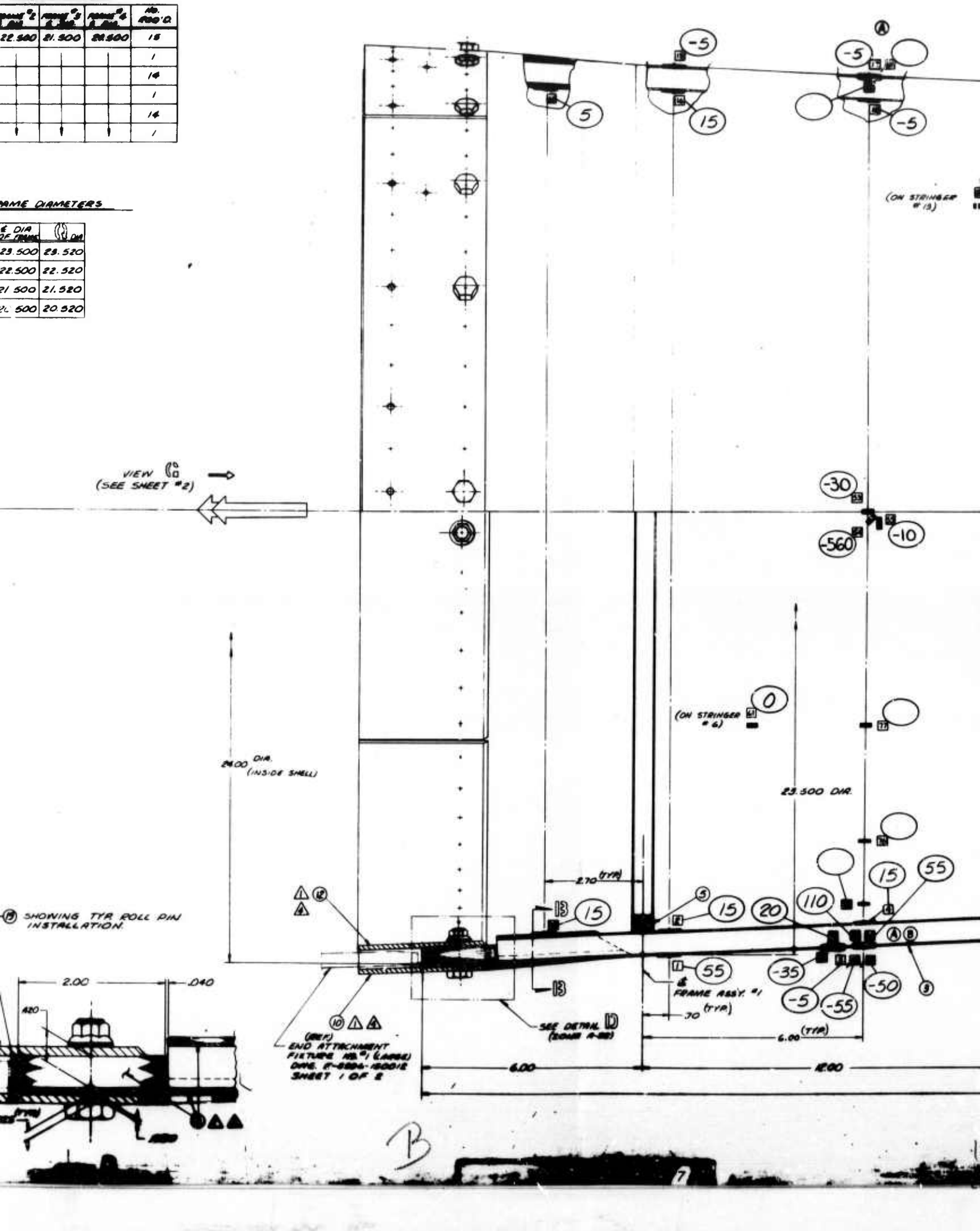

B

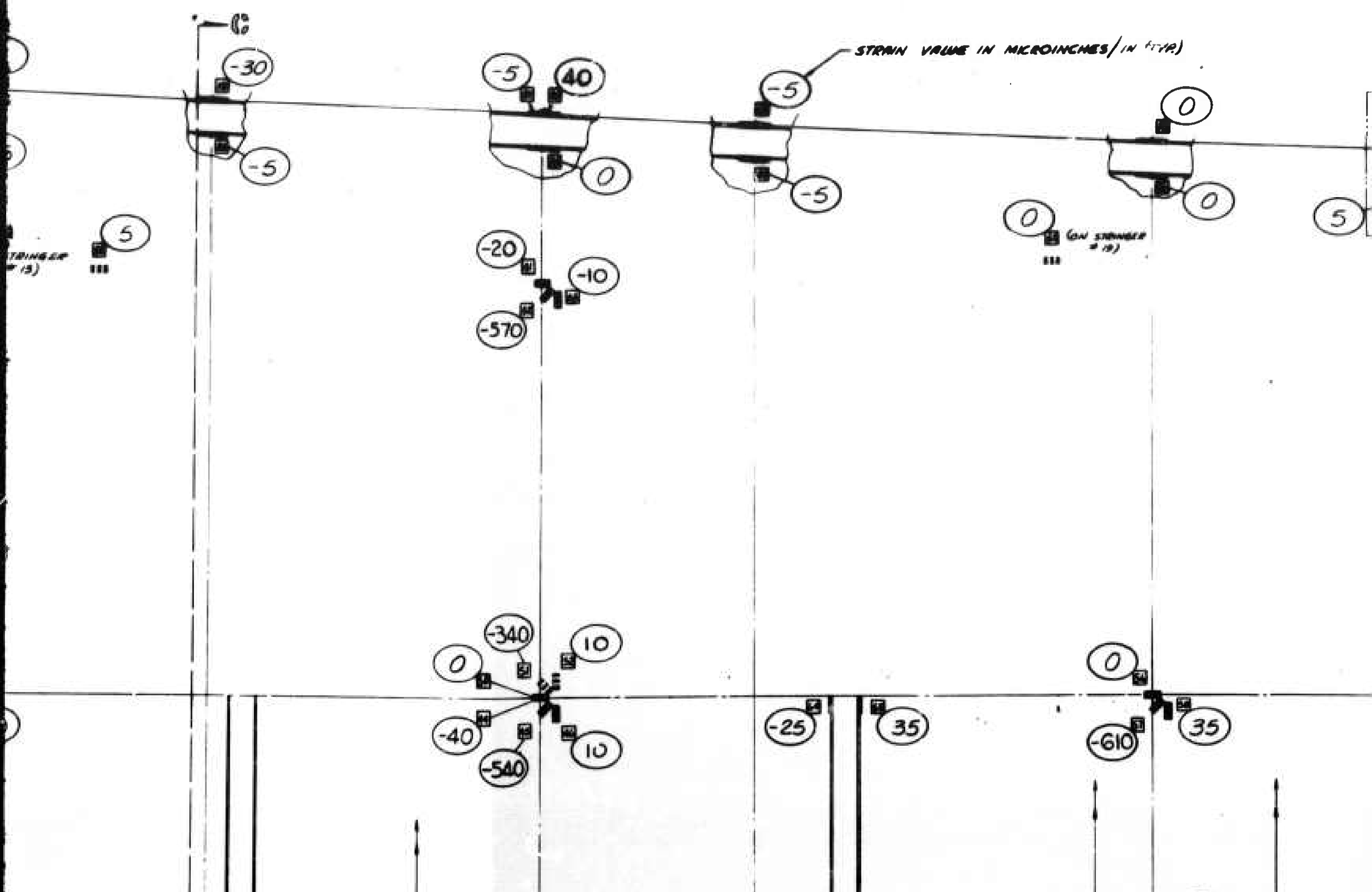

STRAIN VALUE IN MICROINCHES/IN (TYP.)
22.500 DIA.
21.500 DIA.
20.500 DIA.
FRAME ASSY. #2
FRAME ASSY. #3
6.00 (TYP)
1.80 (TYP)
.70 (TYP)
(ON STRINGER #19)

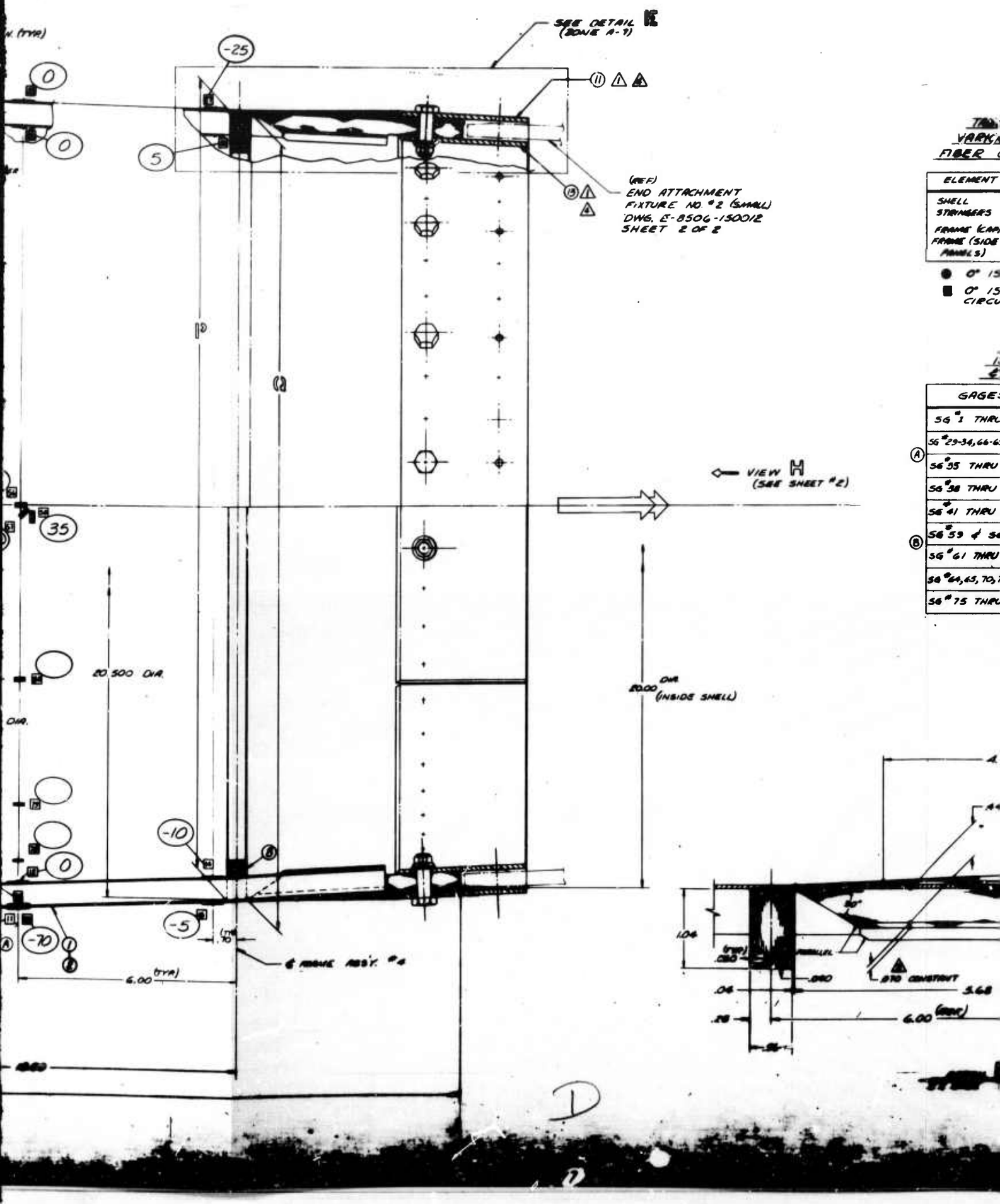

ELEMENT
SHELL
STRINGERS
FRAME (CAP)
FRAME (SIDE PANELS)

GAGES
SG #1 THRU
SG #29-34, 66-6
SG #35 THRU
SG #38 THRU
SG #41 THRU
SG #59 & 6
SG #61 THRU
SG #64, 65, 70,
SG #75 THRU

TABLE SHOWING VARIOUS THICKNESS OF FIBER ORIENTATION

ELEMENT	NUMBER OF LAMINATES	AVERAGE FIBER ORIENTATION
SHELL	4	90°, +15°, -15°, 90° ●
STRINGERS	4	+10°, -10°, -10°, +10° ●
FRAME (CAP)	4	0° ■
FRAME (SIDE PANELS)	3	0°, +45°, -45° ■

● 0° IS ALONG SHELL ℄

■ 0° IS ALONG SHELL CIRCUMFERENTIAL DIRECTION.

TABLE SHOWING INSTRUMENTATION FUNCTION & AXIS OF ORIENTATION

GAGES	ORIENTATION	GAGE FUNCTION
SG #1 THRU SG #28	LONGITUDINAL	STRINGER BENDING
SG #29-34, 66-69, 81 & 82	LONGITUDINAL	SKIN BUCKLING
(A) SG #35 THRU SG #37	CIRCUMFERENTIAL	FRAME STRAINS
SG #38 THRU SG #40	CIRCUMFERENTIAL	SKIN STRAINS
SG #41 THRU SG #58	BIAXIAL PLUS SHEAR	SKIN STRAIN COMPONENTS
(B) SG #59 & SG #60	LONGITUDINAL	FIBERGLASS LOAD TRANSFER
SG #61 THRU SG #63	LONGITUDINAL	STRINGER REPAIR EFFECTIVENESS
SG #64, 65, 70, 71 & 72	CIRCUMFERENTIAL	RING BENDING
SG #75 THRU SG #80	LONGITUDINAL	STRINGER STRAINS

(SHEET #2)

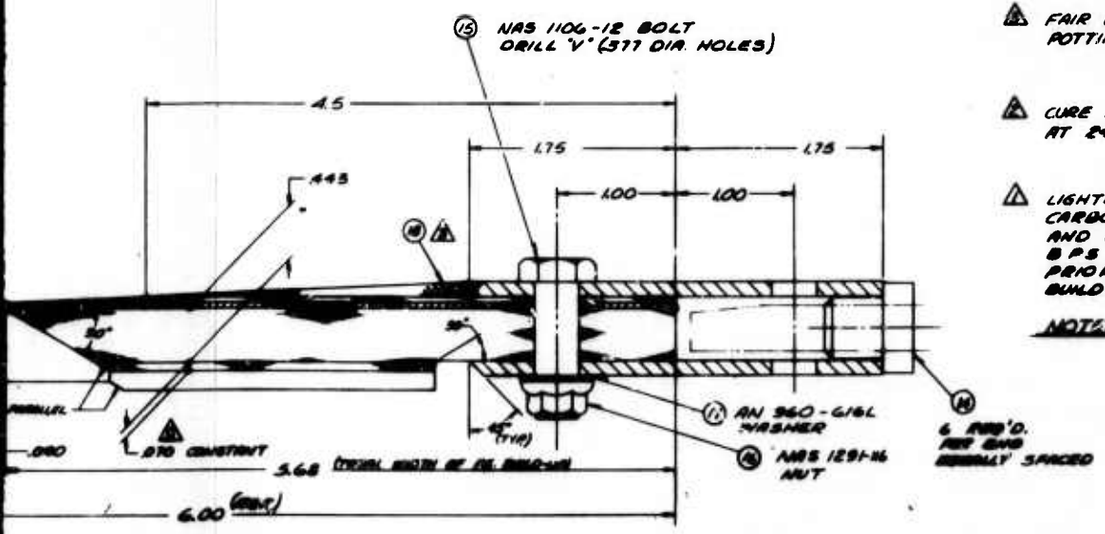

(5) DRAPE .070 FIBERGLASS BUILD-UP PLIES - ONE LAYER AT A TIME.

(4) BOND ON ALUM. PLATES WITH EC 2216.

(3) FAIR WITH ROOM TEMPERATURE CURING POTTING COMPOUND AFTER ASSEMBLY.

(2) CURE IN PLACE FOR 120 ± 5 MINUTES AT 245 ± 10°F AND 40 P.S.I.

(1) LIGHTLY SAND (300 GRIT) AND DEGREASE CARBON LAMINATE WITH MEK AND CLEAN AND ACID ETCH ALUMINUM PLATES PER BPS FW 4852, REV D, METHOD II PRIOR TO BONDING TO FIBERGLASS BUILDUP.

NOTES:

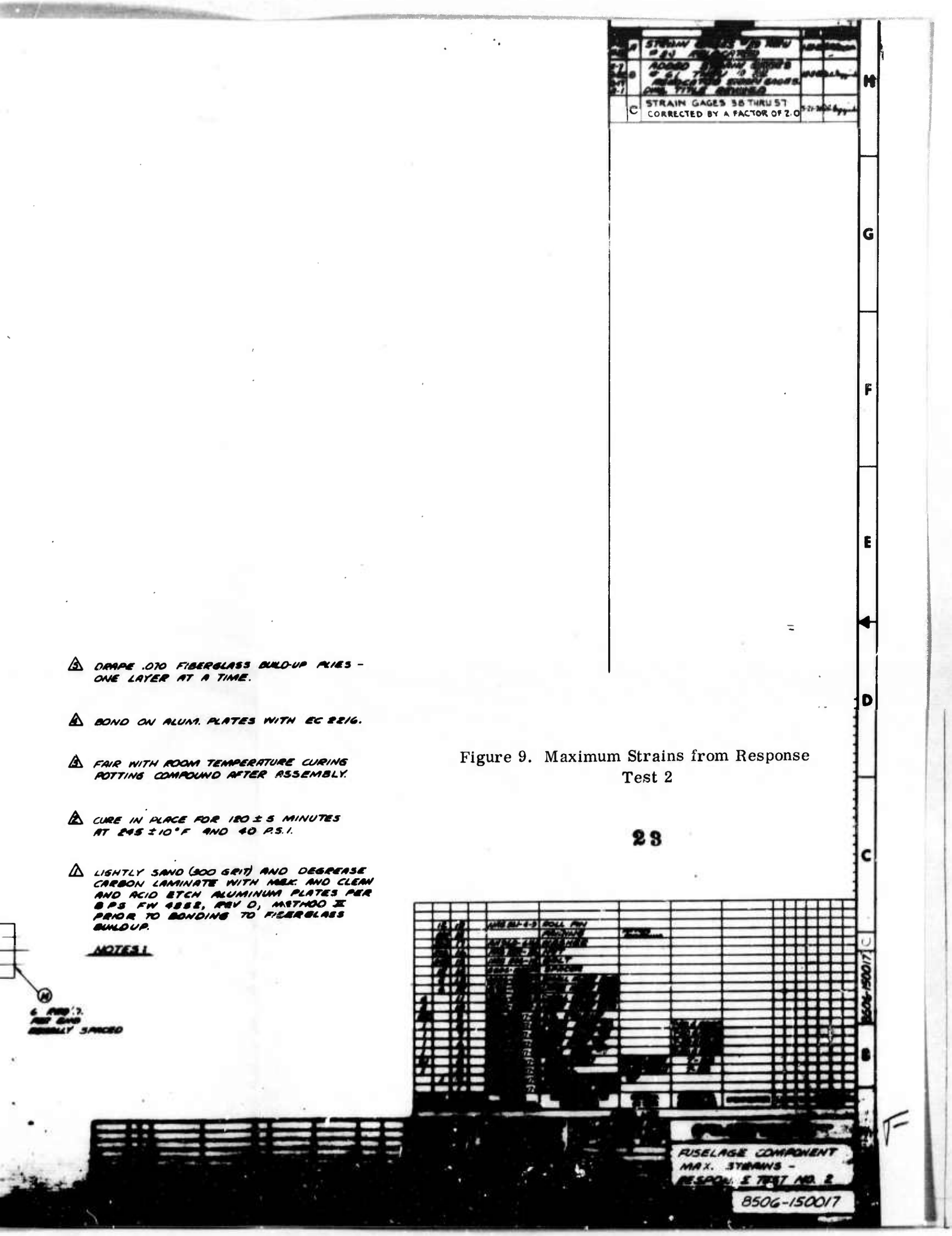

Figure 9. Maximum Strains from Response Test 2

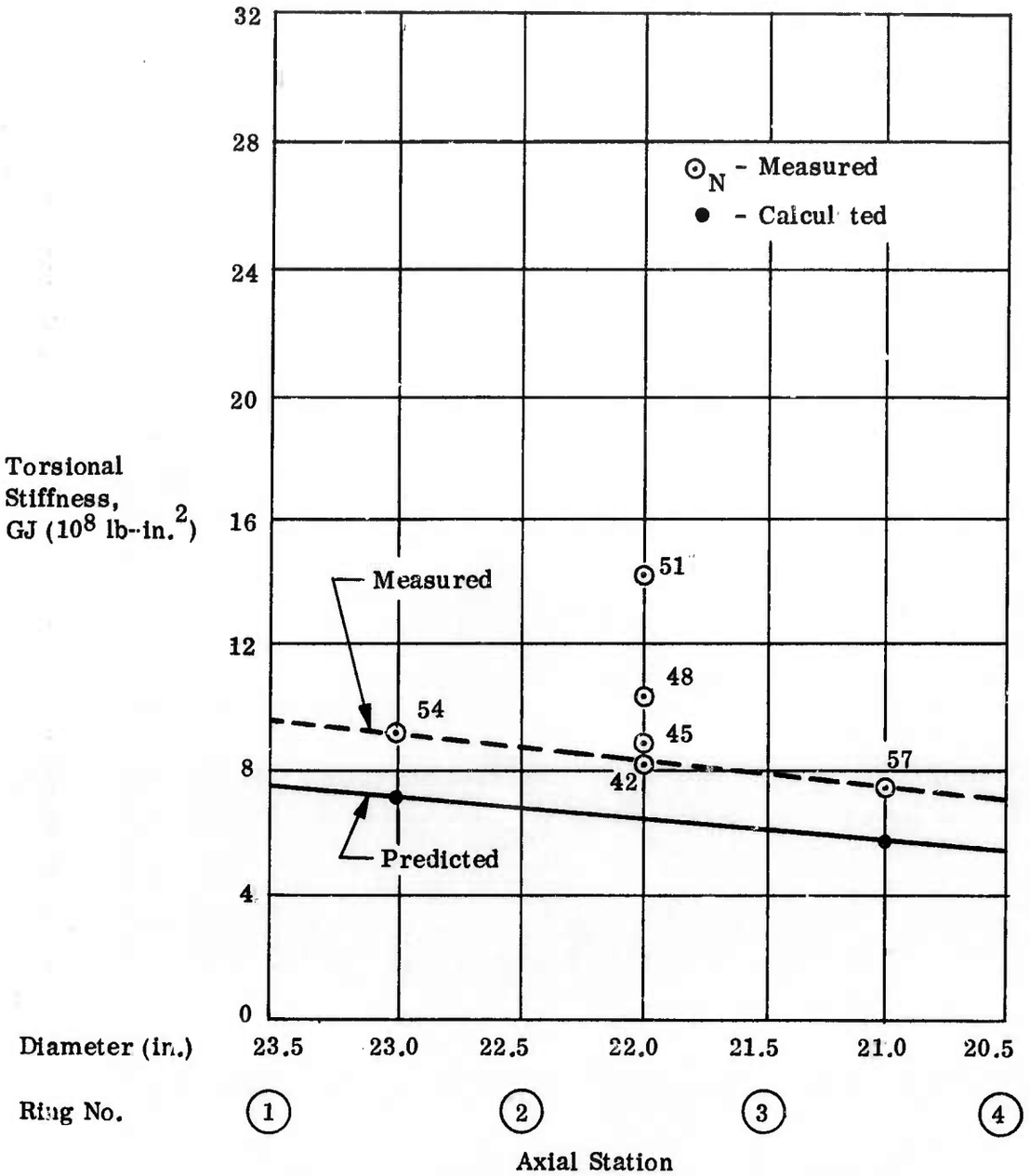

Figure 10. Torsional Stiffnesses from Response Test 2

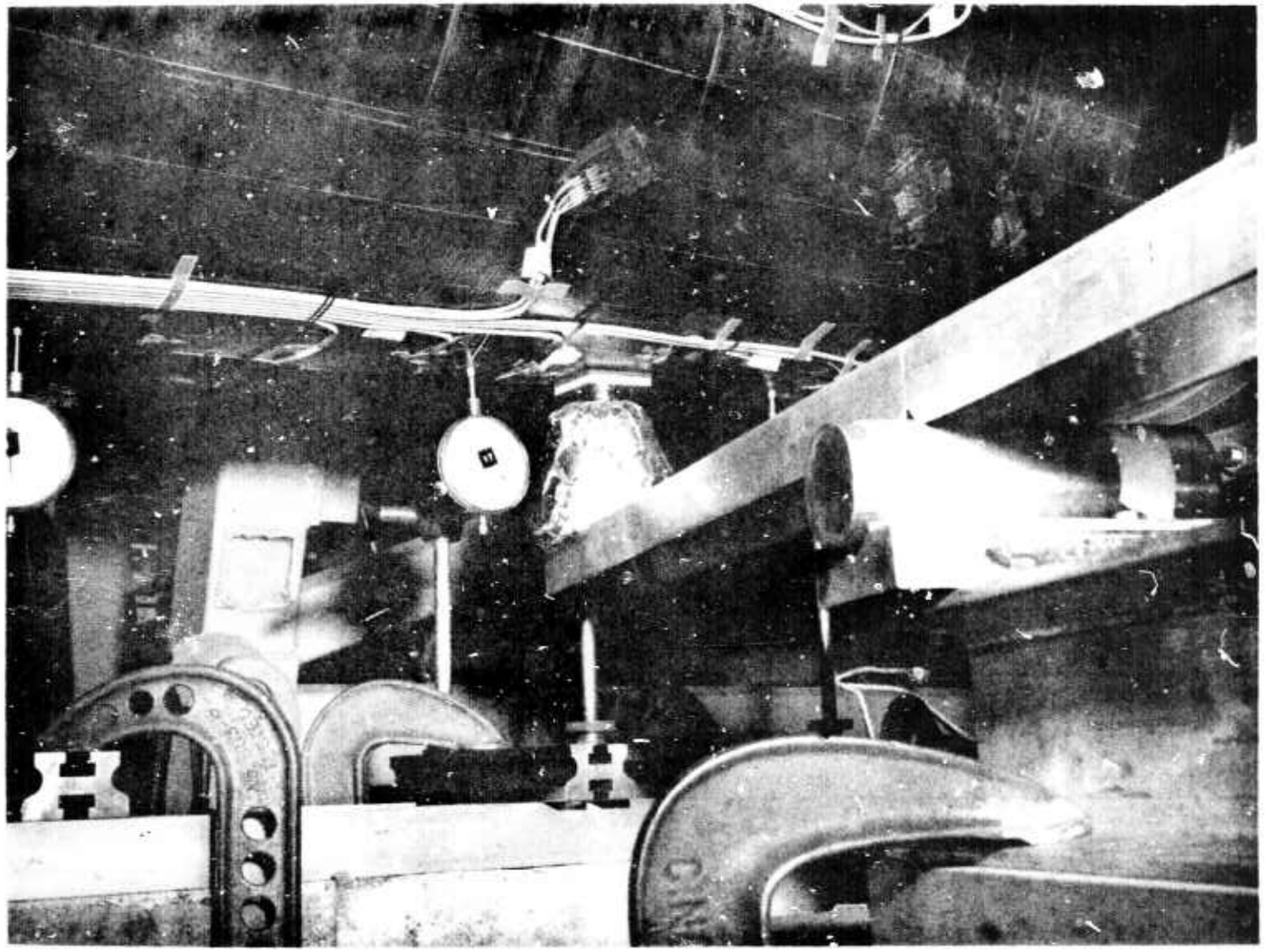

Figure 12. Close-Up of Response Test 4 Local Load Application.

P700067

TABLE SHOWING TYPICAL FRAME CONSTRU...

JOINT LOCATION FROM STIFFENER #1	MATERIAL	ANGLE	FRAME #1 ℄ DIA	FRAME #2 ℄ DIA	FALSE ...
J	BALSA	25° 15' 52"	23.500	22.500	21.50...
K	BALSA	11° 36' 46"	↓	↓	↓
L	THORNEL	25° 13' 52"	↓	↓	↓
M	THORNEL	34° 50' 18"	↓	↓	↓
N	THORNEL	25° 15' 52"	↓	↓	↓
O	THORNEL	34° 50' 18"	↓	↓	↓

TABLE SHOWING FRAME DIAME...

FRAME NO.	P DIA	℄ DIA OF FRAME	Q ...
1	23.480	23.500	23.52...
2	22.480	22.500	22.52...
3	21.480	21.500	21.52...
4	20.480	20.500	20.52...

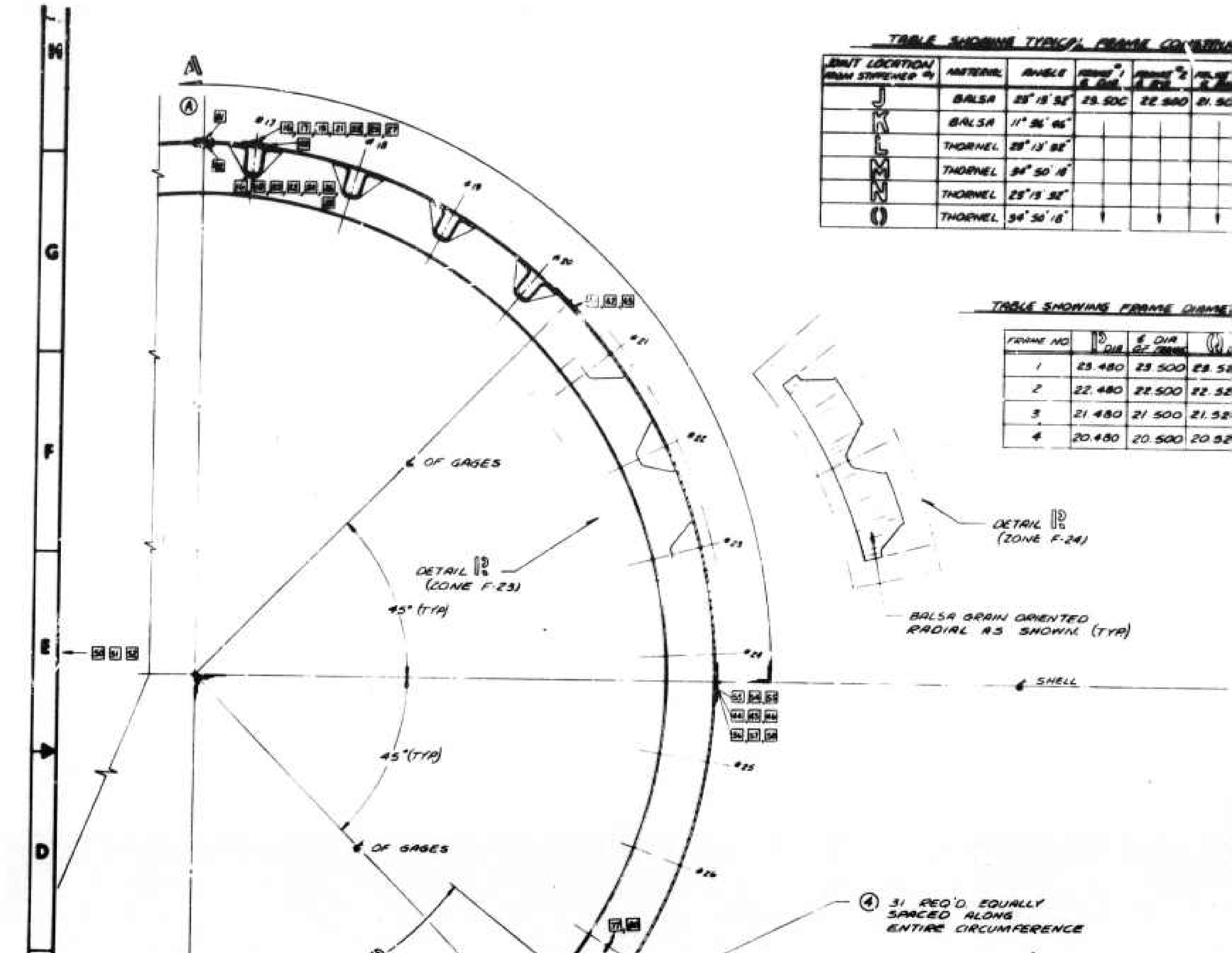

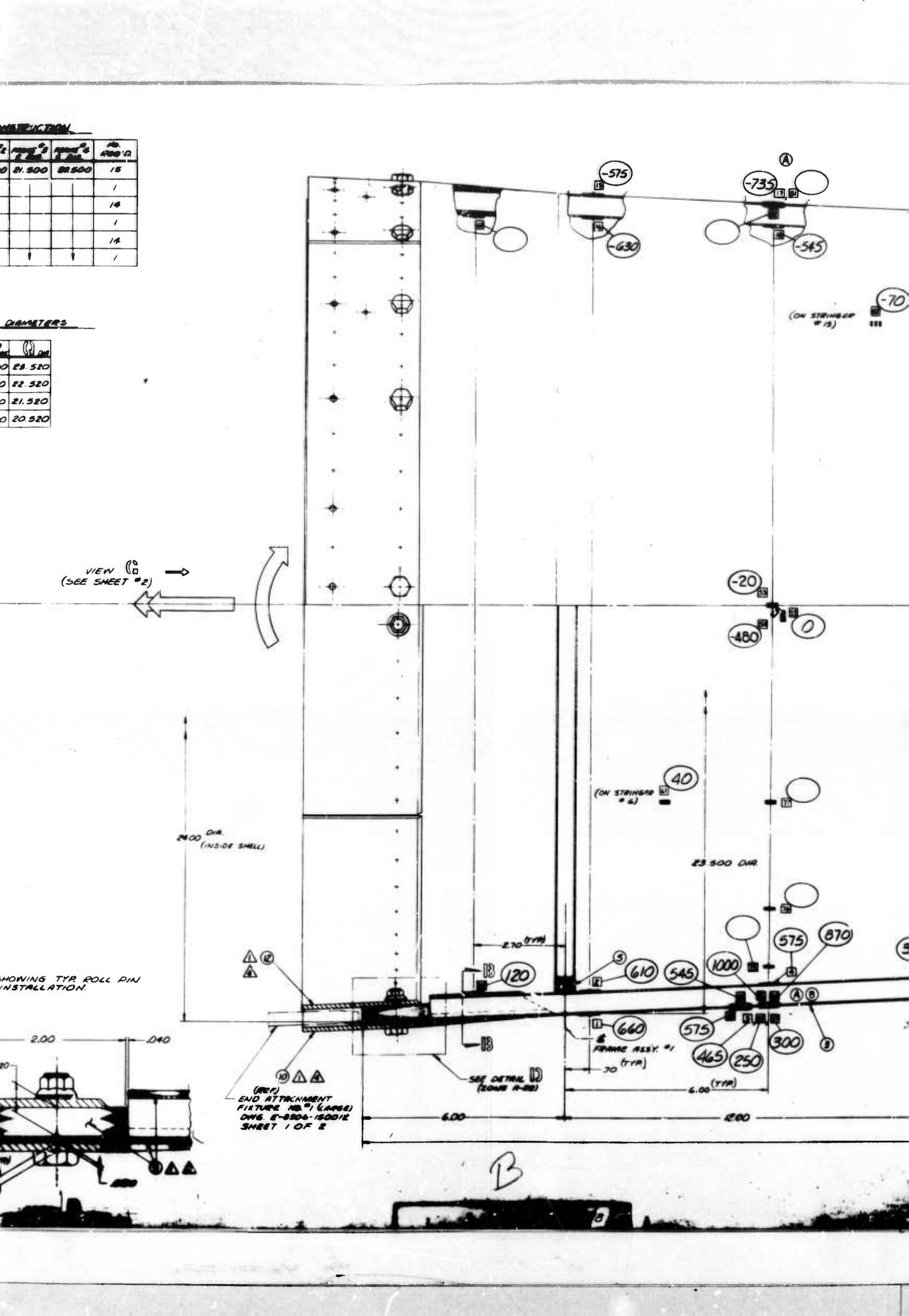
-575
-735
-630
-545
-70
(ON STRINGER #15)
-20
-480
0
VIEW
(SEE SHEET #2)
40
(ON STRINGER #4)
24.00 DIA.
(INSIDE SHELL)
23.500 DIA.
2.70 (TYP)
120
610
545
1000
575
870
660
575
300
465
250
FRAME ASSY. #1
.70 (TYP)
6.00 (TYP)
SEE DETAIL D
(SHEET 4-512)
(REF)
END ATTACHMENT
FIXTURE NO. #1 (LARGE)
DWG. E-8804-150012
SHEET 1 OF 2
6.00
12.00
2.00
.040
SHOWING TYP. ROLL PIN
INSTALLATION.
B

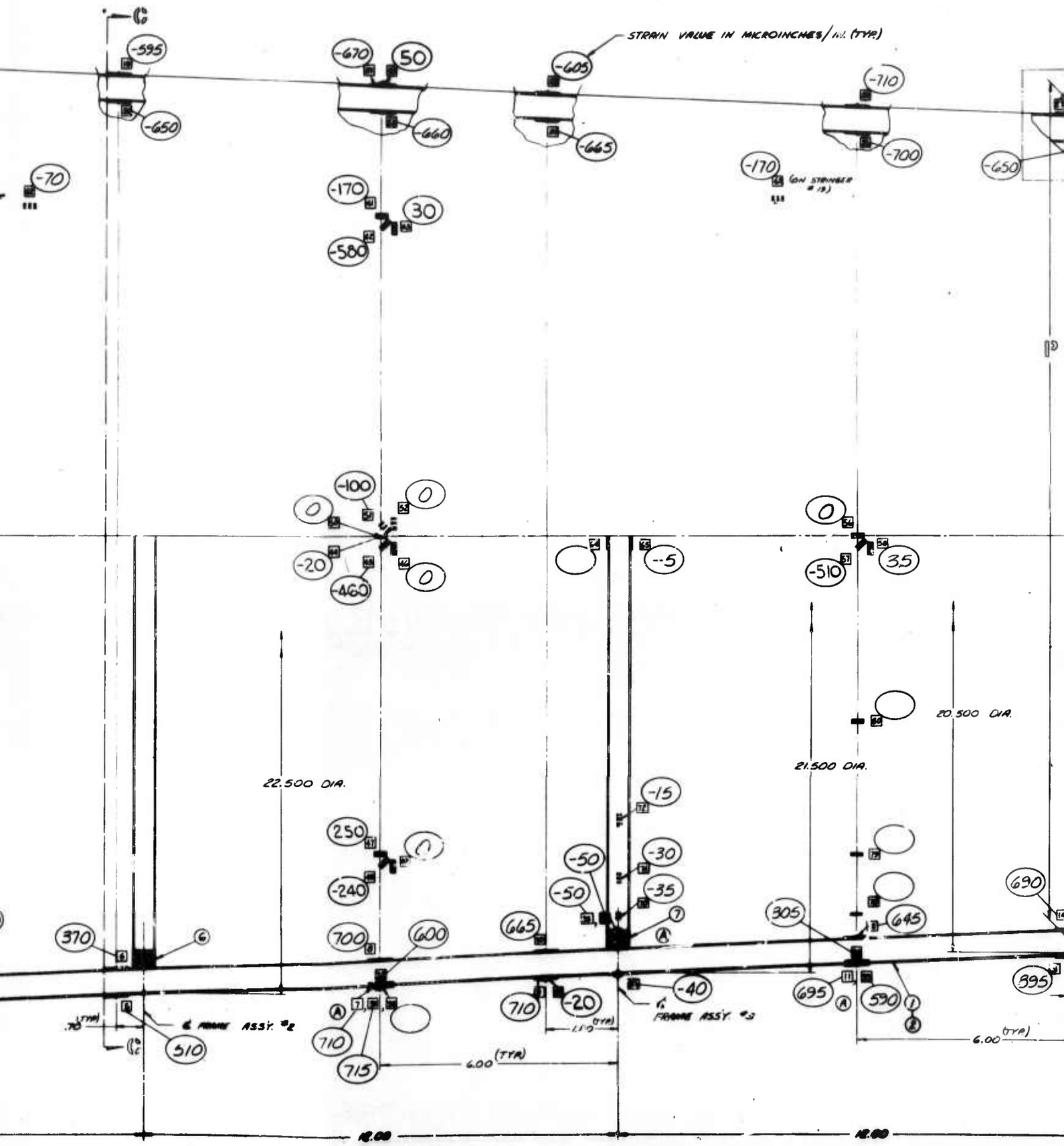
STRAIN VALUE IN MICROINCHES/in. (TYP.)
-595
-650
-670
50
-660
-605
-665
-710
-700
-650
-70
-170
(ON STRINGER # 19)
-170
30
-580
-100
0
0
-20
-460
0
-5
0
-510
3.5
20.500 DIA.
21.500 DIA.
22.500 DIA.
-15
250
0
-240
-50
-30
-50
-35
690
370
700
600
665
305
645
710
-20
-40
695
590
395
.75 (TYP.)
6 FRAME ASSY. #2
510
710
715
6.00 (TYP.)
1.5 (TYP.)
6 FRAME ASSY. #3
6.00 (TYP.)
82.00
82.00

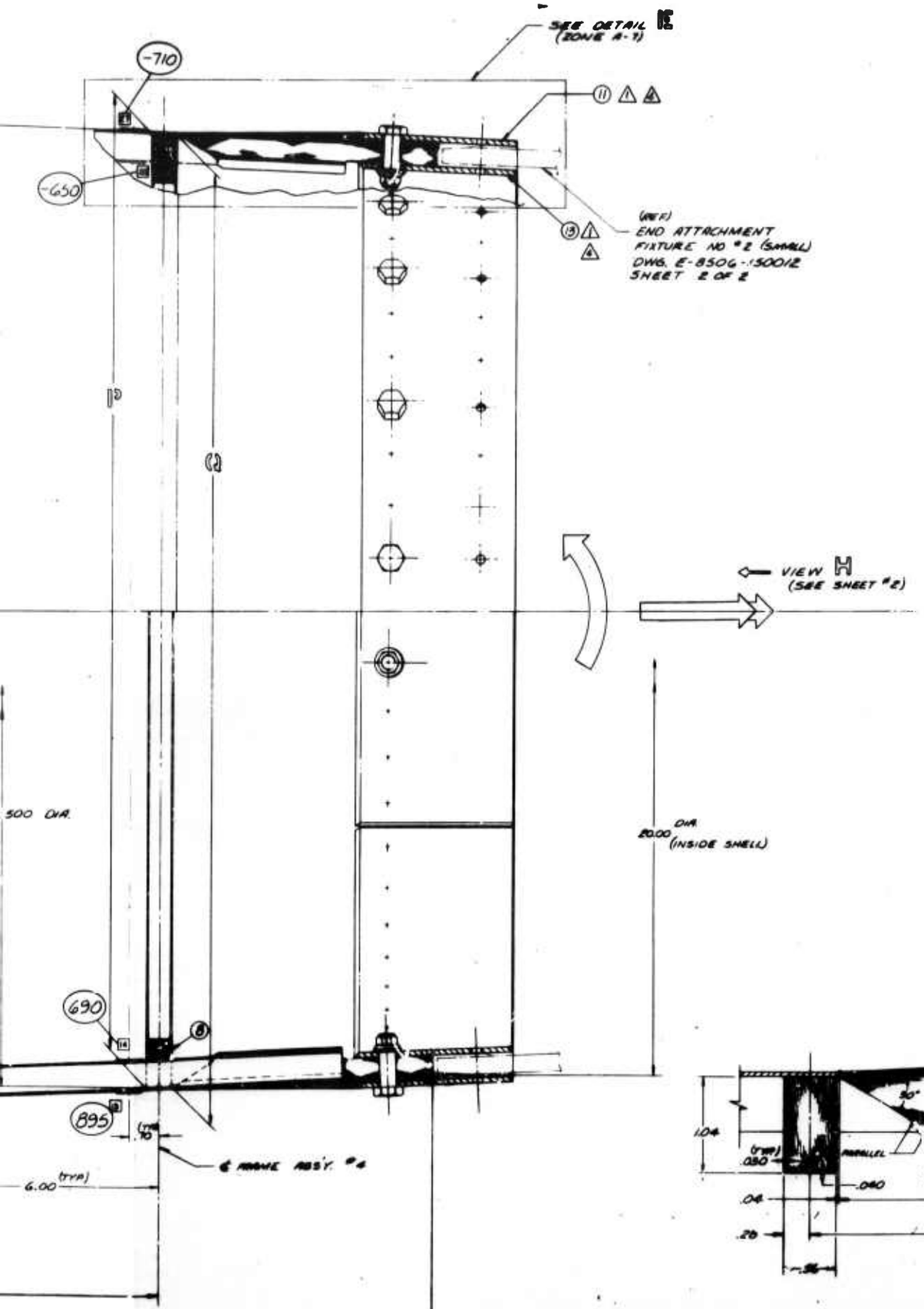

TABLE SHOWING VARIOUS THORNEL FIBER ORIENTATION

ELEMENT	NUMBER OF LAYERS	AVERAGE FIBER ORIENTATION
SHELL	4	90°, +15°, -
STRINGERS	4	+10°, -10°, -
FRAME (CAP)	4	0°
FRAME (SIDE PANELS)	3	0°, +45°, -

● 0° IS ALONG SHELL
■ 0° IS ALONG SHELL CIRCUMFERENTIAL DI

TABLE SHOWI INSTRUMENTATIO & AXIS OF ORIE

	GAGES	ORIENTAT
	SG #1 THRU SG #28	LONGITUD
	SG #29-34, 66-69, 81 & 82	LONGITUDI
(A)	SG #35 THRU SG #37	CIRCUMFERE
	SG #38 THRU SG #40	CIRCUMFERE
	SG #41 THRU SG #58	BIAXIAL PLU
(B)	SG #59 & SG #60	LONGITUDI
	SG #61 THRU SG #63	LONGITUDI
	SG #64, 65, 70, 71 & 72	CIRCUMFERE
	SG #75 THRU SG #80	LONGITUDI

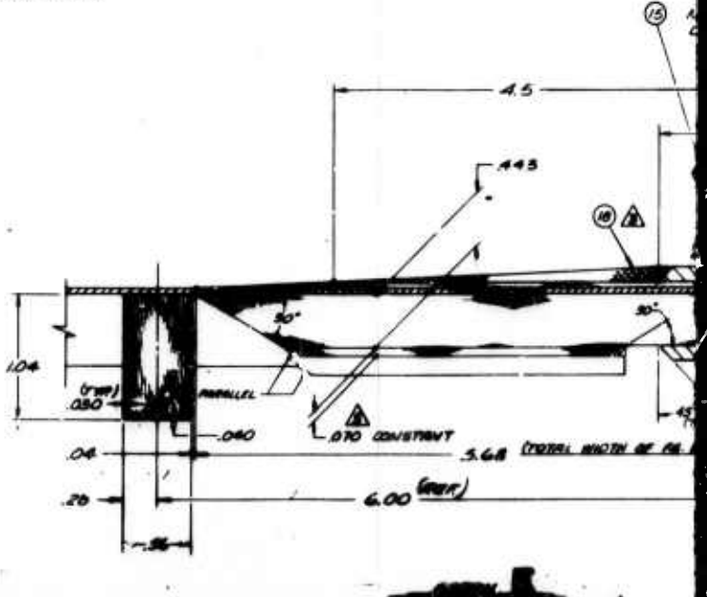

TABLE SHOWING
VARIOUS THORNEL 50
ER ORIENTATION

MCNT	NUMBER OF LAYERS	AVERAGE FIBER ORIENTATION	
L	4	90°, +15°, -15°, 90°	●
MBERS	4	+10°, -10°, -10°, +10°	●
E (CAP)	4	0°	■
E (SIDE ELS)	3	0°, +45°, -45°	■

0° IS ALONG SHELL É
0° IS ALONG SHELL
CIRCUMFERENTIAL DIRECTION.

TABLE SHOWING
INSTRUMENTATION FUNCTION
& AXIS OF ORIENTATION

GAGES	ORIENTATION	GAGE FUNCTION
THRU SG #28	LONGITUDINAL	STRINGER BENDING
34, 66-69, 81 & 82	LONGITUDINAL	SKIN BUCKLING
THRU SG #37	CIRCUMFERENTIAL	FRAME STRAINS
THRU SG #40	CIRCUMFERENTIAL	SKIN STRAINS
THRU SG #58	BIAXIAL PLUS SHEAR	SKIN STRAIN COMPONENTS
& SG #60	LONGITUDINAL	FIBERGLASS LOAD TRANSFER
THRU SG #63	LONGITUDINAL	STRINGER REPAIR EFFECTIVENESS
63, 70, 71 & 72	CIRCUMFERENTIAL	RING BENDING
THRU SG #80	LONGITUDINAL	STRINGER STRAINS

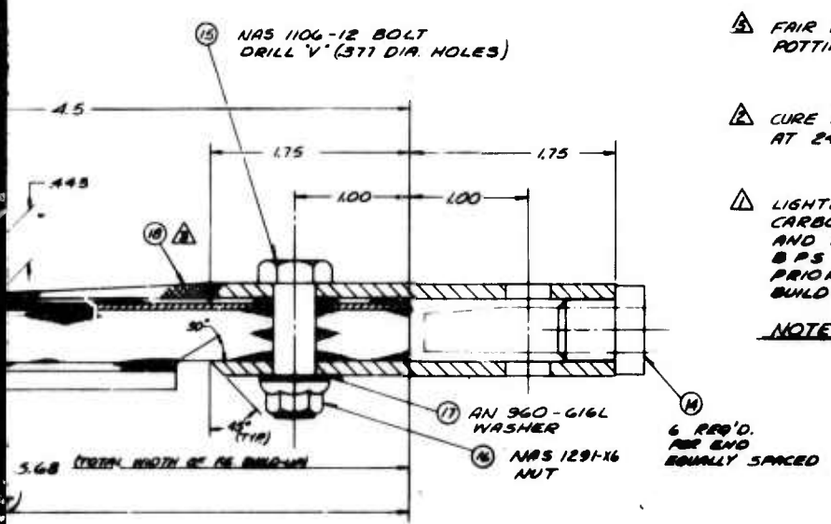

(5) DRAPE .070 FIBERGLASS BUILD-UP PLIES - ONE LAYER AT A TIME.

(4) BOND ON ALUM. PLATES WITH EC 2216.

(3) FAIR WITH ROOM TEMPERATURE CURING POTTING COMPOUND AFTER ASSEMBLY.

(2) CURE IN PLACE FOR 120 ± 5 MINUTES AT 245 ± 10°F AND 40 P.S.I.

(1) LIGHTLY SAND (300 GRIT) AND DEGREASE CARBON LAMINATE WITH MEK. AND CLEAN AND ACID ETCH ALUMINUM PLATES PER BPS FW 4852, REV D, METHOD II PRIOR TO BONDING TO FIBERGLASS BUILDUP.

NOTES:

Figure 11. Max

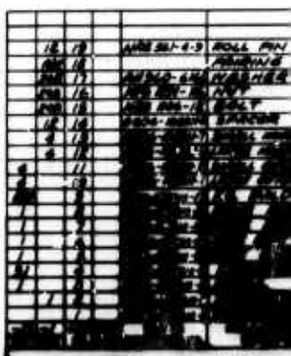

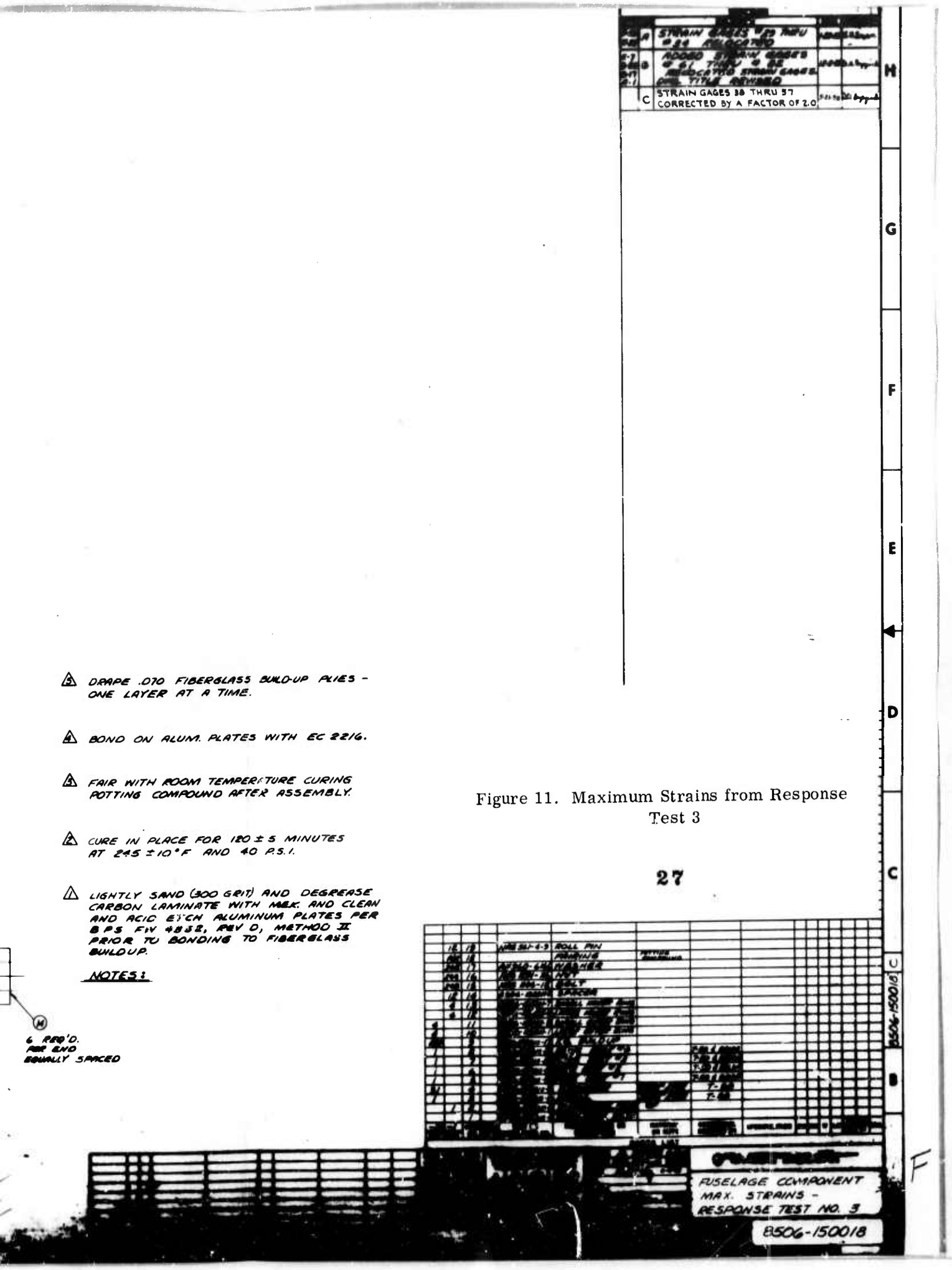

Figure 11. Maximum Strains from Response Test 3

TABLE SHOWING TYPICAL FRAME CONSTRUCT

JOINT LOCATION FROM STRINGER #4	MATERIAL	ANGLE	FRAME #1	FRAME #2	FRAME #3
J	BALSA	28° 13' 32"	23.500	22.500	21.500
K	BALSA	11° 36' 46"			
L	THORNEL	28° 13' 32"			
M	THORNEL	34° 50' 18"			
N	THORNEL	28° 13' 32"			
O	THORNEL	34° 50' 18"			

TABLE SHOWING FRAME DIAMETE

FRAME NO.	I.D. DIA	℄ DIA OF FRAME	O.D. DIA
1	23.480	23.500	23.520
2	22.480	22.500	22.520
3	21.480	21.500	21.520
4	20.480	20.500	20.520

DETAIL B (ZONE F-24)

BALSA GRAIN ORIENTED RADIAL AS SHOWN. (TYP.)

℄ SHELL

DETAIL B (ZONE F-23)

45° (TYP.)

℄ OF GAGES

45° (TYP.)

℄ OF GAGES

(4) 31 REQ'D. EQUALLY SPACED ALONG ENTIRE CIRCUMFERENCE

THESE VIEWS TO SHOW JOINT LOCATION ONLY. (ALL JOINTS TO BE FILLED WITH RESIN).

(REF.) 5°48'11"

SECTION C-C

SECTION B-B

SHOWING INSTALLA

2.00

420

.125 X 45° CHAMFER (TYP.)

.065

A

CONSTRUCTION

500	21.500	20.500	15
			1
			14
			1
			14
			1

E DIAMETERS

DIA	DIA
500	23.520
500	22.520
500	21.520
500	20.520

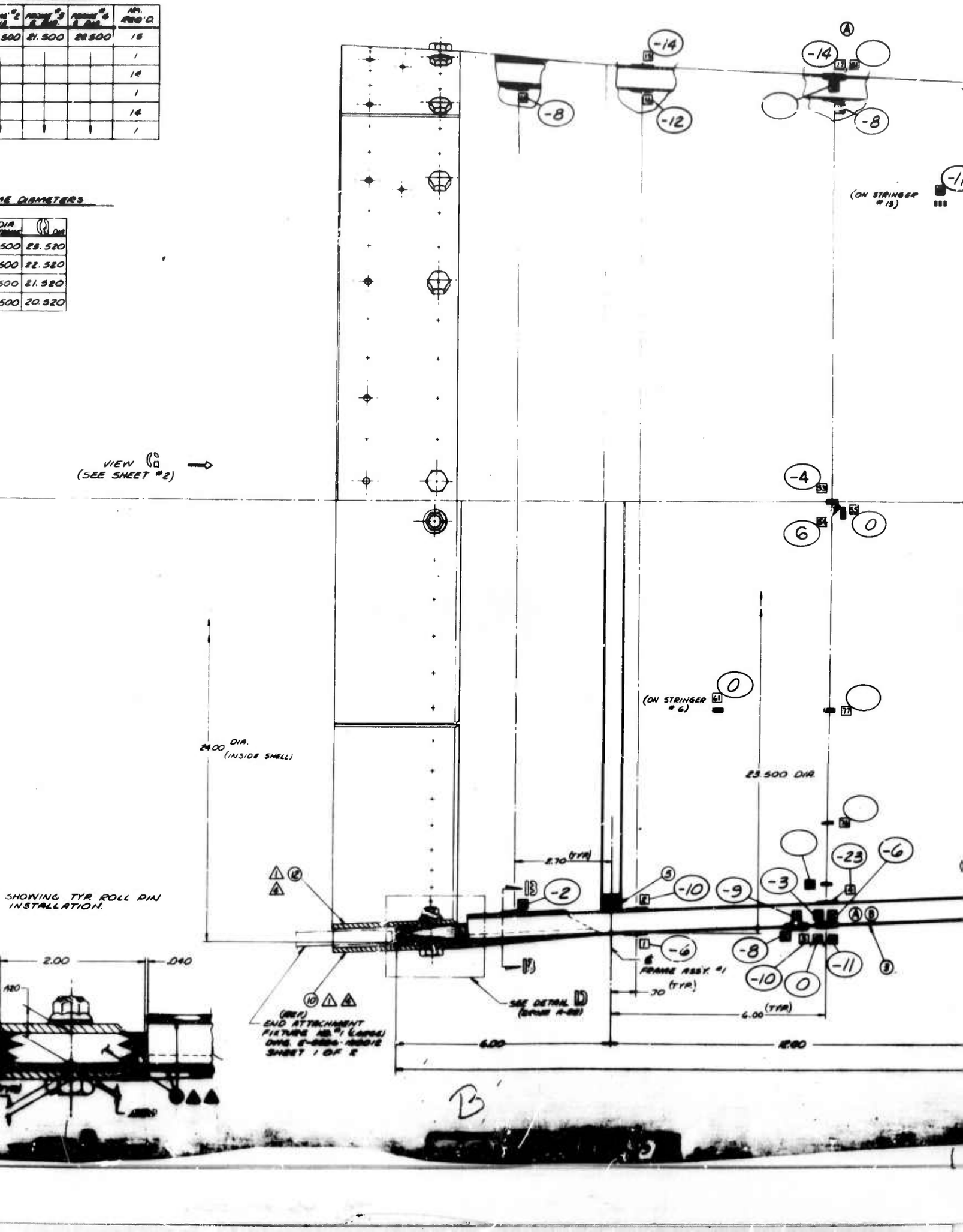

SHOWING TYP. ROLL PIN INSTALLATION.

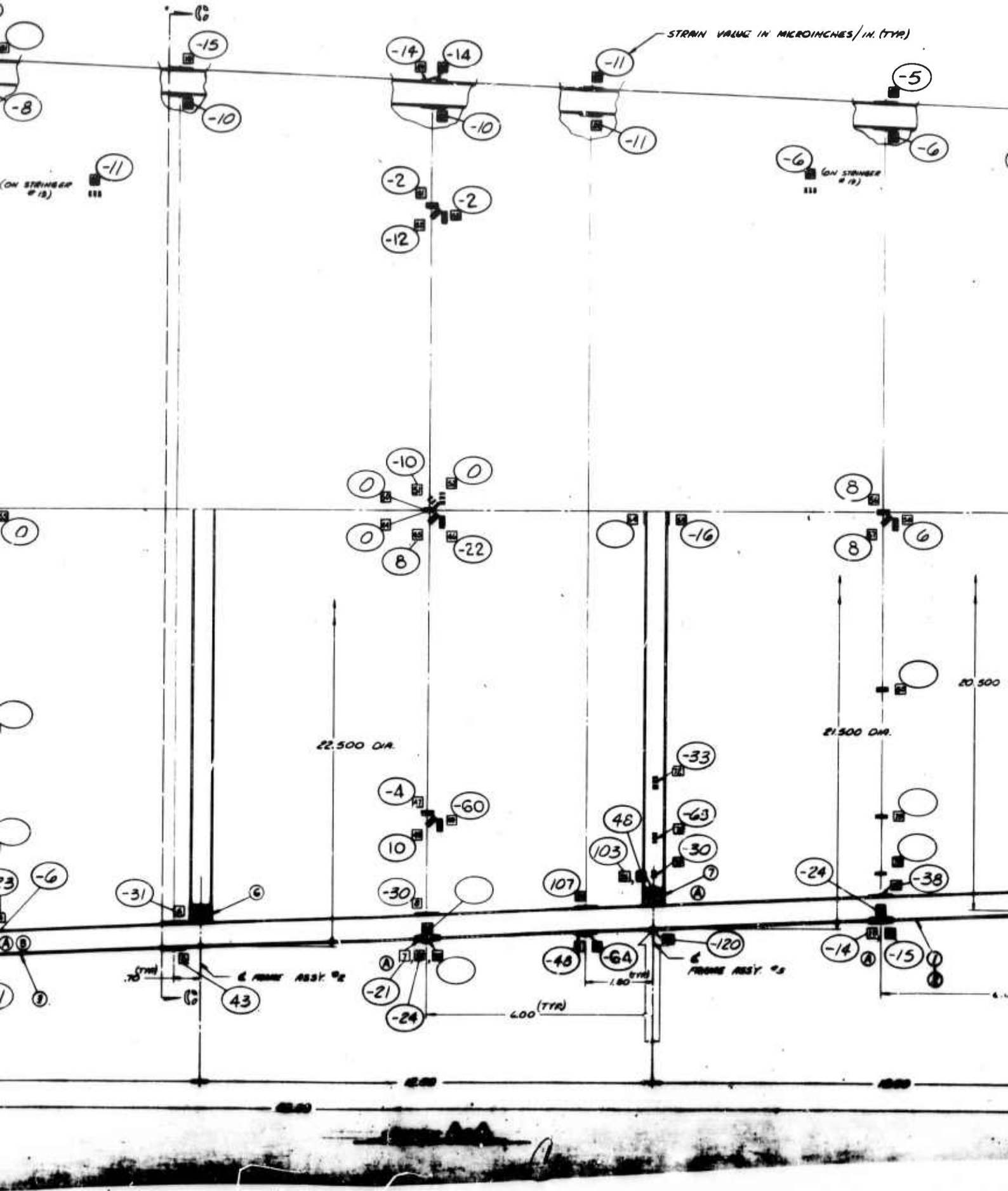
STRAIN VALUE IN MICROINCHES/IN. (TYP.)
22.500 DIA.
21.300 DIA.
4.00 (TYP.)
1.80 (TYP.)
.78 (TYP.)
(ON STRINGER # 15)
(ON STRINGER # 19)

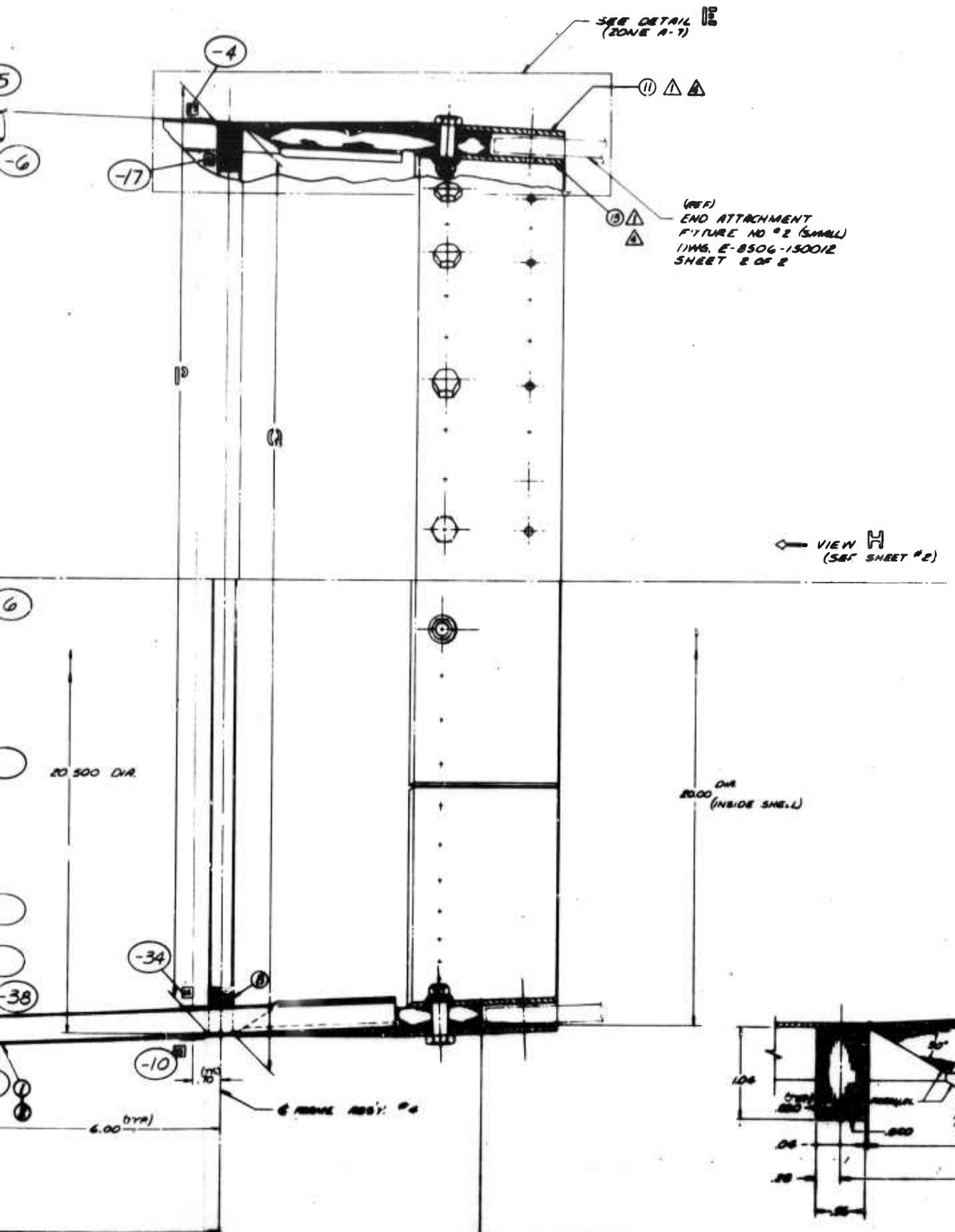

TABLE SA
VARIOUS T
FIBER ORIE

ELEMENT	
SHELL STRINGERS	4
FRAME (CAN	4
FRAME (SAGE FRAME)	3

● 0° IS ALONG
■ 0° IS ALONG CIRCUMFER

TABU
INSTR
& AXIS

	GAGES
	SG #1 THRU SG #28
	SG #29-34, 66-69, 81 & 82
A	SG #35 THRU SG #37
	SG #38 THRU SG #40
	SG #41 THRU SG #58
B	SG #59 & #3 - #60
	SG #61 THRU SG #63
	SG #64, 65, 70, 71 & 72
	SG #75 THRU SG #80

TABLE SHOWING
VARIOUS THORNEL 50
FIBER ORIENTATION

ELEMENT	NUMBER OF PLIES	AVERAGE FIBER ORIENTATION	
SHELL	4	90°, +15°, -15°, 90°	●
STIFFENERS	4	+15°, -15°, -15°, +15°	●
FRAME (CAP)	4	0°	■
FRAME (SIDE PANELS)	3	0°, +45°, -45°	■

● 0° IS ALONG SHELL ℄

■ 0° IS ALONG SHELL CIRCUMFERENTIAL DIRECTION

TABLE SHOWING
INSTRUMENTATION FUNCTION
& AXIS OF ORIENTATION

GAGES	ORIENTATION	GAGE FUNCTION
SG #1 THRU SG #28	LONGITUDINAL	STRINGER BENDING
SG #29-34, 66-69, 81 & 82	LONGITUDINAL	SKIN BUCKLING
SG #35 THRU SG #37	CIRCUMFERENTIAL	FRAME STRAINS
SG #38 THRU SG #40	CIRCUMFERENTIAL	SKIN STRAINS
SG #41 THRU SG #58	BIAXIAL PLUS SHEAR	SKIN STRAIN COMPONENTS
SG #59 & SG #60	LONGITUDINAL	FIBERGLASS LOAD TRANSFER
SG #61 THRU SG #63	LONGITUDINAL	STRINGER REPAIR EFFECTIVENESS
SG #64, 65, 70, 71 & 72	CIRCUMFERENTIAL	RING BENDING
SG #73 THRU SG #80	LONGITUDINAL	STRINGER STRAINS

(A)

(B)

⚠ DRAPE .070 FIBERGLASS BUILD-UP PLIES - ONE LAYER AT A TIME.

⚠ BOND ON ALUM. PLATES WITH EC 2216.

⚠ FAIR WITH ROOM TEMPERATURE CURING POTTING COMPOUND AFTER ASSEMBLY.

⚠ CURE IN PLACE FOR 180 ± 5 MINUTES AT 245 ± 10°F AND 40 P.S.I.

⚠ LIGHTLY SAND (600 GRIT) AND DEGREASE CARBON LAMINATE WITH MEK. AND CLEAN AND ACID ETCH ALUMINUM PLATES PER BPS #W 4852, REV D, METHOD II PRIOR TO BONDING TO FIBERGLASS BUILDUP.

NOTES:1

Figure 1

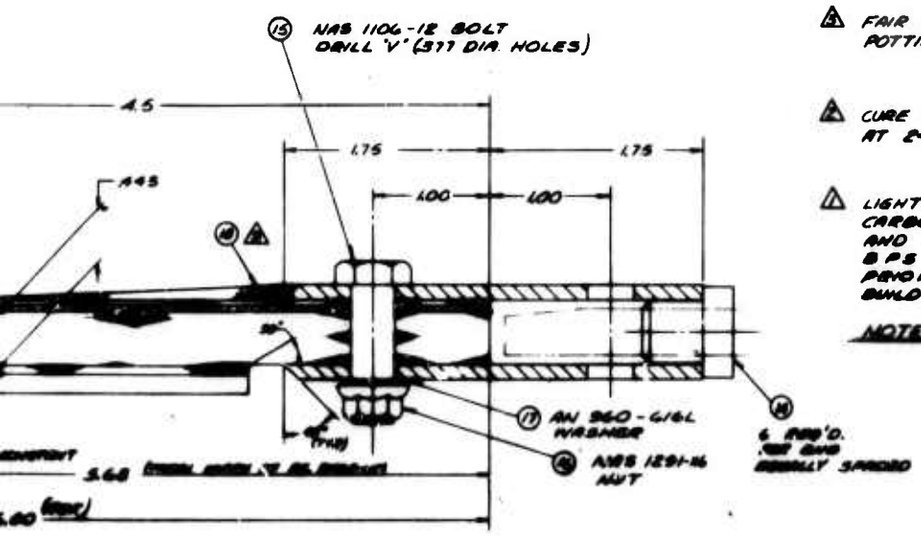

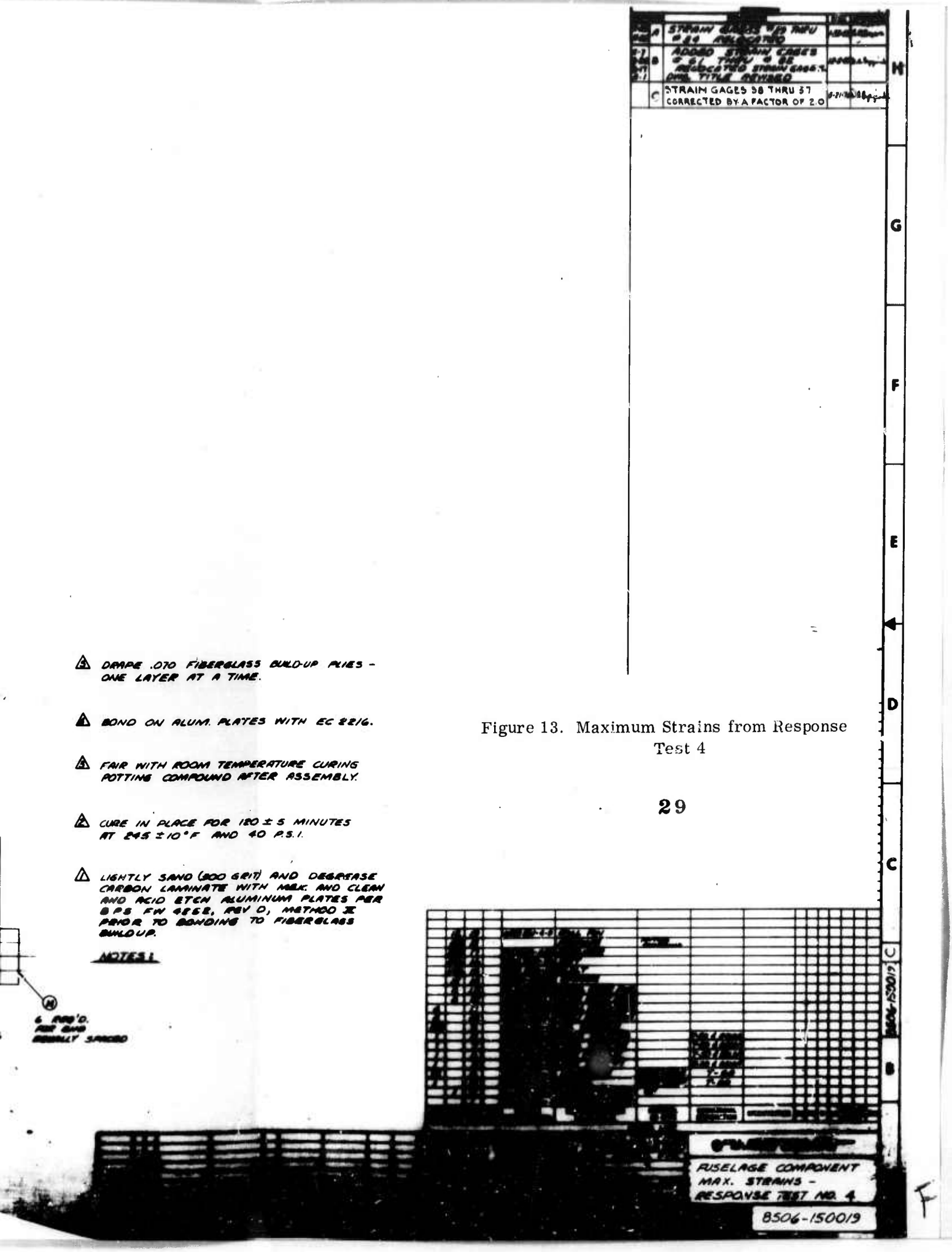

Figure 13. Maximum Strains from Response Test 4

Dial gages positioned on either side of the loading region recorded deflections of 0.006 and 0.003 in.; 0.001-in. tip deflection was measured. Discrete element analysis predictions were 0.0024, 0.0022, and 0.00103 in., respectively. The agreements are very good, considering the accuracy of dial gages and the relatively rough surface finish of the component, which permits some gage motion during loading.

D. Destruct Test
(S.L. Cross, L.H. Kocher, and D.P. Hanley, Bell Aerospace)

Prior to the destruct test, all response test data were reviewed to assess the component structural integrity and update the planned loading sequence. Additional strain gages (75 to 80) were installed on stringers to measure load diffusion and another pair of back-to-back gages (81 and 82) was added to measure skin bending. A single uniaxial gage was also added alongside rosette gage 47, and the rosette gage 47 was disconnected so that the new gage 47 output could be compared with that of gage 41. A plexiglass shield was installed around the component as a protective measure. Closed circuit zoom-lens television was set-up for observation of the test in the data room. A microphone was placed inside the component and connected to a tape recorder to monitor noise during test. Two movie cameras were focused on the large diameter end (top and bottom) of the component, where failure was expected.

A review meeting was held at Bell on November 24, 1969 with the Air Force Program Manager, Union Carbide, and Case-Western Reserve University to present a summary of previous test results and the planned procedure for the destruct test. The test procedure included:

1. Plotting the planned loading profile and strain predictions for critical areas for in-test monitoring.

2. Pretest checks of the hydraulic load system, hardware tie-down, dial gage positioning, photographic and data room set-up.

3. Application of combined bending and shear loads in increments at prescribed rates and hold times, data recording, and movie coverage starting when maximum strain reached 2000μ in./in.

4. Continuation of step loading to failure.

5. Post-test inspection, photography, and tear-down.

Arrangement for the destruct test is given in Figure 14 and shows dial gage positioning, safety shield envelope (dotted line), and load cylinder configuration. The planned loading profile is shown in Figure 15. The upper profile represents bending load/cylinder and the lower is the shear load. A 100-second load time/step was used up to step 5 where the loading increments were 1085 lb/cylinder bending and 840 lb/shear. Subsequent steps were completed in 50 seconds, with bending load increments of 543 lb/cylinder and shear increments of 420 lb. Specified N_x limit loading was between steps 8 and 9 and predicted N_x ultimate was at step 15. The loading combination was planned so that the N_{xy} shear load at the small end was one-tenth the N_x bending load at the large end.

As shown in Figure 15, failure occurred upon reaching load step 9. Maximum bending load at failure was 1980 lb/in. or 110% of the 1800-lb/in. design requirement. It was, however, only 76% of the expected 2610-lb/in. ultimate load. The fuselage component carried a shear load at failure of 200 lb/in., or 10% in excess of the 180-lb/in. design requirement for shear. Film coverage established that failure originated at the bottom of the component (tensile side) and progressed up to the top. The general plane of failure (Figures 16 and 17) was at ring frame 2.

During load application between steps 4 and 5 a loud, sharp noise was heard. The internally mounted microphone clearly recorded the sound. A number of strain gages showed a change in slope at this step and one gage (6) positioned on the bottom stringer cap (large end) showed constant strain with increasing load. It is suspected that stringer 1 cracked at the limit load level while loading from steps 4 to 5. Further cracking noises were heard and recorded at catastrophic failure while holding at step 9.

Shown in Figure 18 are strains as a function of load for a number of strain gages. The B gages shown by the outer two curves indicate severe local bending as was seen in the response tests. The B' gages however, 1-inch away from the B gages, did not show severe bending. This again confirmed the localized extent of the bending. All four gages showed a discontinuity slightly past 1200 lb/in. which corresponded to the recorded noise. Shown also in Figure 18 are outputs from gages in Regions C and D near Frame 2. Gage C_i was on the No. 1 stringer cap and C_o was on the outside skin. The D gages were back-to-back on the skin directly above Region C. There, also, the break in the curves was seen. Note from the bottom right curve that gage C_i on the Stringer 1 cap showed constant strain as load increased. An arrested crack in Stringer 1 may have accounted for this effect.

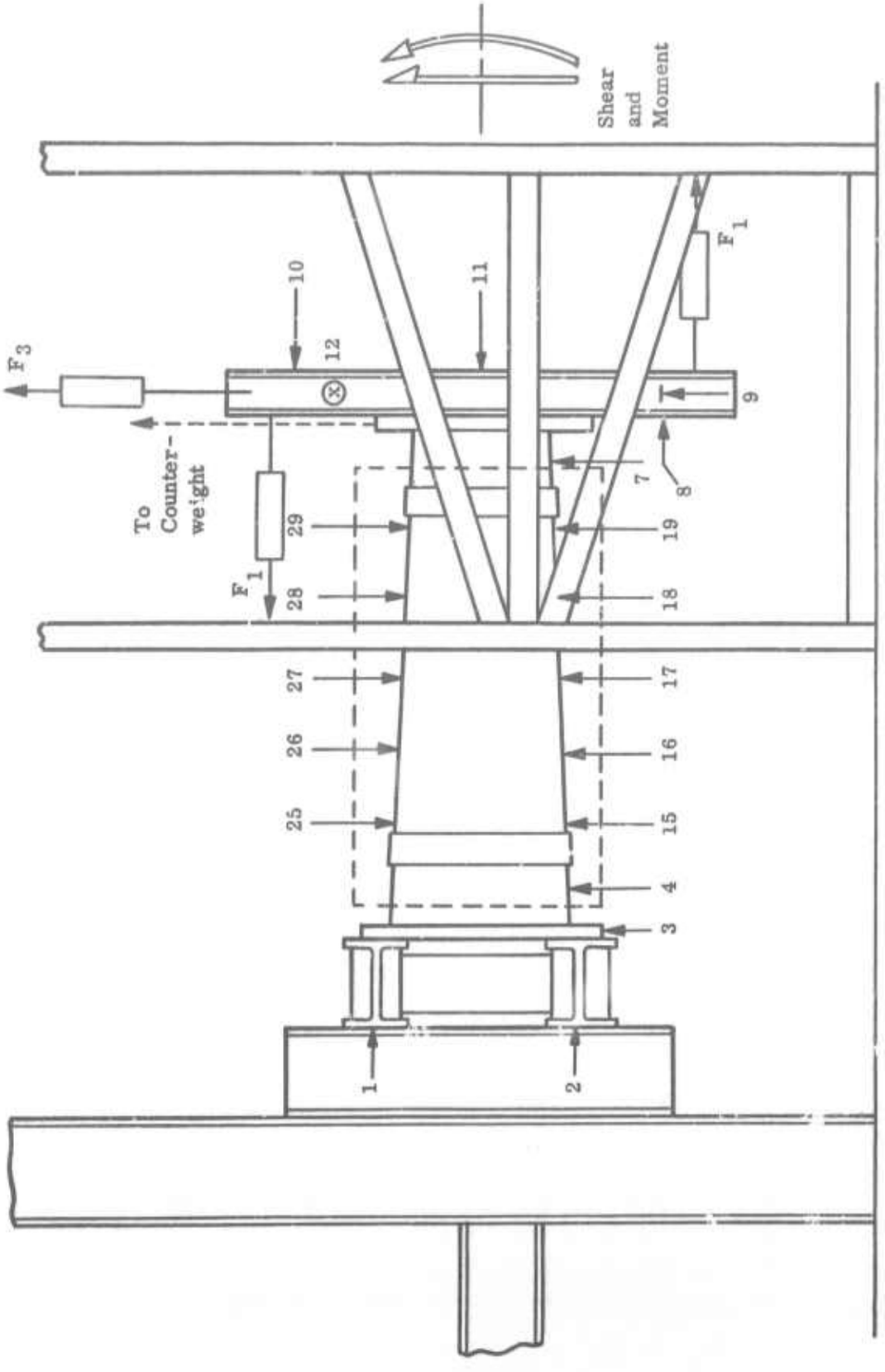

Figure 14. Destruct Test Arrangement

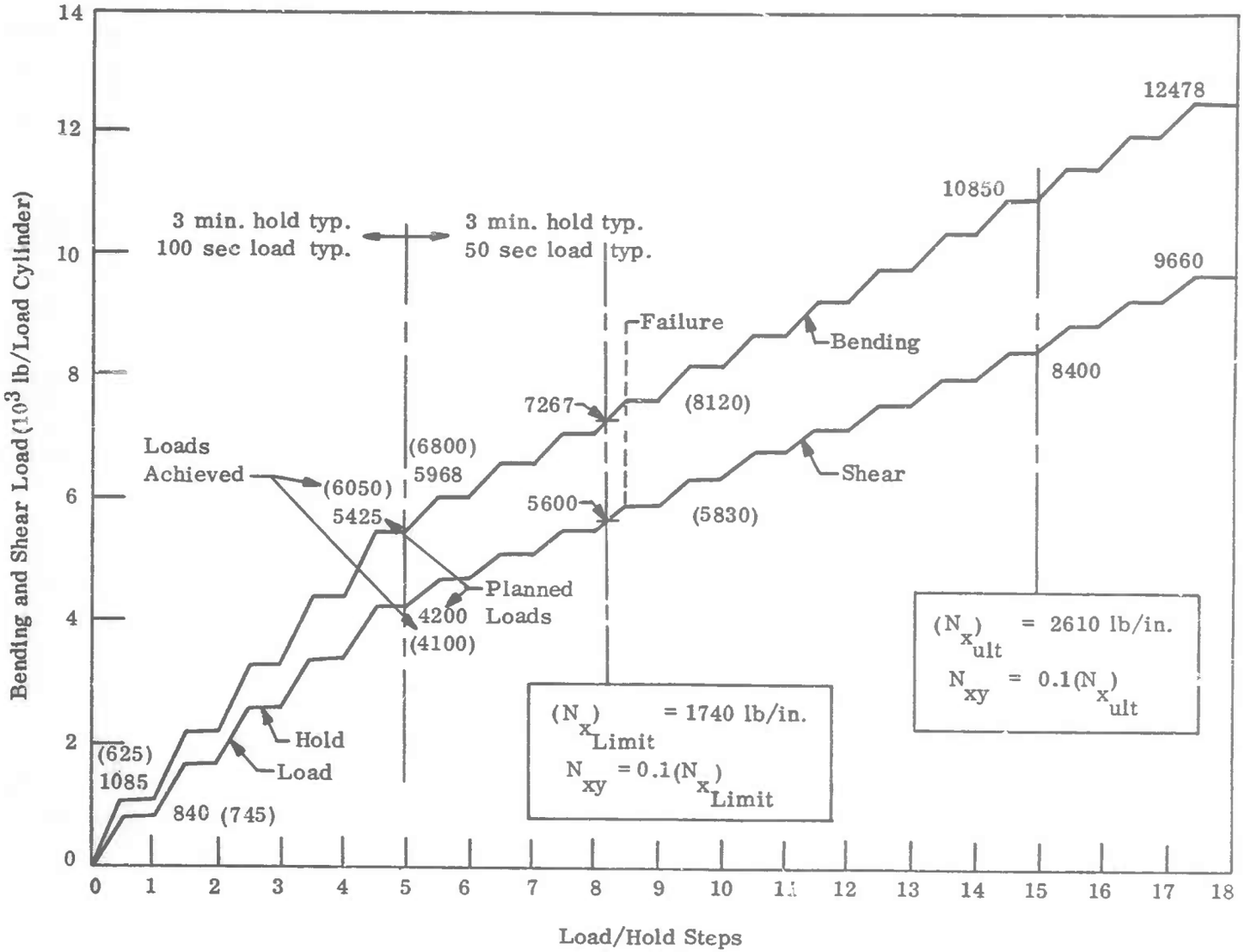

Figure 15. Destruct Test Load Profile

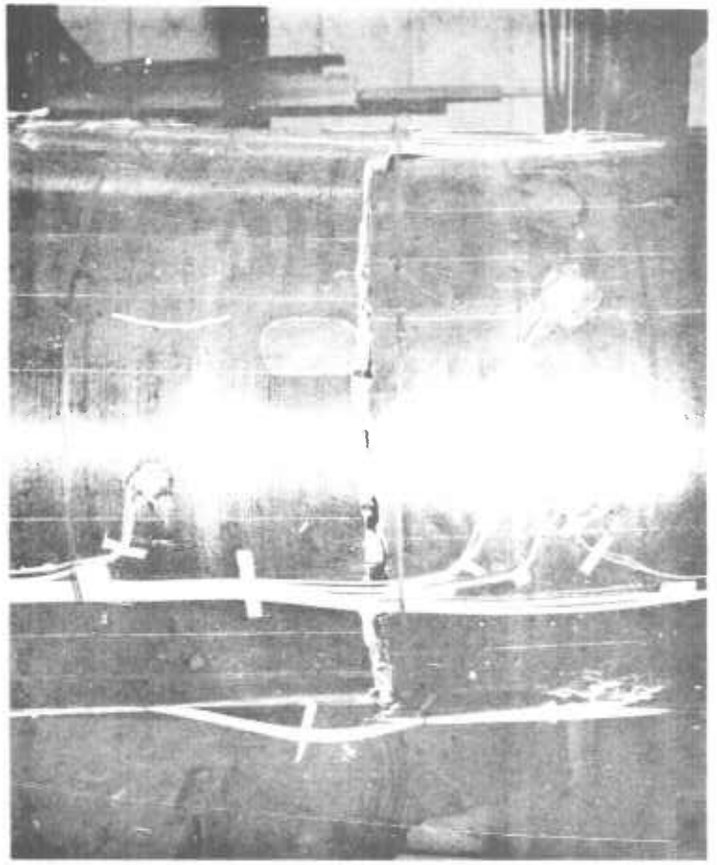

Figure 16(a). Left Side of Failed Component

P700065

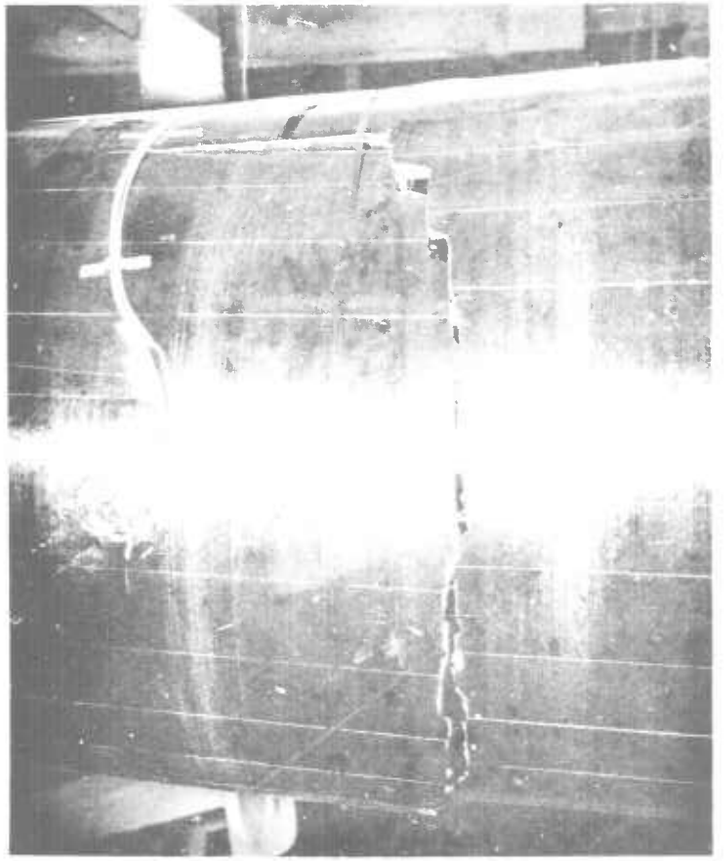

Figure 16(b). Right Side of Failed Component

P700066

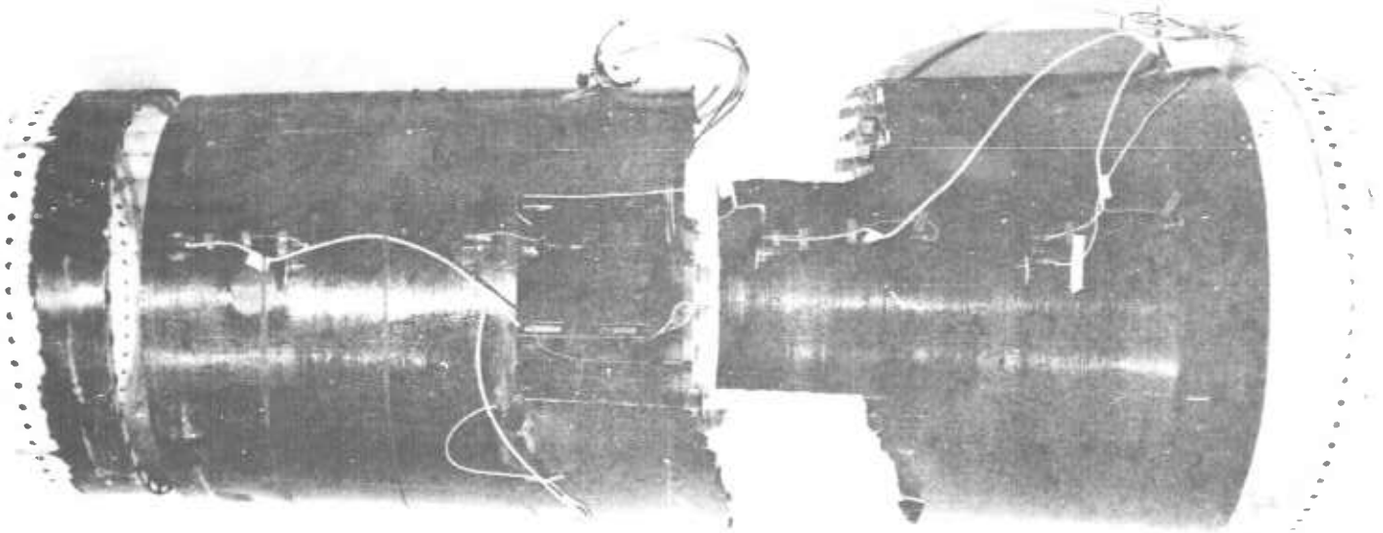

Figure 17. Top View of Failed Component (Shown After Cutting "Tongue" and Sawing Off End Buidlups)

P00069

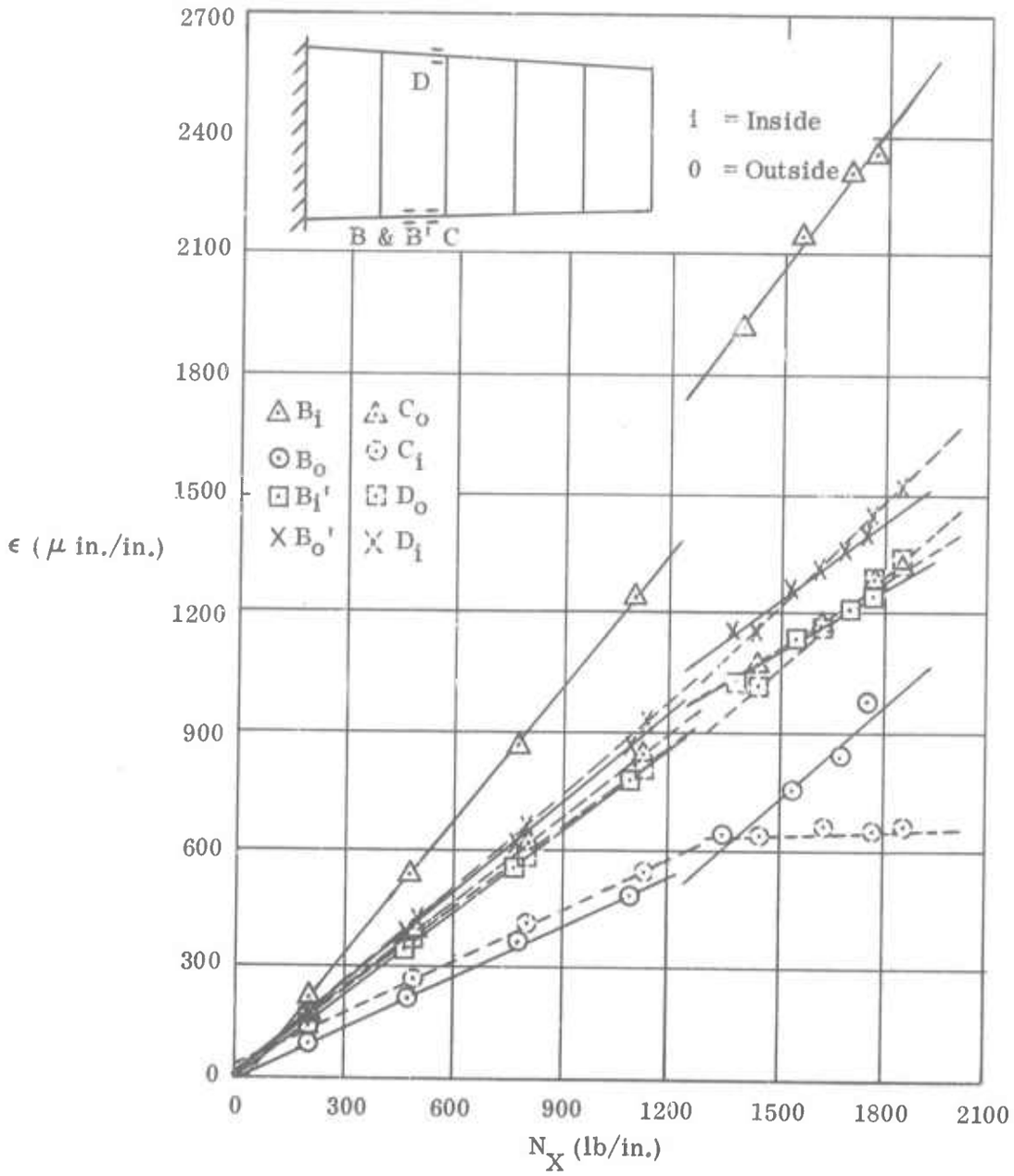

Figure 18. Strain-Load Curves from Destruct Test

Practically all gage outputs showed some evidence of a little jiggle at load Step 4 as shown in Figure 18; however, away from the localized bending region, the curves were all very nearly linear. Load deflection plots, as well, were all linear. Belief that failure first occurred locally was therefore given further support. The failure load occurred upon reaching load Step 9 at 1980 lb/in. The curves shown in Figure 18 are extended to that measured load level since timing did not permit strain recordings.

Maximum strains recorded at load Step 8 are shown in Figure 19. Since failure occurred immediately after reaching load level 9, strain gage readings were not obtained at that step. Maximum recorded strains were in tension, 2410μ in./in. on gage 66 and 2000 μ in./in. on gage 30. These strains occurred in the same area noted in the response tests where local skin bending occurred. Local skin bending was also observed in the added pair of back-to-back gages (81 and 82) 180 degrees away from gage pairs 29 and 30 and 66 and 67. Strains at the frame 2 station where failure occurred were lower than at the large mid-bay suggesting a possible crack propagation failure at this station caused by a local defect or further failure of stringer 1 if it had partially failed at steps 4 to 5. Plots of strain distribution through the depth of the shell verified that plane sections remained plane during loading and removed doubt that loads were not being properly diffused. A comparison of prerun and post-test strain readings indicated that no significant permanent creep occurred in the component during the destruct test. Calibration showed that most gages were still operational after the destruct test. Post-failure examination of the failed component revealed that the previous repairs of the fuselage component were highly successful. Fractographic examination of the failed structure was undertaken by Case-Western Reserve University (Section VI F).

Deflection data obtained at load Step 8 are shown in Figure 20. The solid curve represents data from dial gages positioned along the bottom of the component, and the dashed curve represents data from gages along the top. Relative deflections between top and bottom in the large end glass buildup area and within the first bay show that slight ovalling occurred. Figure 21 gives deflections as a function of axial loading. Dial gage numbers are listed to the right of the curves and correspond with locations given in Figure 14. Deflections are remarkably linear; however, gages 7, 25, 26, and 27 "tailed off" after reaching 1600 lb/in. loading whereas gages 15, 17, 18, 19 and 29 show a deflection slope increase after 1700 lb/in. loading.

TABLE SHOWING TYPICAL FRAME CONST

JOINT LOCATION FROM STIFFENER #1	MATERIAL	ANGLE	FRAME #1 ℄ DIA	FRAME #2 ℄ DIA	FRA ℄
J	BALSA	29°19'32"	23.500	22.500	21.
K	BALSA	11°36'46			
L	THORNEL	29°19'32"			
M	THORNEL	34°50'18"			
N	THORNEL	29°19'32"			
O	THORNEL	34°50'18"			

TABLE SHOWING FRAME DIA

FRAME NO.	℄ DIA OF FRAME	℄ DIA OF FRAME	
1	23.480	23.500	23
2	22.480	22.500	22
3	21.480	21.500	21.
4	20.480	20.500	20

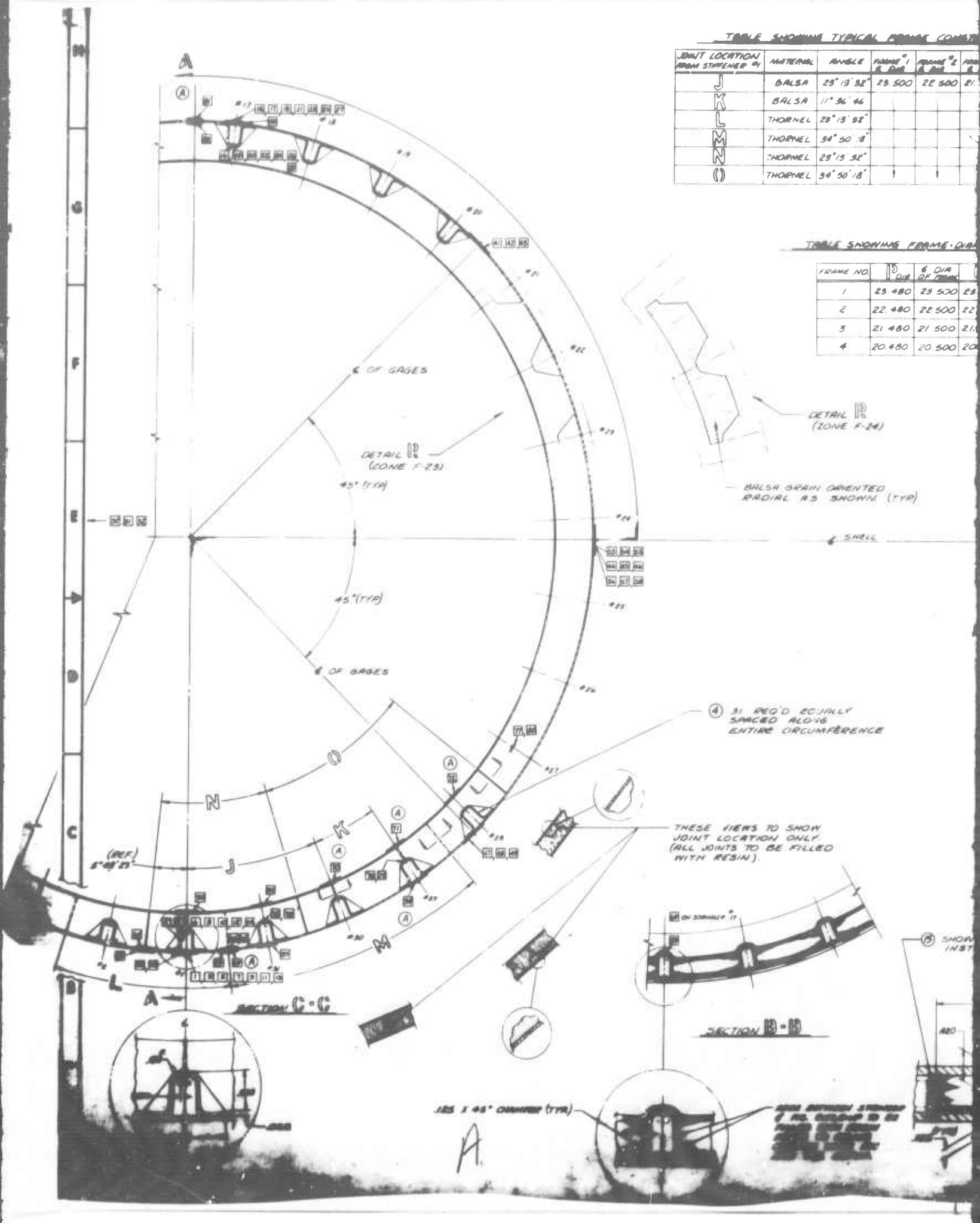

FRAME CONSTRUCTION

FRAME #1	FRAME #2	FRAME #3	FRAME #4	NO. REQ'D
23 500	22 500	21 500	20 500	15
				1
				14
				1
				14
				1

FRAME DIAMETERS

DIA	℄ DIA OF FRAME	OM
480	23 500	23 520
480	22 500	22 520
480	21 500	21 520
480	20 500	20 520

(TYP)

VIEW (SEE SHEET #2)

-1480

-1905

-850

-190

-1325

-1740

-1235

(ON STRINGER # 15)

0

-10

440

65

(ON STRINGER # 6)

655

890

1130

1265

2410

24.00 DIA (INSIDE SHELL)

23 500 DIA

270 (TYP)

160

1300

1230

2000

1490

1380

1110

735

950

FRAME ASSY. #1

30 (TYP)

6.00 (TYP)

SHOWING TYP. ROLL PIN INSTALLATION

2.00

.040

.420

(REF.) END ATTACHMENT FIXTURE NO. 1 (LARGE) DWG. E-6224-10000-2 SHEET 1 OF 2

B

20

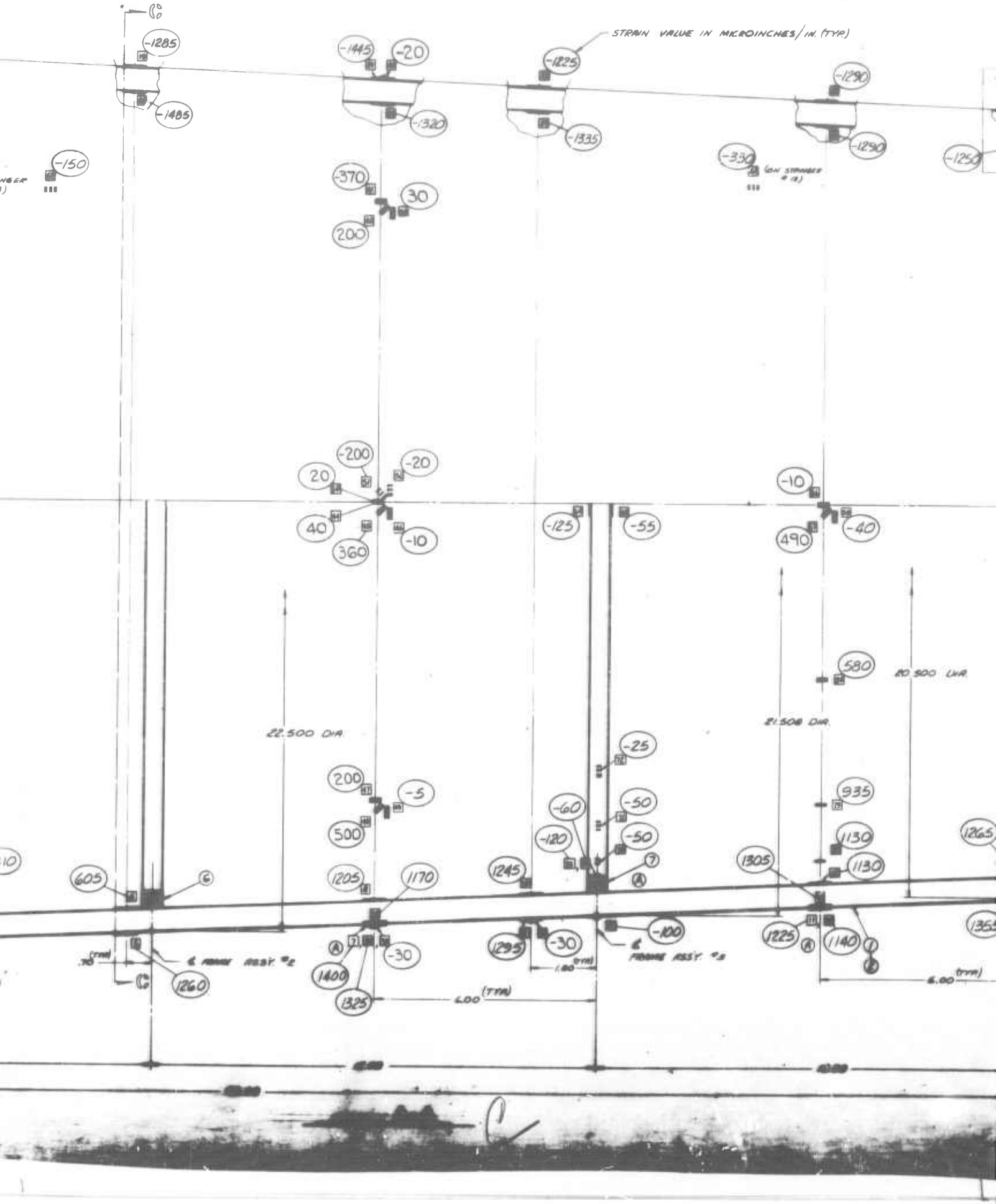
STRAIN VALUE IN MICROINCHES/IN. (TYP.)
-1285
-1485
-1445
-20
-1320
-1225
-1335
-1290
-1290
-330
(ON STRINGER # 13)
-1250
-150
-370
30
200
-200
20
-20
40
360
-10
-125
-55
-10
490
-40
580
RO 900 LNR
22.500 DIA
21.508 DIA
-25
200
-5
500
-60
-50
-120
-50
935
1130
1130
1265
605
1205
1170
1245
1305
1225
1140
1355
1295
-30
-100
1400
-30
1325
1260
6.00 (TYP)
6.00 (TYP)
6.00 (TYP)
6 PRIMARY ASSY. #2
6 PRIMARY ASSY. #3

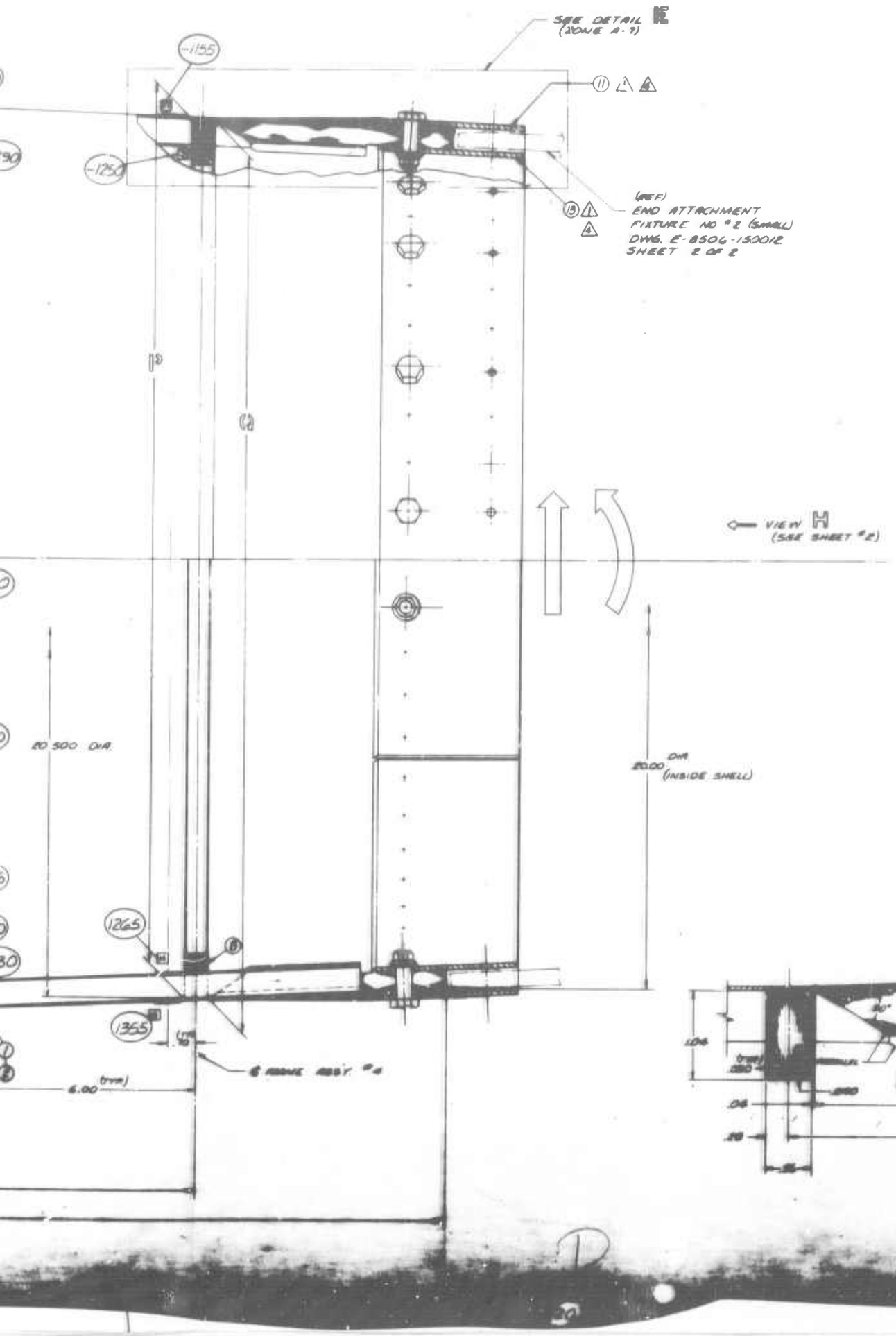

TABLE SHO
VARIOUS THO
FIBER ORIENT

ELEMENT	
SHELL	4
STRINGERS	4
FRAME (CAP)	4
FRAME (SIDE PANELS)	3

● 0° 15 ALONG
■ 0° 15 ALONG
CIRCUMFEREN

TABLE
INSTRUM
& AXIS O

	GAGES	
	SG "1 THRU SG "28	
(A)	SG "29-34, 66-69, 81 & 82	LO
(A)	SG "35 THRU SG "37	CI
(A)	SG "38 THRU SG "40	CI
(A)	SG "41 THRU SG "58	BI
(B)	SG "59 & SG "60	LO
(B)	SG "61 THRU SG "63	LO
(B)	SG "64, 65, 70, 71 & 72	CI
(B)	SG "75 THRU SG "80	LO

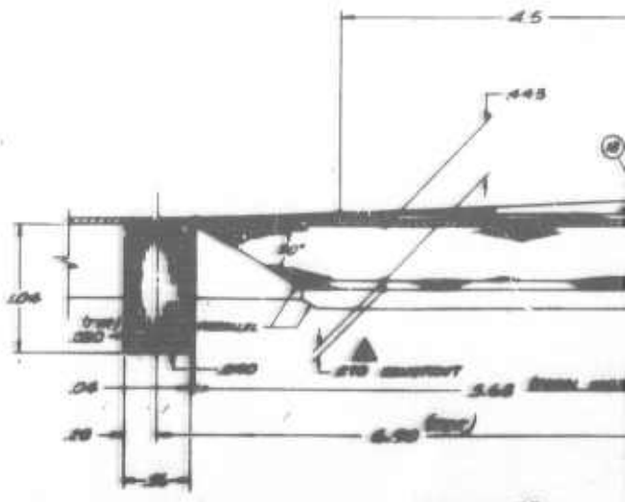

TABLE SHOWING
VARIOUS THORNEL 50
FIBER ORIENTATION

ELEMENT	NUMBER OF LAYERS	AVERAGE FIBER ORIENTATION	
SHELL	4	90°, +15°, -15°, 90°	●
STRINGERS	4	+10°, -10°, -10°, +10°	●
FRAME (CAP)	4	0°	■
FRAME (SIDE PANELS)	3	0°, +45°, -45°	■

● 0° IS ALONG SHELL ℄

■ 0° IS ALONG SHELL CIRCUMFERENTIAL DIRECTION

TABLE SHOWING
INSTRUMENTATION FUNCTION
& AXIS OF ORIENTATION

GAGES	ORIENTATION	GAGE FUNCTION
SG #1 THRU SG #28	LONGITUDINAL	STRINGER BENDING
SG #29-34, 66-69, 81 & 82	LONGITUDINAL	SKIN BUCKLING
SG #35 THRU SG #37	CIRCUMFERENTIAL	FRAME STRAINS
SG #38 THRU SG #40	CIRCUMFERENTIAL	SKIN STRAINS
SG #41 THRU SG #58	BIAXIAL PLUS SHEAR	SKIN STRAIN COMPONENTS
SG #59 & SG #60	LONGITUDINAL	FIBERGLASS LOAD TRANSFER
SG #61 THRU SG #63	LONGITUDINAL	STRINGER REPAIR EFFECTIVENESS
SG #64, 65, 70, 71 & 72	CIRCUMFERENTIAL	RING BENDING
SG #75 THRU SG #80	LONGITUDINAL	STRINGER STRAINS

⑤ DRAPE .010 FIBERGLASS BUILD-UP PLIES - ONE LAYER AT A TIME.

④ BOND ON ALUM. PLATES WITH EC 2216.

③ FAIR WITH ROOM TEMPERATURE CURING POTTING COMPOUND AFTER ASSEMBLY.

② CURE IN PLACE FOR 120 ± 5 MINUTES AT 245 ± 10°F AND 40 P.S.I.

① LIGHTLY SAND (400 GRIT) AND DEGREASE CARBON LAMINATE WITH MEK. AND CLEAN AND ACID ETCH ALUMINUM PLATES PER BPS FW 4852, REV D, METHOD II PRIOR TO BONDING TO FIBERGLASS BUILDUP.

NOTES:

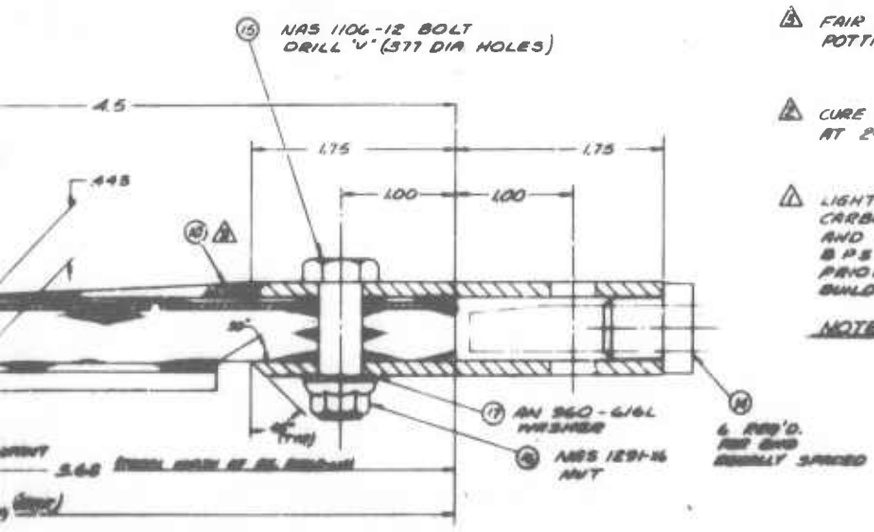

Figure 19. M
Te

	A	STRAIN [illegible] REV [illegible]	
	B	ADDED STRAIN GAGES [illegible] AS INDICATED STRAIN GAGES [illegible]	
	C	STRAIN GAGES 58 THRU 97 CORRECTED BY A FACTOR OF 2.0	

5 DRAPE .010 FIBERGLASS BUILD-UP PLIES - ONE LAYER AT A TIME.

4 BOND ON ALUM. PLATES WITH EC 2216.

3 FAIR WITH ROOM TEMPERATURE CURING POTTING COMPOUND AFTER ASSEMBLY.

2 CURE IN PLACE FOR 120 ± 5 MINUTES AT 245 ± 10°F AND 40 P.S.I.

1 LIGHTLY SAND (300 GRIT) AND DEGREASE CARBON LAMINATE WITH MEK. AND CLEAN AND ACID ETCH ALUMINUM PLATES PER BPS FW 4852, REV D, METHOD II PRIOR TO BONDING TO FIBERGLASS BUILDUP.

NOTES:

(M) 4 REQ'D. FWD AND ASSEMBLY SPACED

Figure 19. Maximum Strains from Destruct Test (Load Step 8)

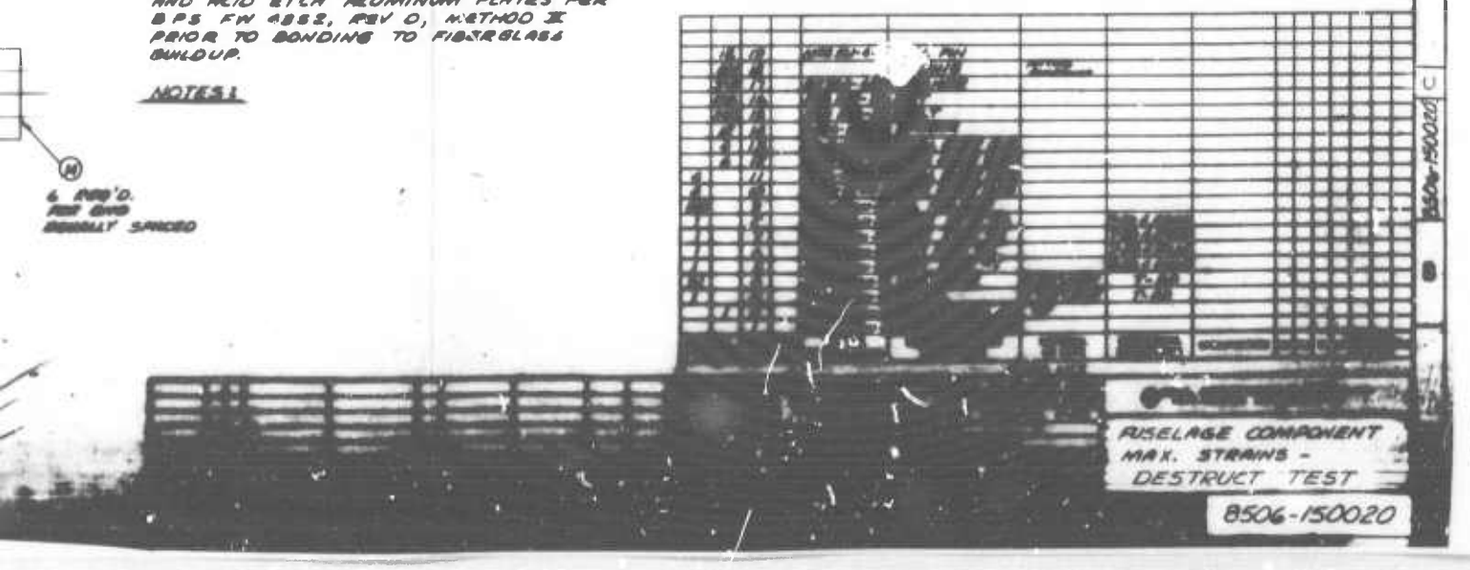

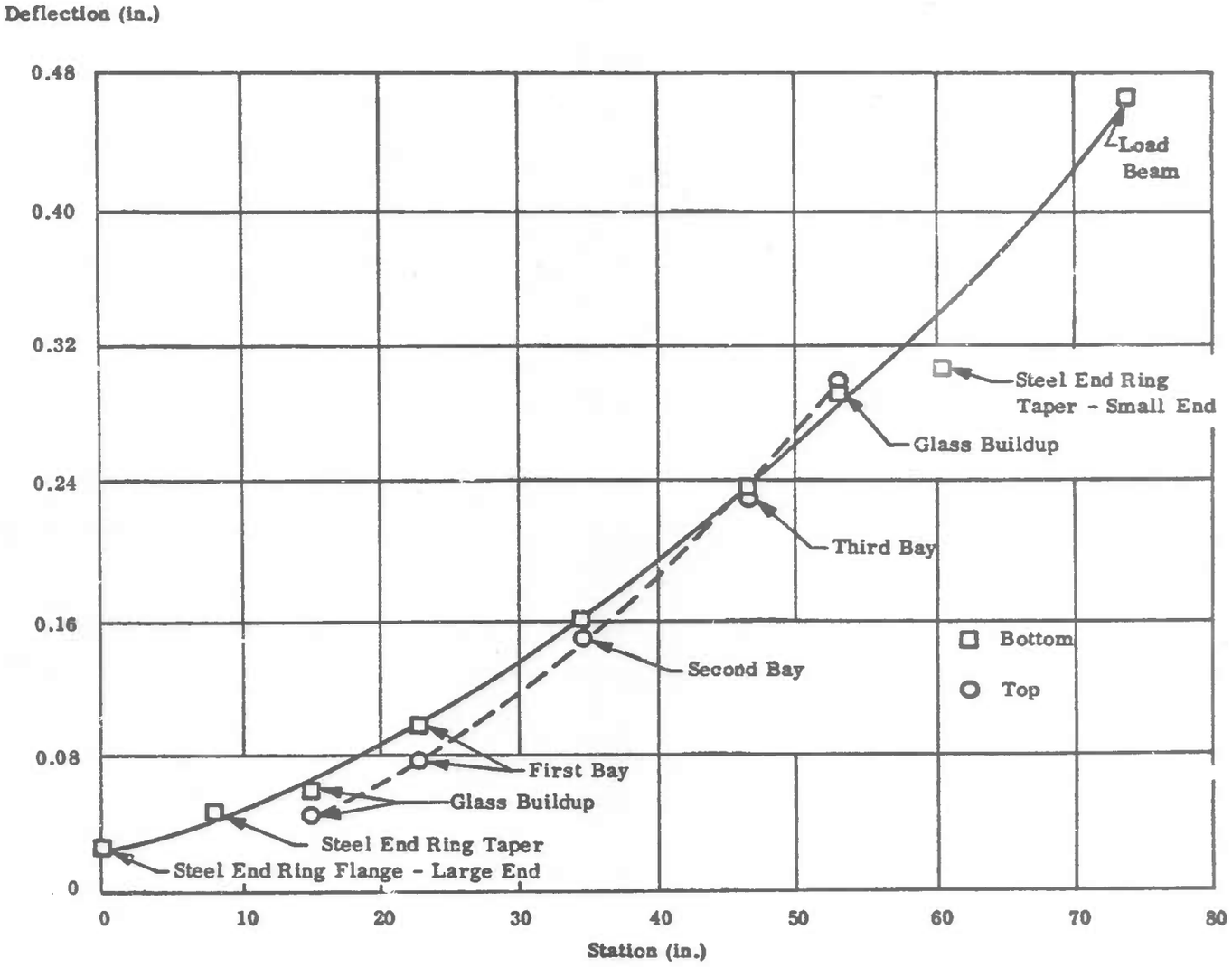

Figure 20. Destruct Test Deflections versus Axial Station

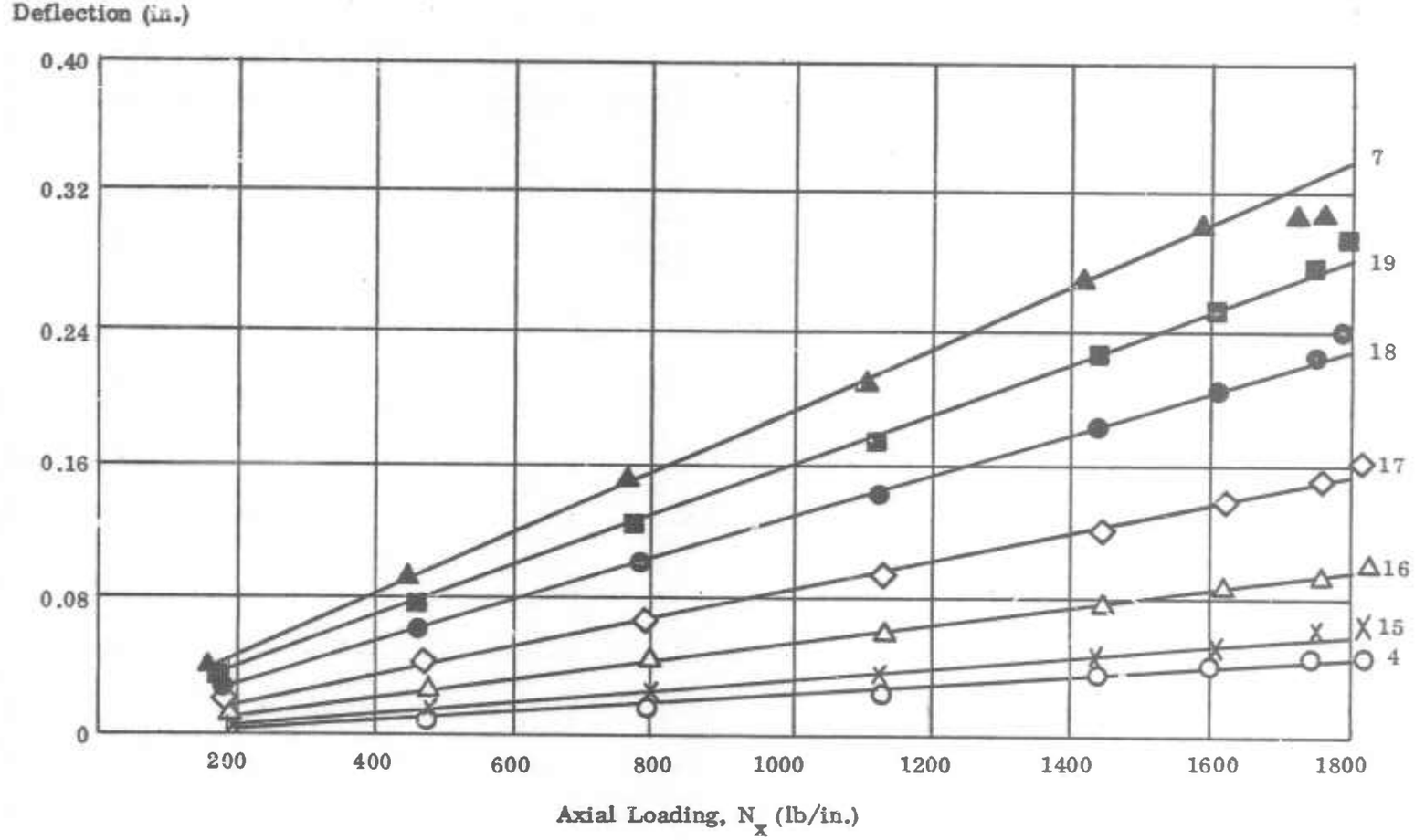

Figure 21(a). Deflections versus Load at Bottom of Structure from Destruct Test

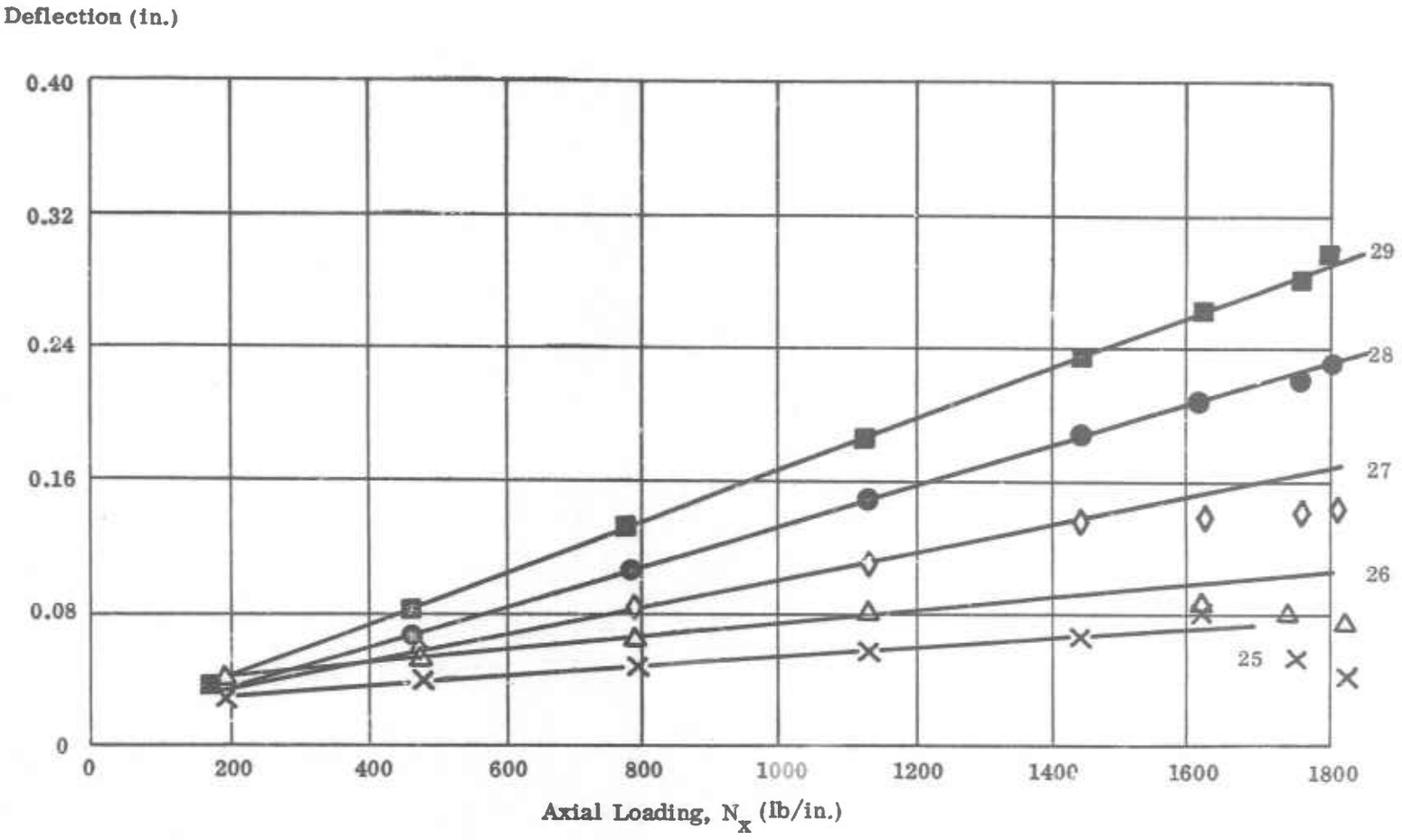

Figure 21(b). Deflections versus Load at Top of Structure from Destruct Test

SECTION IV

FUSELAGE COMPONENT STRESS ANALYSIS

This section describes accomplishments covering finalized material properties, updated discrete element analyses, and a brief discussion of other analytical methods employed to predict the fuselage component performances.

A. Final Material Properties

(D.P. Hanley and L.H. Kocher, Bell Aerospace)

Section III B of Reference 6 presented results of the shell stress analysis based on nominal (calculated or assumed) material properties for treated "Thornel" 50 graphite yarn; however, the loading conditions were those associated with a "Thornel" 40 component. During this period the shell structure was reanalyzed using more refined material properties (primarily measured ones) and the loading conditions for the "Thornel" 50 component based on end attachment specimen tests as given in Section IV B of Reference 6. Table IV of the present report summarizes the material properties used in the more recent shell stress analysis (these are labeled "as fabricated" properties), and Table V presents comparisons of predicted and measured properties to show the confidence level in the material properties used in the updated analysis.

Table IV gives the "design" and "as fabricated" properties for the skin and stringers of the fuselage component. The "design" values were those used originally. Fiber volume contents (V_F) and thicknesses (t) are shown along with elastic constants and strengths. Subscripts 1 and 2 in the elastic constants refer to axial and hoop directions; X,Y, and T indicate longitudinal, transverse, and shear strengths and T&C subscripts designate tension and compression. The design V_F and t values were derived from the combined results of preliminary design, analytical studies of structural elements, and from consideration of manufacturing processes.

Measured average values of skin and stringer thicknesses and stringer V_F's given in Table IV are seen to differ considerably from the design values. Both skin and stringers were thicker than desired, consequently their V_F's are lower than design. These differences were due to extrapolation of design data with "Thornel" 40 to the "thickness per ply - V_F" relationship for the smaller diameter "Thornel" 50 fiber and to the fabrication processes themselves. These data indicate that both the "as fabricated" stringer and skin strengths and moduli were about 25 to 30% less than the design goals.

The skin strengths given in Table IV are believed conservative by about 12-25% by virtue of the comparison given in

TABLE IV

MATERIAL PROPERTIES USED IN SHELL ANALYSIS

		Skin (90, ±15, 90°)		Stringer (±10, ±10°)	
		Design	As Fabricated	Design	As Fabricated
V_F	(%)	50	36	65	53
t	(in.)	0.047	0.0562 (1)	0.033	0.0375 (3)
E_1	(10^6 psi)	11.65	8.52	29.82	20.0
E_2		13.26	9.68	1.30	-
G		1.30	0.895	1.71	-
$\nu 12$		0.083	0.088	0.929	-
$\nu 21$		0.094	0.100	0.040	-
X_T	(ksi)	30.3	21.9 (2)	61.7	45.0 (4)
X_C		34.6	22.5	55.0	50.0
Y_T		32.5	23.6	-	-
Y_C		36.8	23.8	-	-
T		11.0	7.35	-	-

(1) Measured average thickness; estimated V_F.

(2) Calculated properties based on predicted unidirectional properties w/V_F = 36% (E_1 = 18.4, E_2 = 0.977, G = 0.351, ν_{12} = 0.321, ν_{21} = 0.017) and estimated strengths (X_T = X_C = 45, Y_T = 2.5, Y_C = 28.0, T = 6.0); X_T and X_C conservatively proportioned from 70 ksi estimated at V_F = 57%.

(3) Measured average in top quadrant critical stringers.

(4) Stringer compression strength is measured average in top quadrant critical stringers (see Table XIV of Reference 6); stringer tensile strength estimate is based on flat laminate properties (see Table XI of Reference 6).

TABLE V

TREATED "THORNEL" 50 PROPERTY COMPARISONS (1)

		Predicted	Measured(2)
Unidirectional Laminate (V_F =57%)			
	E_1	= 28.7	25.5
	E_2	= 1 00	0.94
	G_{12}	= 0.489	-
	ν_{12}	= 0.298	0.34
	ν_{21}	= 0.010	0.011

		Pred.(3)	Meas.(4)	Pred.(5)	Meas.	
Skin Laminate (V_F =48%)						
	E_1	=11.1	9.8	X_T =28.1	32	(4)
	E_2	=12.7	11.3	X_C =30.0	30	(4)
	G_{12}	= 1.14	-	Y_T =30.7	41	(4)
	ν_{12}	= 0.081	0.081	Y_C =30.8	40	(4)
	ν_{21}	= 0.092	0.084	T = 9.43	10.7	(6)

		Pred.	Meas.(7)	Pred.	Meas.(7)
Stringer Laminate (V_F =61%)					
	E_1	=27.8	24.0	X_T =71.0	65
	E_2	= 1.01	0.95	X_C =56.2	70
	G_{12}	= 1.38	-	Y_T = 2.58	-
	ν_{12}	= 1.08	1.03	Y_C =21.7	24
	ν_{21}	= 0.039	-	T =11.6	-

(1) Elastic moduli (10^6 psi); Ultimate strength (ksi).
(2) Table IX (6).
(3) Based on predicted unidirectional elastic properties.
(4) Table X (6).
(5) Based on predicted unidirectional elastic properties and estimated unidirectional strength properties.
(6) Table LX, (3), $(N_{xy})_{ult}$ = 416 lb/in., t_{skin} = 0.038.
(7) Table XI (6).

Table V for the skin strengths at different V_F's. Similar comparisons have been made for the stringer properties and are given in Table V. Therein, an unconservative tensile strength prediction is seen in comparison with the test results. The overall properties of the component were expected to be within 10-15% of actual properties. Strength estimates were conservative; skin stiffness predictions, however, were expected to be slightly greater than actual due to the differences illustrated in the unidirectional properties as shown in Table V. Sections VI C and D present measured properties obtained after the component test and gives comparisons with the predicted values.

B. Component Stress Analysis
(D.L. Turner and S. Jordan, Bell Aerospace)

Preliminary analysis of the fuselage structure utilized nominal shell geometry, computed material properties, and arbitrary but representative load conditions (Section III B of Reference 6). Further analyses have been conducted by using better defined material properties and thicknesses as given in the previous report section along with better defined loading conditions for the test program. The structural idealization is the same as that described in Section III B of Reference 6. Four loading conditions were analyzed in the "Nominal Analysis"(6) and five loads were considered in the "Current Analysis" as summarized in Figure 22.

Margins of Safety were computed for the shell elements of the structure based on the "Hill-Laminate" criteria referred to in Reference 6. The following discussion summarizes the gross behavior of the structure for the loading conditions given in Figure 22.

1. Load Condition 1 - Bending and Shear

Figure 23 presents a contour plot on the developed shell of the computed skin margins of safety. Similar contour plots from the earlier (nominal) analysis for Load Condition 1 (shear only) and Load Condition 2 (moment only) were given in Figures 5 and 9 of Reference 6. L.C. 1* is seen to represent primarily bending. However, comparison with previous results (Reference 6, Figures 5 and 9), shows that the influence of shear is significant. The influence of bending due to shear in L.C. 1 is sufficient to reverse the contour pattern generated by bending stresses in the top and bottom regions of the structure. In the case of Figure 9, (6), the taper in the structure caused

*Loading condition is abbreviated hereafter L.C.

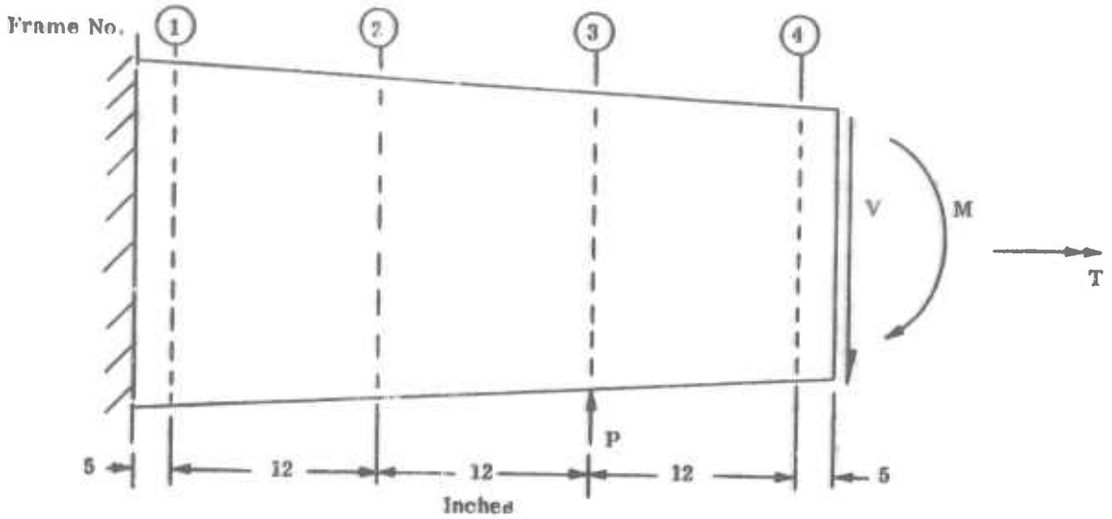

Load Cond	M (in. lb)	V (lb)	T (in. lb)	P (lb)
	Nominal Analysis			
1		7,350		
2	576,000			
3			114,600	
4				80
	Test Analysis (Current)*			
1	308,000	2,080		
2			42,600	
3	135,000		28,200	
4				80
5	631,000	13,400		

*Loads Correspond to Table XXXVIII (6)

Figure 22. Summary of Load Conditions - Nominal and Current Analyses

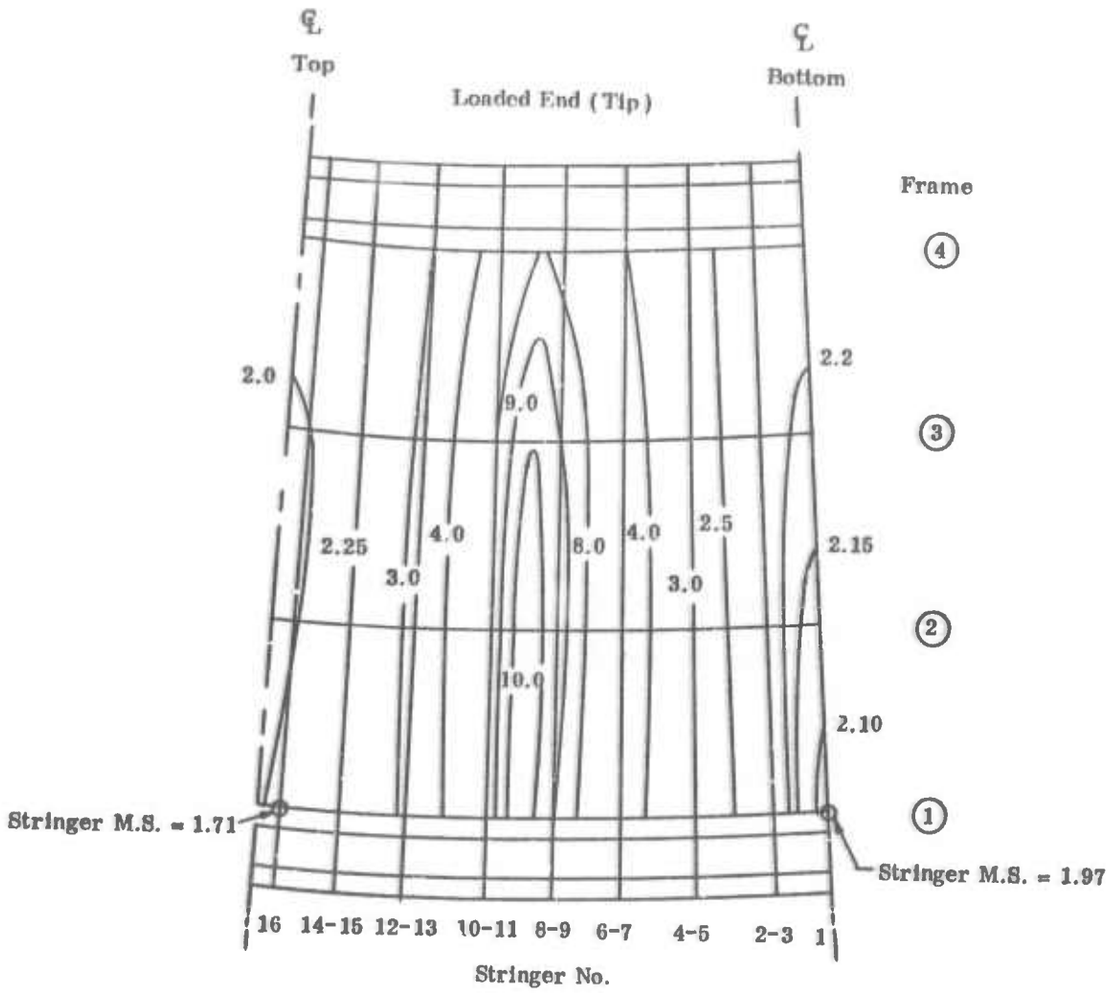

Figure 23. Margin of Safety Distribution (Developed Shell) Load Condition 1 - Moment and Shear

margins to increase from tip to root whereas in the present case (Figure 23) the additional bending moment generated by the shear load is sufficient to nearly offset the effect of taper and shift the minimum (bending) margins of safety (top and bottom) to the root.

Comparison of Figure 23 with Figure 5 of Reference 6 also verifies that tension and compression allowables are more nearly equal in the current analysis (Table IV) than in the earlier analysis (Table II of Reference 6), i.e., the minimum margins in the upper and lower surfaces are much closer than was the case in the nominal analysis.

In looking at the side panel elements of Figure 23, which are governed by shear stresses, comparison of the current case with L.C. 1 of the earlier analysis (Figure 5 of Reference 6) is of value. Here the influence of the shear load appears in the half-loop between stringers 8-9 and 10-11 of Figure 23 (as opposed to the virtual absence of such loops in the bending only case of Figure 5 in Reference 6). Direction of the loops is, however, reversed due to effects of the applied bending moment. It is also noted that distortion of the loops as shown in Figure 9 of Reference 6, caused by the relatively large difference between tension and compression allowables, is greatly reduced in the present case. Despite the apparently large changes in the M.S.* pattern in the region governed by shear stresses, it is noted that the minimum M.S., though large in this case, still occurs at the loaded end (tip).

Minimum margins of safety based on axial load have been determined for the stringers under tension and compression. These appear on Figure 23. The stringer M.S.'s are less than those for the skin and the critical stringer is in tension (M.S. = 1.71).

Figure 24 shows the vertical displacement of the structure for L.C.'s 1 and 3. Comparison of Figure 24 (a) with Figures 8 and 11 of Reference 6, (corresponding displacements for shear only and moment only, respectively, from the nominal analysis) shows the expected combined effects of shear and bending loads.

2. Load Condition 2 - Torsion

L.C. 2 reiterates the situation established for L.C. 3 of the nominal analysis where the loading condition was identical though of different magnitude. Once again the M.S. contours show curves parallel to the ring frames with values ranging from 7.25 at Frame 1 to 5.3 at Frame 4. Figure 25 (a) shows the tangential displacement of the shell for this load condition.

*M.S. : abbreviation for margin of safety.

(a) Load Condition 1 (Moment and Shear)

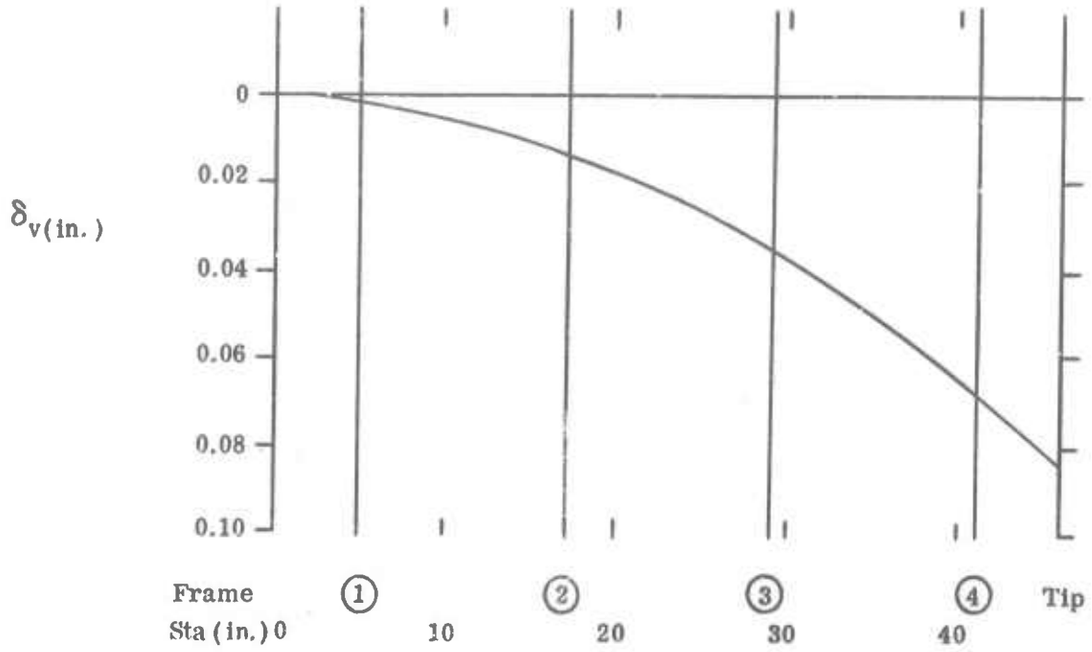

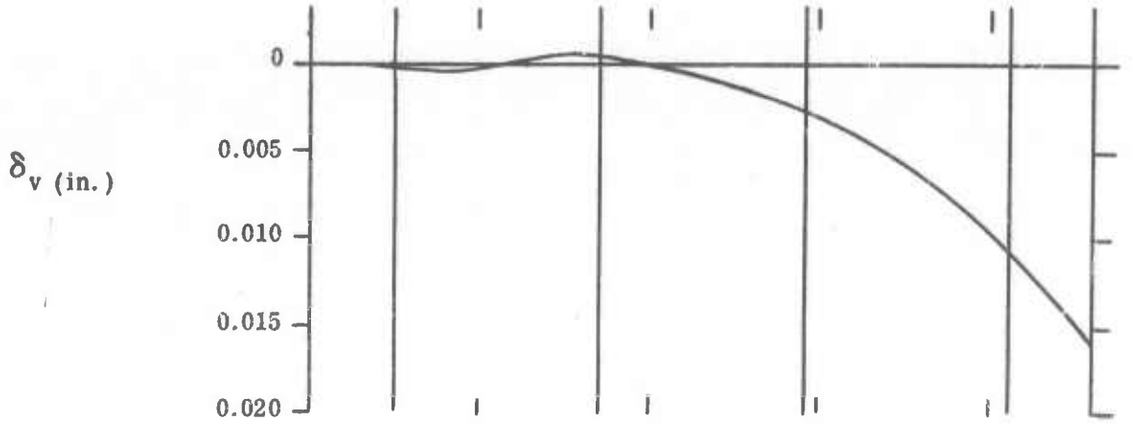

(b) Load Condition 3 (Moment and Torsion)

Figure 24. Vertical Displacements of Fuselage Shell - Loading Conditions 1 and 3

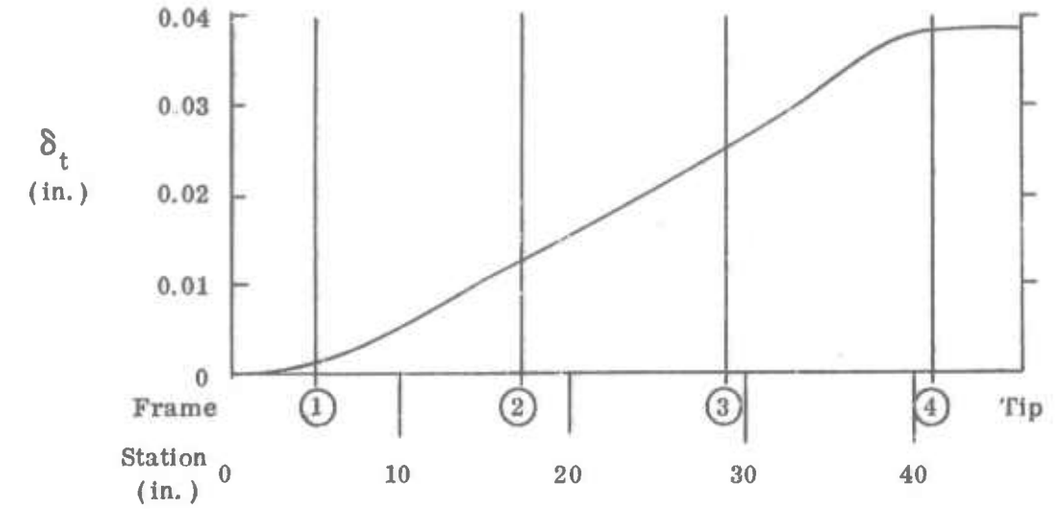

(a) Tangential Displacement of Stringer 1 (Bottom) for Load Condition 2 (Torsion)

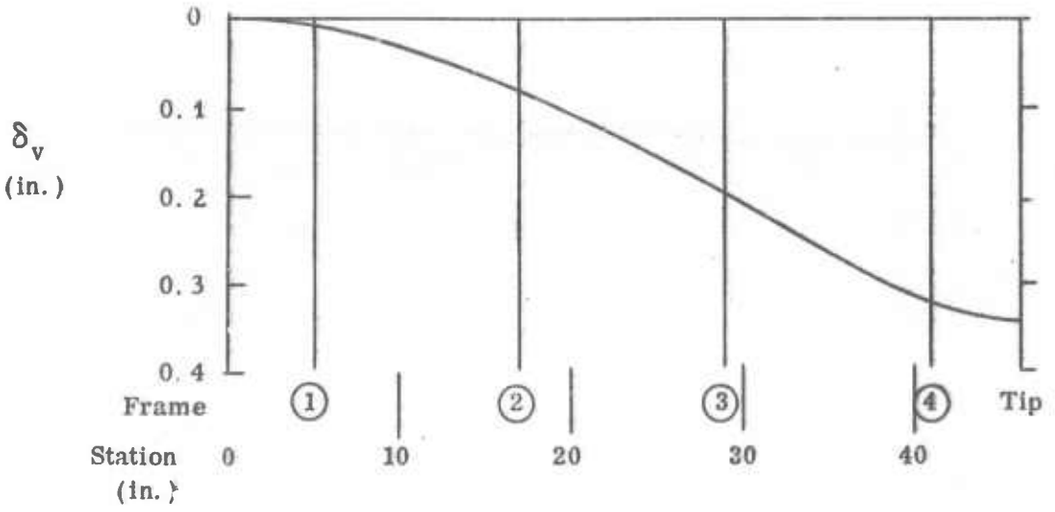

(b) Radial Displacement of Stringer 1 (Bottom) for Load Condition 5 (Moment and Shear - Ult.)

Figure 25. Displacements of Fuselage Shell - Loading Conditions 2 and 5

3. Load Condition 3 - Bending and Torsion

Figure 26 presents a contour plot of predicted safety margins for the skin panels indicating the gross shell structure behavior. Here again, as in L.C. 1, the M.S.'s in the upper and lower surfaces are nearly equal at a given station, reflecting the almost equal tension and compression allowables. As expected, the M.S. contours appearing in Figure 26 are essentially the same as those generated for L.C. 2 (bending only) of the nominal analysis (See Figure 9 of Reference 6) because the effect of torsion should not change the pattern. In contrast to L.C. 1 where the stringer M.S.'s were less than those for the shell skin, the situation is reversed in Figure 26 where the minimum M.S.'s (3.5 in the top and bottom of the shell) in the skin are less than those in the critical stringers.

Figure 24 (b) shows the vertical displacement of the structure. Similarity with L.C. 2 (bending) of the nominal analysis is apparent (See Figure 11 of Reference 6).

Figure 27 (a) shows the variation of axial stress across the shell at each of the four frames. As for all shear and/or bending loading cases, a linear (simple beam) distribution applies. The effect of taper results in greater upper and lower surface stresses at the tip than at the root. Figure 27 (b) shows the distribution of shear stress around the shell at each of the four frames. Comparison of these results with those from the nominal analysis under a bending load only shows that the effect of moment plus torsion simply offsets the shear curves from the origin by an amount equal to the shear flow due to torsion, the latter being constant at any section. Figure 28 shows a computer plot of the displaced structure under the L.C. 3 loading system.

4. Load Condition 4 - Concentrated Load

L.C. 4 is the same as that in the nominal analysis. The shell skin properties are, however, different in the two analyses as previously described. Figure 29 shows frame radial displacements under this loading and gives the maximum frame displacement. The maximum displacement at Frame 3 is approximately 11% greater than in the nominal analysis because of the reduced material properties.

Figure 30 shows a plot of shell margins of safety for L.C. 4. The margins of safety are large; however, the contours are presented to illustrate the expected pattern. Figure 31 shows a computer plot of the displaced shape of the structure with a large scale-up factor.

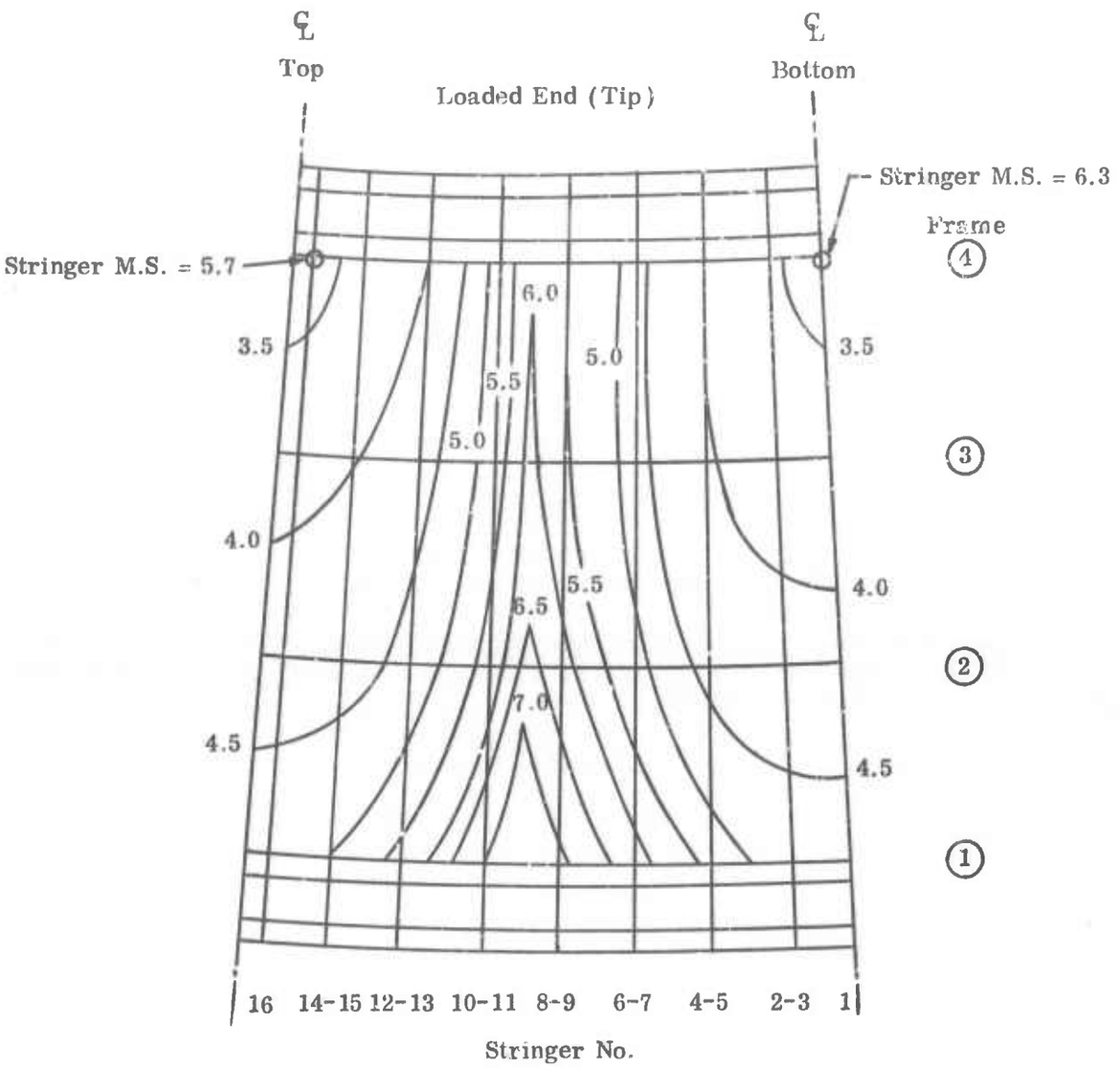

Figure 26. Margin of Safety Distribution (Developed Shell)
Load Condition 3 - Moment and Torque

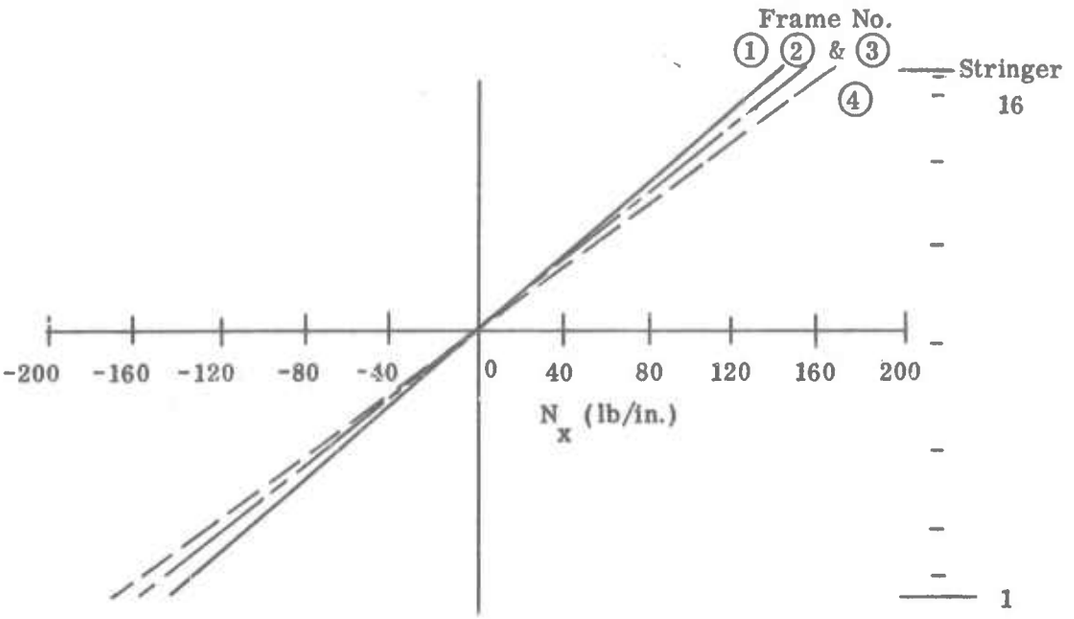

(a) Axial Stress Distribution

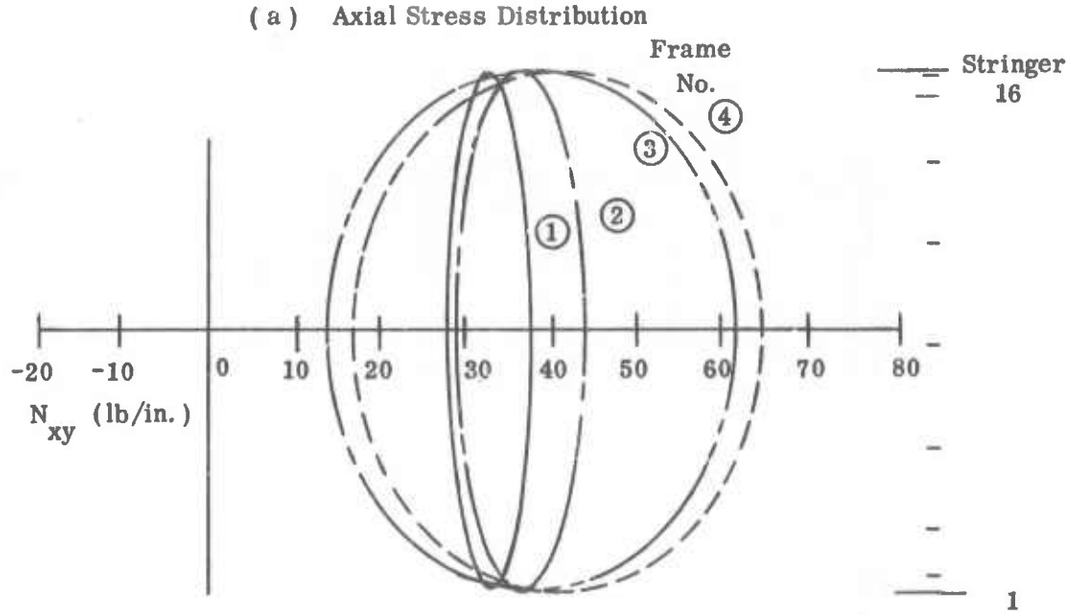

(b) Shear Stress Distribution

Figure 27. Stress Distribution at Ring Frames of Fuselage Shell - Load Condition 3 (Moment and Torsion)

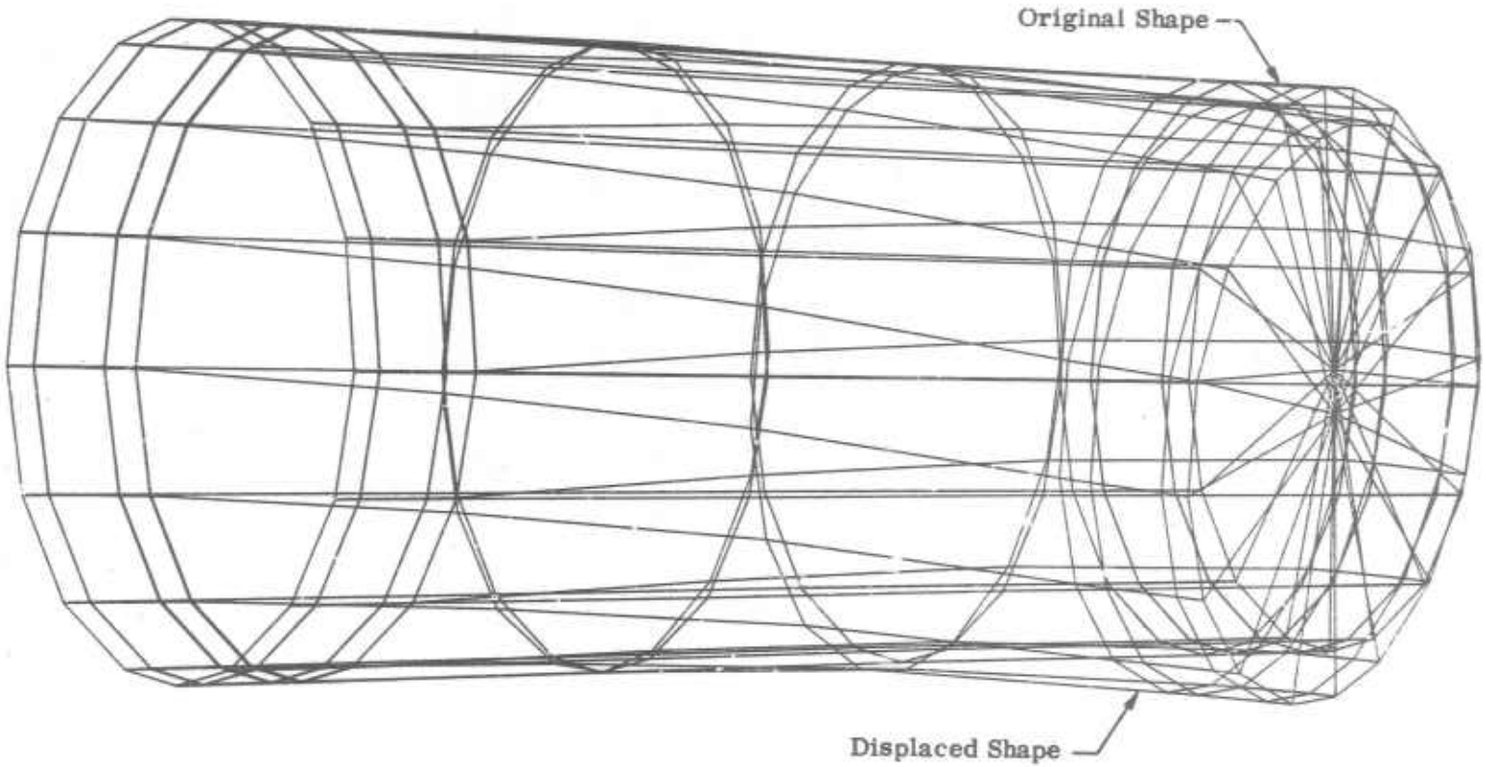

Figure 28. Computer Drawn Displacement Plot for Load Condition 3

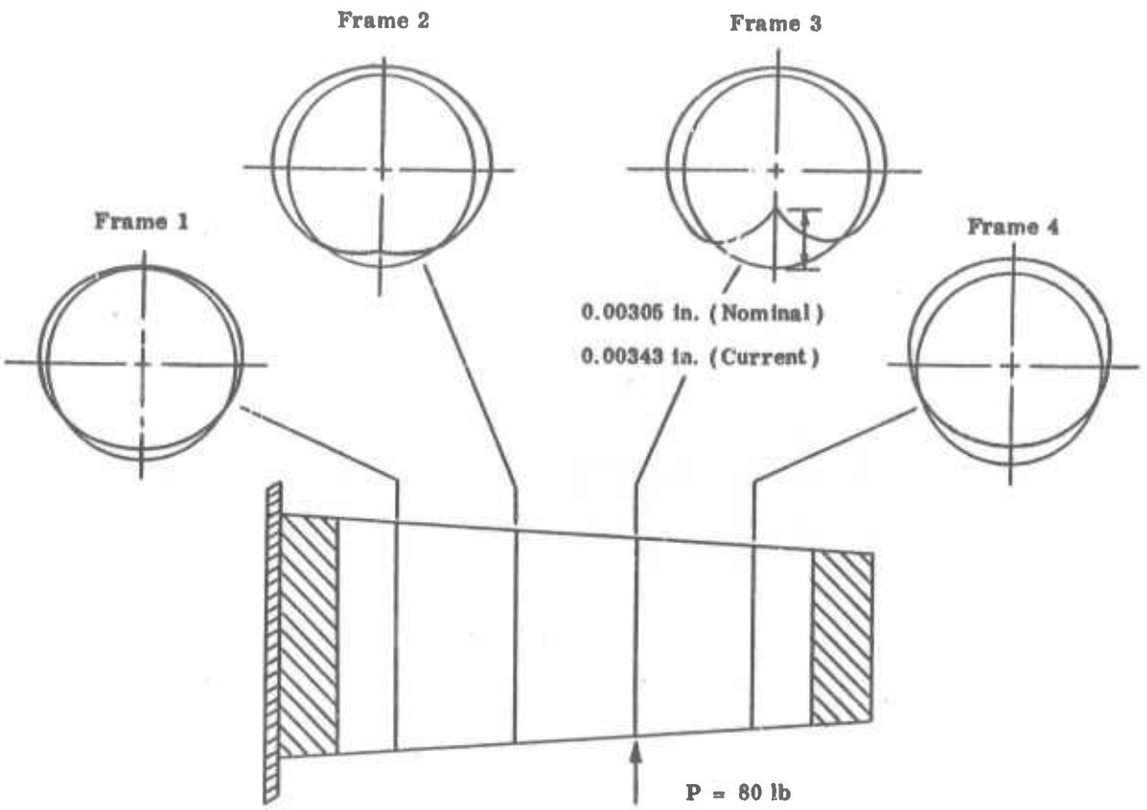

Figure 29. Frame Deflections with Local Applied Load

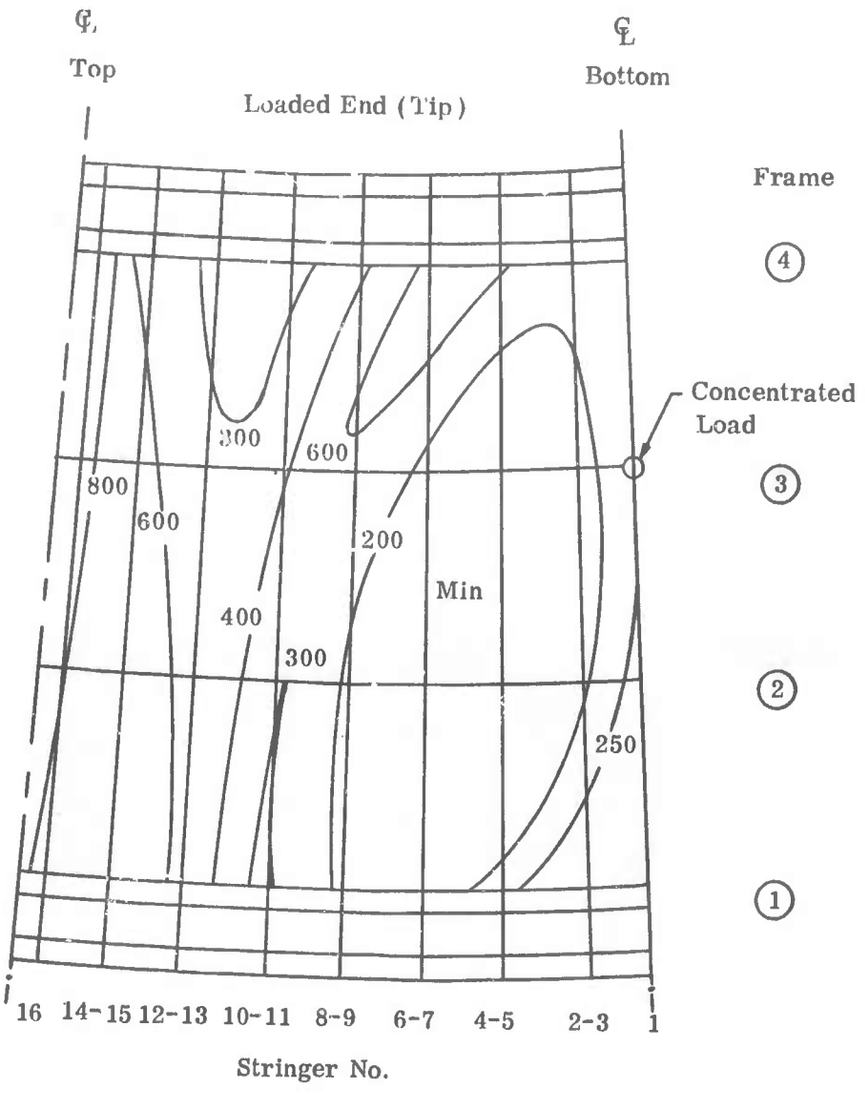

Figure 30. Margin of Safety Distribution (Developed Shell)
Load Condition 4 - Concentrated Load

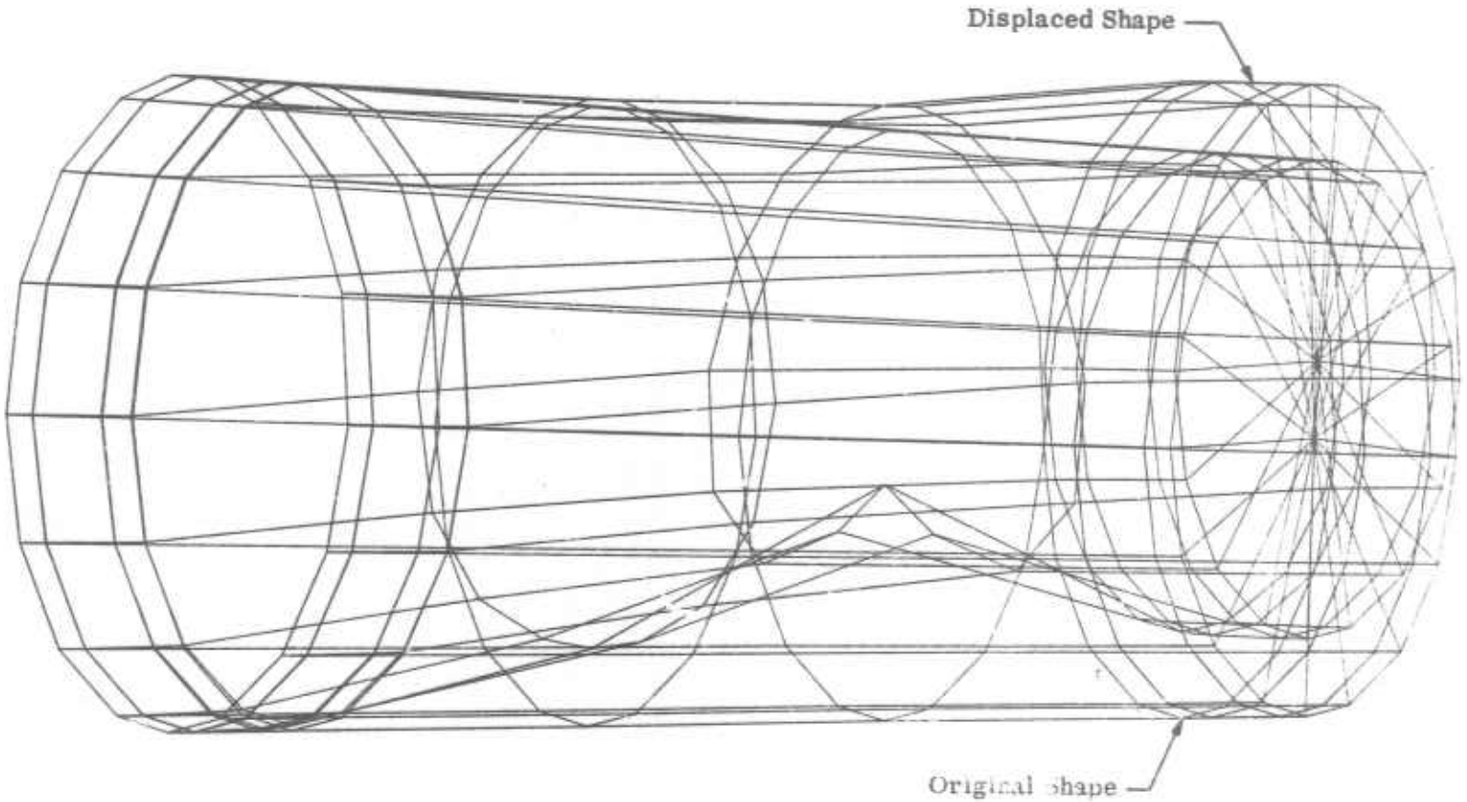

Figure 31. Computer Drawn Displacement Plot for Load Condition 4

5. Load Condition 5 - Bending and Shear (Ultimate)

L.C. 5 was the ultimate load condition tentatively established for the destruct test of the fuselage component. This load condition was subsequently changed as discussed in Section III D. A contour plot of the computed shell margins of safety for the original load condition is given in Figure 32. Comparison with Figure 23 for L.C. 1 shows significant differences. These differences reflect the fact that in L.C. 5 the shear load relative to the bending moment is considerably larger. Thus, in many respects, the M.S. contour plot bears a greater similarity to that for shear loading only as established in the nominal analysis (See Figure 5 of Reference 6) than to Figure 23. As for L.C. 1, the minimum L.C. 5 margins of safety for the upper and lower surfaces occur at the root, the absolute minimum occurring, as expected, on the tension (top) surface due to the slightly lower tension allowable. These margins are negative and are indicated by the hatched regions of Figure 32. However, it should be noted that the lowest margins do not appear at the extreme top and bottom of the structure, but several stringers away from the top and bottom positions. The negative zones are seen also to move further away from the extreme top and bottom, going from the root toward the tip. This action is accounted for by the interaction of shear and bending stresses due to the shell taper and end conditions. Since shear stress is essentially zero at the extreme top and bottom of the structure, the M.S. values there are essentially tension or compression values. However, moving away from the extremities, the shear stress increases, and since the shear allowable is quite low, the combined stress M.S. drops off. In addition, moving from the root to the tip, the bending stresses drop off (See Figure 33 (a)) but, initially, the shear stresses increase (See Figure 33 (b)). Hence the negative margins persist, but tend to shift towards the midpanels where shear stress governs.

Minimum M.S.'s were computed for several of the critical stringers and are given in Figure 32. Figure 25 (b) shows the vertical displacement of the structure for L.C. 5. Here the influence of both shear and bending loads is apparent, the influence of shear being, as expected, much more pronounced than was the case for L.C. 1.

Based on the shell stress analyses, the following conclusions were drawn:

(1) Predicted results for simple distributed load conditions (torsion, shear, bending) validate use of simple beam theory.

(2) Composite shell response for non-distributed loads (e.g., a local concentrated load) requires more sophisticated analysis.

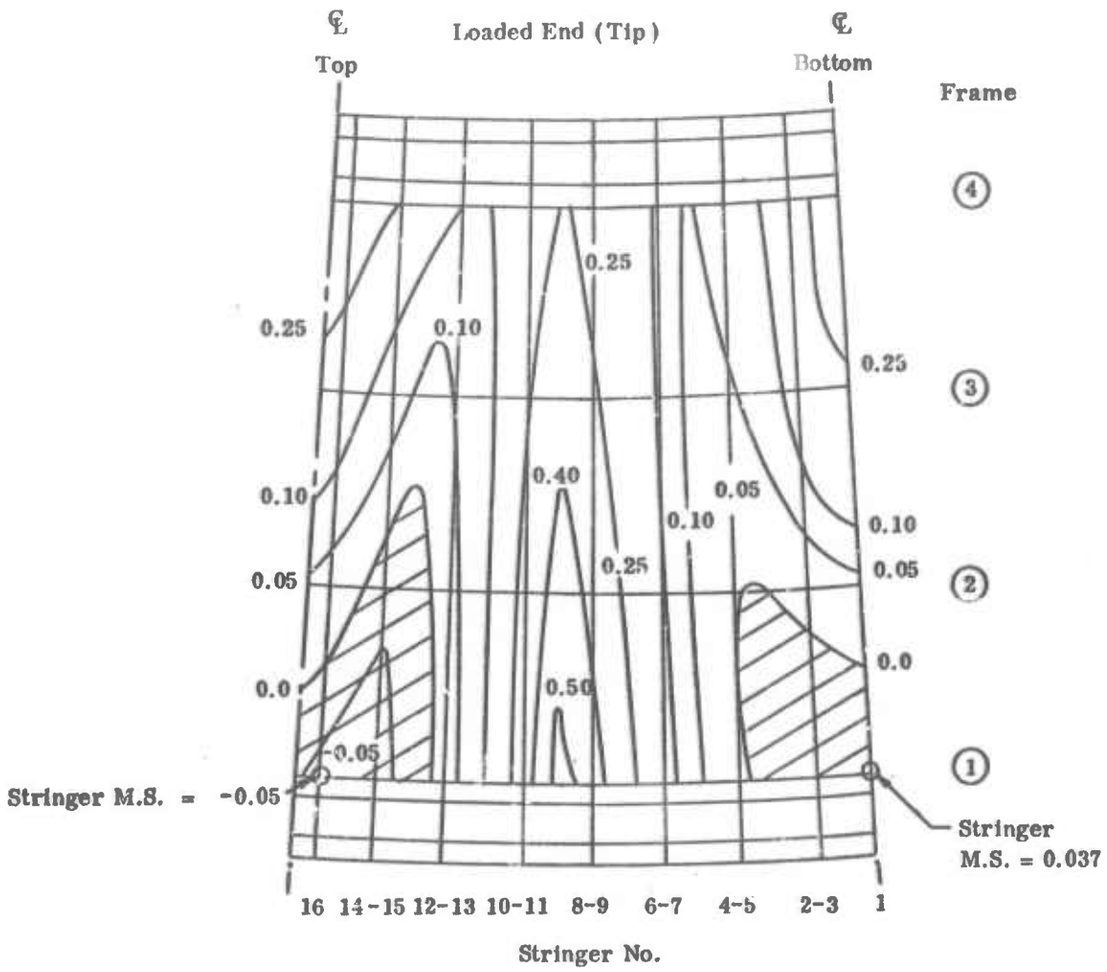

Figure 32. Margin of Safety Distribution (Developed Shell)
Load Condition 5 - Moment and Shear (Ult.)

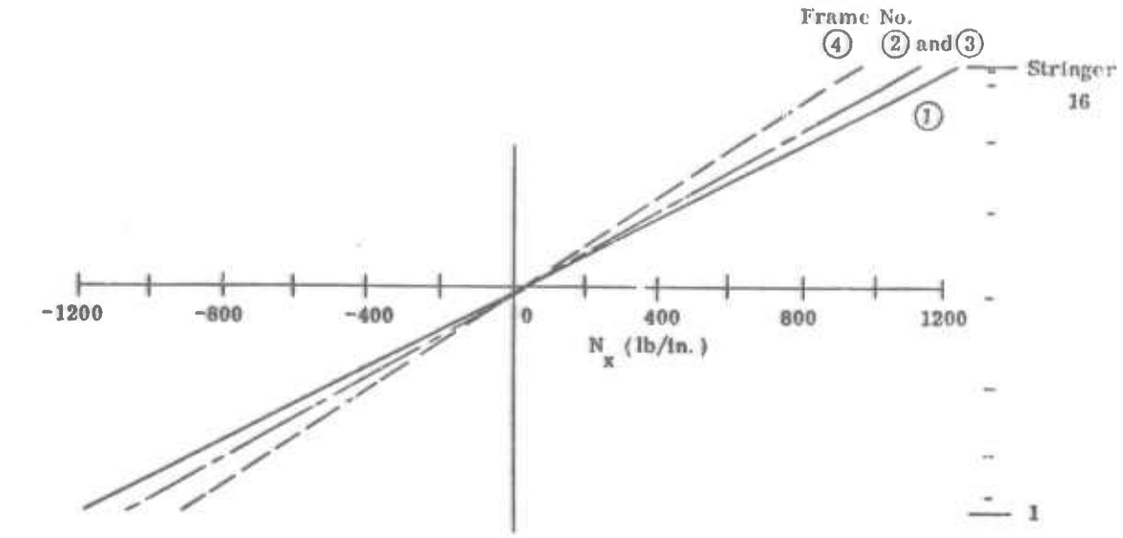

(a) Axial Stress Distribution

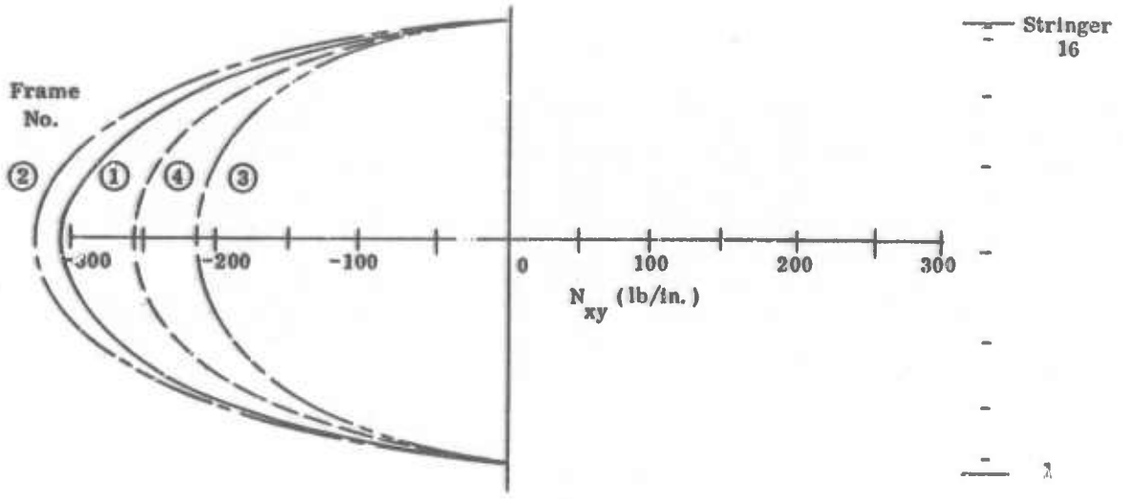

(b) Shear Stress Distribution

Figure 33. Stress Distribution at Ring Frames-Load Condition 5 Moment and Shear (Ult.)

(3) Influences of material changes, shell taper and combinations of loads have been qualitatively defined.

(4) Margins of safety for the fuselage structure destruct test indicate probable zones of failure as follows:

a. Shell skin tension side at root.

b. Extreme stringer on tension side at root.

c. Shell skin on compression side at root.

d. Extreme stringer on compression side at root.

For the actual destruct test, the shear loading was reduced based on the discrete element analysis results to favor the shell failure mode in bending since the shear allowables were less firmly established than the tension and compression values.

C. Other Analytical Methods
(W.N. Meholick and D.P. Hanley, Bell Aerospace)

Composite stiffness predictions were based on Bell's computer program for laminate property determination. Strength predictions made use of the Hill-Tsai failure criteria which is employed in the same laminate property prediction program. Check cases were also made using the Air Force developed RD-5 program (7), and good agreements were obtained.

Local buckling stresses were determined using orthotropic plate theory with reduced stiffnesses due to membrane/flexural coupling with theory developed by Case Western Reserve University. Calculated stresses compared very well with results obtained using the RA-5 program described in Reference 8. Post-buckling strength referenced in Section V was calculated by multiplying the ultimate skin strength and the effective skin width according to theory also developed by Case and adding to this quantity the load carrying capability of the stringers at the same strain level.

Stringer column buckling allowables were determined from wide column theory by assuming that skin and stringer together act as an isolated pin-ended column 12 inches long. For general bending instability, the method of Reference 9 was used. This computer program was developed and obtained from NASA/Langley.

SECTION V

PERFORMANCE EVALUATIONS

Analytical evaluations of the representative fuselage component were made to summarize expected and achieved performance and to project performance of the component if it were made with presently available "Thornel" 50S fiber. This section summarizes stiffnesses and strengths of the component, and presents comparisons with aluminum structure.

The following assumptions were made in the performance evaluations: (1) geometry was maintained constant, i.e., same spacing, shape, and size of stringers and rings; (2) ply lay-ups were the same as in the fabricated component; (3) equivalent aluminum designs in 7075-T6 were based on the same load capacities as composite designs; and (4) five failure modes were considered: material strength, skin and/or stringer element buckling, stringer column buckling, and general instability.

A. Stiffness Comparisons with Aluminum

(W.N. Meholick and D.P. Hanley, Bell Aerospace)

Measured and predicted stiffnesses of the components are shown in Figure 34 for axial, bending, and torsion loads. These AE, EI, and GJ quantities are fundamental to predictions of static and dynamic response for any structure. The key in Figure 34 designates A for aluminum and C for composite. P is predicted, M is measured, and the upper and lower bounds correspond to the end diameters of the shell. The average C_m values for AE and EI are twice that of an equivalent load capacity aluminum structure while the composite GJ is half that of aluminum. This points up the well known nature of 'tailoring' a composite structure. Good agreements are seen between predicted and measured EI and GJ for the composite.

The composite AE measured about 25% less than predicted. That difference is thought due to the fact that moduli were considered equal in tension and compression and to factors such as thickness variations. The equivalent E for the component was 13 million psi, 30% greater than aluminum. The equivalent G was 1.34 million psi, 12% greater than the minimum 1.2 million psi design requirement. Thus, the composite GJ values shown represent adequate torsional stiffness.

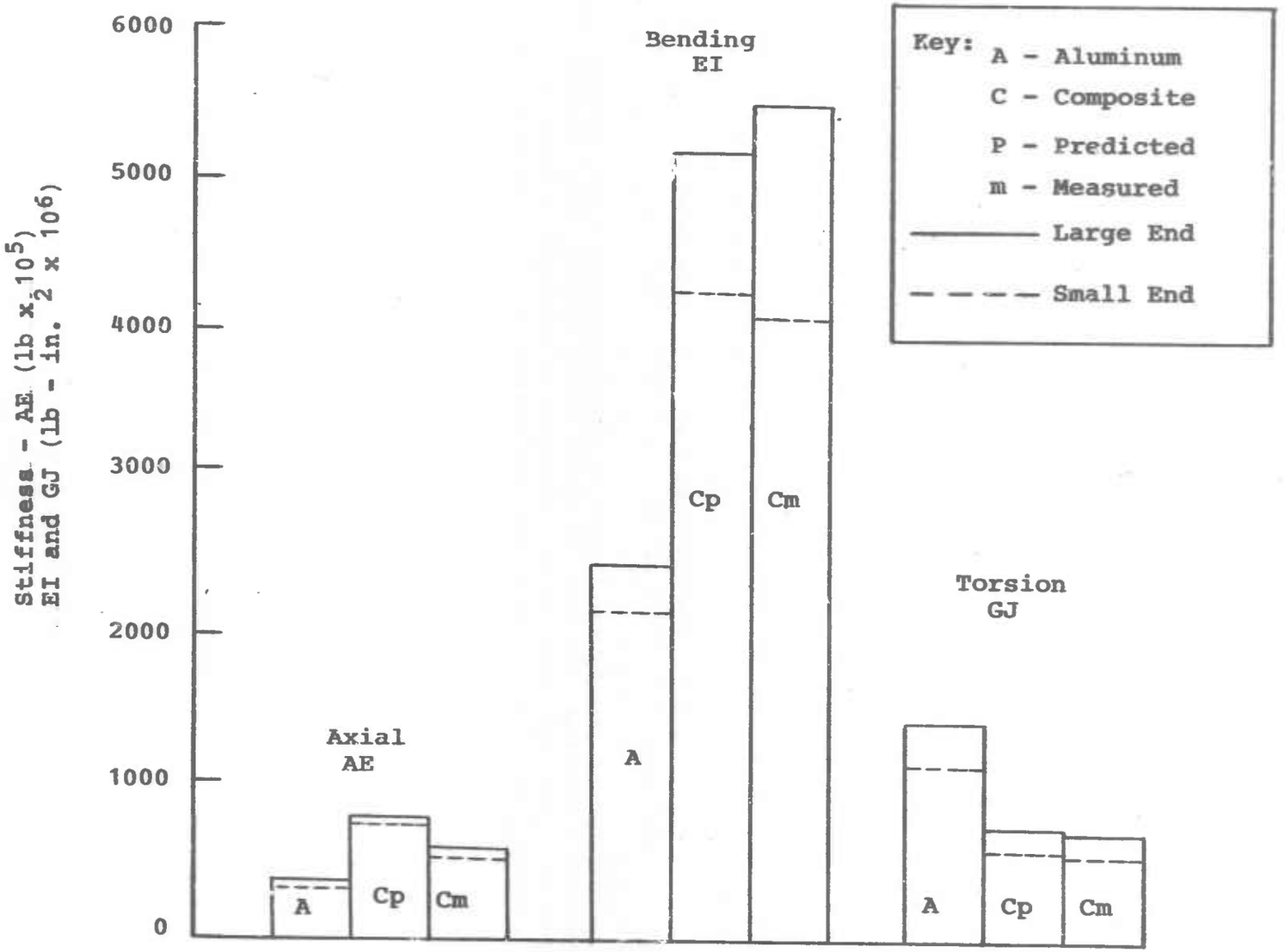

Figure 34. Fuselage Stiffnesses

B. Present Potential of Graphite Fiber Composites
(W.N. Meholick and D.P. Hanley, Bell Aerospace)

Table VI summarizes performance of the fuselage component in terms of strength, stiffness, and weight. The original aluminum shell, designed for 1800 lb/in., weighted 0.95 psf. The actual component failed at 1980 lb/in. and weighed 0.70 psf. The demonstrated weight savings over equivalent aluminum structure was 27% instead of the expected 36%. The stiffness advantage was a factor of 2 and the stiffness-to-weight advantage was a factor of almost 3.

Had the "design goal" fiber volume contents and thicknesses of skin and stringers been achieved in fabrication as given in Table VI, the weight savings would have been 43%. This structure would fail at 3150 lb/in. The EI/weight advantage would be a factor of 3.3.

Improvements in treated "Thornel" 50 have been made with yarn tensile strength increased from 220,000 to 250,000 psi. Composite property increases in compression and shear are also being obtained: values of 100,000 psi and 10,000 psi, respectively, have been measured. Performance of the fuselage with present day material is given last in Table VI. A weight savings of 49% is shown with a slight decrease in $(N_x)_{ult}$ to 3120 lb/in. This failure level is based on an instability failure rather than strength as in the other designs. For this design, post-buckling theory recently developed at Case Western Reserve University was used. The aluminum designs given in Table VI were based on several combinations of skin thicknesses (25 and 32 mils) and stringer thicknesses (32 and 40 mils) and very slight changes in stringer flange widths so as to achieve load capacities equivalent to the composite designs.

TABLE VI

PERFORMANCE SUMMARY AND PROJECTIONS

	(N_x) ult (lb/in.)	EI (10^6 lb/in.^{2})	Weight (psf)	Wt Savings (%)
• Original Aluminum Design	1800	2300	0.95	-
• As Fabricated Component				
Composite { Expected	2610	4710	0.70	36
Composite { Actual	1980	4810	0.70	27
• Equivalent Aluminum	1980	2310	0.96	-
	2610	2650	1.10	-
• Design Goal				
Composite	3150	5525	0.67	43
Aluminum	3150	2960	1.17	-
• "Thornel" 50S, March 1970				
Composite	3120	4600	0.59	49
Aluminum	3120	2960	1.16	-

SECTION VI

FUSELAGE COMPONENT POST-TEST EVALUATIONS

To aid in evaluation of the fuselage component test results, several additional tests were performed on portions of the fuselage component and on similar composite shapes. A 6 x 10-inch stiffened panel was cut from the side of the component and tested in compression for verification of the rosette strain gage readings. Tests were conducted on specimens cut from Union Carbide's practice skin (made from untreated "Thornel" 25), which had the same lay-up as the actual fuselage skin, so that specimen preparation, instrumentation, and test methods could be evaluated. Tension and compression tests were conducted on specimens cut from the fuselage component skin for verification of predicted properties. Tensile tests were performed on specimens cut from unused stringers and on skin-stringer combinations cut from the fuselage component. A fractographic evaluation was made of the failure surfaces of the fuselage component.

A. Stiffened Panel Test

(L.H. Kocher, Bell Aerospace)

The objective of this test was to verify rosette strain gage readings. A 6 x 10-inch stiffened panel was cut from the side of the fuselage component for compression testing. New individual gages were mounted in the same orientation and as close as possible to the original rosette gage elements as seen in Figure 35(a). One of the gages of the original rosette was damaged during handling. Comparisons of the other two rosette gage readings with those of the new gages showed some discrepancy. Differences were believed due to effects of gage positioning on the stiffened panel since a similar test on an unstiffened aluminum tensile specimen showed identical outputs of rosette and uniaxial gages. The major finding from the stiffened panel test was that of uncovering an error in the rosette gage factors used in reducing the fuselage test data. This error amounted to a factor of two difference in the rosette strains. Those corrections have been applied to Figures 7, 9, 11, 13 and 18.

Catastrophic failure of the test panel occurred at a load of 2090 lb/in. and at a strain level of 1940 μ in./in. See Figure 35(b). This failure load in compression was only slightly greater than the 1980 lb/in. tensile failure load of the fuselage component.

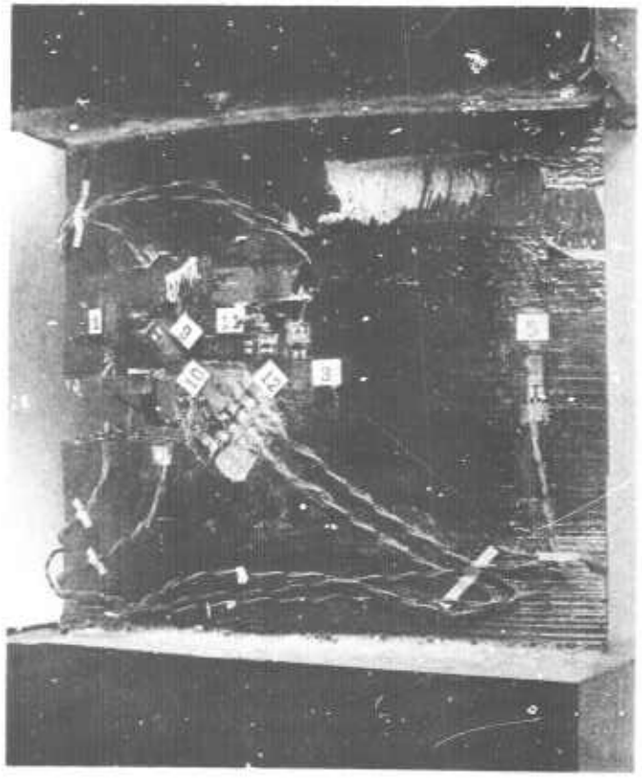

a) Back-Side View

P00076

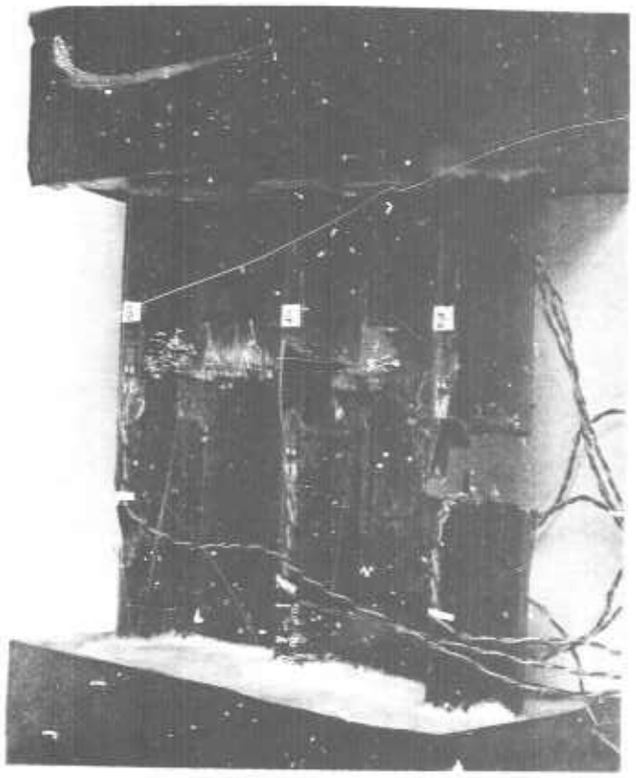

b) Front-Side View

P00075

Figure 35. Panel from Fuselage Component After Compression Test.

B. Tests on Practice Skin
(L.H. Kocher and D.P. Hanley, Bell Aerospace)

Two specimen widths (0.5 and 1.0 inch) were employed in tests of tension and compression specimens to determine effect on property measurements. After specimens were cut from the practice skin section, considerable longitudinal curvature and twist was observed. These effects were believed due to differences in thicknesses and resin contents of the inner and outer 90^{o} plies and anti-symmetry of the $\pm 15^{o}$ plies. Although curvature and twist accounted for considerable prestrain in the skin ($\sim \mu \pm 600$ μin./in.), its effect on tensile strength was estimated to be $<\pm 2\%$ of measured ultimate. The reason for this small effect is that the main load-carrying $\pm 15^{o}$ plies are close to the neutral axis, thus resulting in relatively small flexural stresses.

1. Tensile Tests

A summary of tension test results on the practice skin fabricated from "Thornel" 25 is shown in Table VII. Average tensile strength was 10.43 ksi ±1.0% with an average laminate modulus of 3.08×10^{6} psi. There was no significant effect of the two gage widths.

Transverse curvature of specimens due to the cylindrical shape of the skin were considered negligible for the 0.5 inch wide specimens, and glass end tabs were applied using Epon 828/Versamide adhesive. However, for 1-inch width specimens, the glass tabs were sanded to match specimen curvature prior to bonding.

On a number of specimens, the strain gages were mounted on small and smoothed epoxy pads applied to the skin exterior so that the gages laid flat. Results indicated no significant difference in strains compared with gages mounted directly on the rough skin. Most specimens were instrumented with at least two pairs of back-to-back gages. Considerable divergence of back-to-back strain gage readings was measured on all specimens and gage readings on the skin exterior were consistently larger than those of companion gages mounted on the inside of the skin. Laminate modulus calculations in Table VII were based on averages of back-to-back strain readings. These readings showed good uniformity and compared favorably with values measured by extensiometers.

TABLE VII

PRACTICE SKIN TEST RESULTS

Specimen	Gage Width (in.)	Ultimate Stress		Modulus (10^6 psi)
		First Test (ksi)	Retest (1) (ksi)	
LT-1 (2)	1.0	10.68	11.10	-
LT-2		10.40	-	3.12
LT-3		10.30	-	2.80
LT-4	1.0	10.20	-	2.95
LT-5	0.5	9.43	11.60	3.60
LT-6		10.50	-	2.76
LT-7		11.00	-	-
LT-8		10.50	11.30	3.25
LT-9	0.5	10.90	-	-
		10.43 Avg.	11.33 Avg.	3.08 Avg.
LC-3 (3)	0.5	24.8	-	2.89
LC-4		25.3	-	-
LC-5		24.0	-	-
		24.7 Avg.		2.89

(1) After first test failure, remaining portion was retabbed and tested.

(2) LT = longitudinal tension

(3) LC = longitudinal compression

2. Compression Tests

One-inch width specimens were tested in compression using potted ends. These specimens proved unsuccessful due to severe buckling. This result was probably caused by difficulties in maintaining specimen alignment during potting because of twist and curvature. The 0.5 inch width specimens also showed considerable local bending during test; however, compressive strengths (24.7 ksi average as shown in Table VII) were more than twice the tensile strengths. Measured compression modulus of one specimen was 2.89×10^6 psi, slightly less than the measured average tensile modulus.

C. Tests on Fuselage Skin
(L.H. Kocher and D.P. Hanley, Bell Aerospace)

Eight skin tensile tests were performed on specimens taken from the fuselage component. All specimens were taken from the bottom of the shell with four specimens taken on either side of the failure region. Four skin compression tests were also performed on specimens taken from the top of shell in the region of the "tongue" (See Figure 17). A photograph of the specimens after test is shown in Figure 36.

Warping and twisting of specimens was noted after cutting, similar to that observed with the practice skin. Longitudinal strain required to force the specimens to lay flat was calculated as ~ ±400 μ in./in. This strain agreed with measurements recorded by strain gages during test. The measured degree of twist along specimens was ~1.4°/inch of length.

1. Tensile Tests

Tensile specimens were instrumented with at least one pair of back-to-back gages, and strains were recorded from these gages and from any existing gages applied during the component instrumentation. One specimen, LE 31-1, contained several of the "problem gages" (Nos. 29, 30, 68 and 69). These gages showed responses similar to those experienced during the component tests (i.e., 29 and 30 showed high local bending; 68 and 69 did not). The new gages in general did not exhibit high local bending. Averages of both sets of gages agreed well.

Test results are summarized in Table VIII. It is curious to note that the average ultimate strength of specimens taken from the bay toward the large-end side of the failure, denoted LE, were approximately 27% higher than those from the small end (SE) side of the failure. A similar discrepancy was observed in moduli. It may also be noted in Table VIII that the strength and modulus of the treated "Thornel" 50 skin was two to three times that of the practice skin. (Table VII).

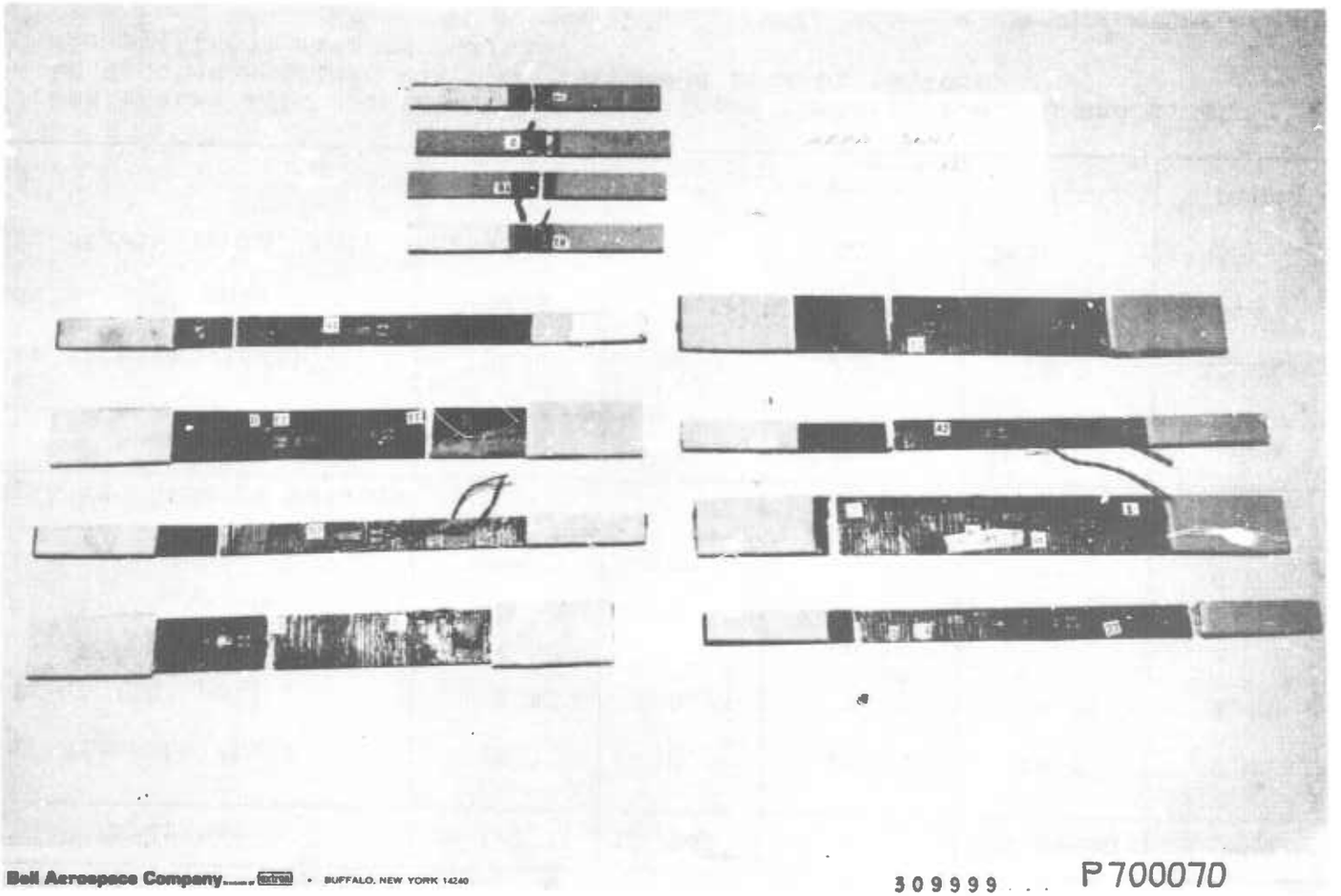

Figure 36. Failed Tension and Compression Specimens Taken from Fuselage Skin.

P700070

TABLE VIII

SUMMARY OF FUSELAGE SKIN TENSION TESTS

Large End Side of Failure					
Specimen	LE 3-2[1]	LE 2-1	LE 1-31	LE 31-30	Avg.
Ult. Strength (ksi)	30.7	30.7	29.0	28.7	29.8±3.3%
Modulus (10^6 psi)	9.85	8.71 7.75	9.00 9.68 9.48	9.35	9.11
Ult. Strain (μ in./in.)	3120	3720	3085	3150	3260
ν_{12}	---	---	0.0667	---	0.0667
Small End Side of Failure					
Specimen	SE 3-2	SE 2-1	SE 1-31	SE 31-30	Avg.
Ult. Strength (ksi)	22.8	22.2	23.8	24.0	23.2±4.3%
Modulus (10^6 psi)	8.9	8.70	7.54	9.18	8.47
Ult. Strain (μ in./in.)	2575	2665	3150	2630	2755
ν_{12}	---	---	---	0.043	0.043

(1) Designates skin specimen between stringer numbers, i.e., 3 and 2, etc.
LE denotes specimen taken on large-end side of failure;
SE, small-end side of failure.

2. Compression Tests

Results of the compression tests are summarized in Table IX.

TABLE IX

SUMMARY OF FUSELAGE SKIN COMPRESSION TESTS

Specimen	C 14-15	C 15-16	C 16-17	C 17-18	Avg.
Ult. Strength (ksi)	28.0	21.2	30.6	28.2	27.0
Modulus (10^6 psi)	8.20	8.37	8.30	8.45	8.33
Ult. Strain (μ in./in.)	3420	2530	3680	3340	3240

Considerable bending was observed as in the practice skin tests; average strength was 27.0 ksi. This result confirmed the expected balance in tension and compression strengths. Average compression modulus of the fuselage skin was slightly lower than tensile modulus as was observed in the practice skin test results.

3. Property Comparisons with Prediction

Measured properties discussed in the previous sections are summarized in Table X and compared with predicted values from Table IV.

The data shown in Table X indicate that the skin strength predictions were quite good. As expected, average measured strengths exceeded prediction, reflecting the known design conservatisms. The predictions, in fact, correspond very closely to the minimum measured strengths. With respect to the fuselage component performance, the data also indicate that the stringer tensile strain was limiting: that value was predicted as 2250 μ in./in. and is less than the minimum 2577 μ in./in. measured skin ultimate tensile strain. Experimental data on stringer tensile strength and strain generated by Union Carbide are given in the next report section.

TABLE X

COMPARISON OF PREDICTED AND MEASURED FUSELAGE SKIN PROPERTIES

Property	Predicted	Measured				
		Minimum	Min. Avg.	Avg.	Max. Avg.	Maximum
V_F (%)	36	--	--	42	--	--
V_w (%)	--	--	--	1.22	--	--
$(E_1)_T$ (10^6psi)	8.52	7.54	8.47	8.85	9.11	9.85
$(E_1)_C$ (10^6psi)	8.52	8.20	--	8.33	--	8.45
ν_{12}	0.088	0.043	--	0.055	--	0.0667
X_T (ksi)	21.9	22.2	24.0	26.5	29.8	30.7
ε_T (μ in./in.)	2570	2577	2755	3010	3260	3720
X_C (ksi)	22.5	21.2	--	27.0	--	30.6
ε_C (μ in./in.)	2640	2530	--	3240	--	3680

D. Tests on Stringers

(T. Weng, Union Carbide Corporation)

The destruct test of the fuselage component resulted in a tensile failure, which was almost certainly initiated by failure of stringer No. 1. Thus, experimental verification of stringer tensile strength estimates, derived from flat laminate properties and used in component performance predictions (see Table IV this report) were of particular interest. The tests were conducted on stringers left over from the fuselage fabrication program, since it was not possible to remove stringers from the failed component without damage to the stringer flanges.

Four hat-shaped stringer specimens were tested. The stringer specimen assembly for the tensile test is shown in Figure 37. The specimen assembly was designed to apply a tensile load through the centroid of the cross-section of the stringer so that a uniform tensile stress-field could be produced in the stringer. The specimen is 12-inches long and has potted ends, 1 x 1.08 x 4 inches (see Item B in Figure 37). The potting compound used is the same material as that used for potting the ends of the compression stringers specimens (Section IX-F of Reference 3). The ends were potted in a fixture which held the specimen in such a position that the centroid of the cross-section of the stringer coincided approximately with the symmetry axes of the potted ends. The centroid of the stringer specimen and the symmetry axes of the potted ends did not coincide exactly because the location of the centroid was pre-calculated with the dimensions of a typical stringer rather than with those of the individual stringer. The Fixtures C and D in Figure 37 were cemented to the specimen with Scotch-Weld Structural Adhesive 2216.* Bolts E, which pass through the symmetry plane of potted ends, were used to align and grip the test specimen to the fixtures. Correction for minor misalignment between the centroids of the stringer and the symmetry axes of the potted end was accomplished by adjusting the location of Pin F in the slot with Set Screws G and by lateral movement of Block H along the pin. A slot was not provided in Fixture D.

Three strain gages, one on the cap and one on each flange, were attached to the stringer specimen to measure longitudinal strains. Initially, a small load was applied to check out the alignment of the test specimen. If the strain read-outs from the strain gages on both flanges were different, an adjustment of the location of Block H was made. If the strain read-outs from the strain gages on the cap and the flanges were different, the location of Pin F was adjusted.

The results of tensile tests on stringer specimens are given in Table XI. Three specimens were cut from stringer No. H50-223 and one specimen was cut from stringer No. H50-233.

*Product of 3M Company.

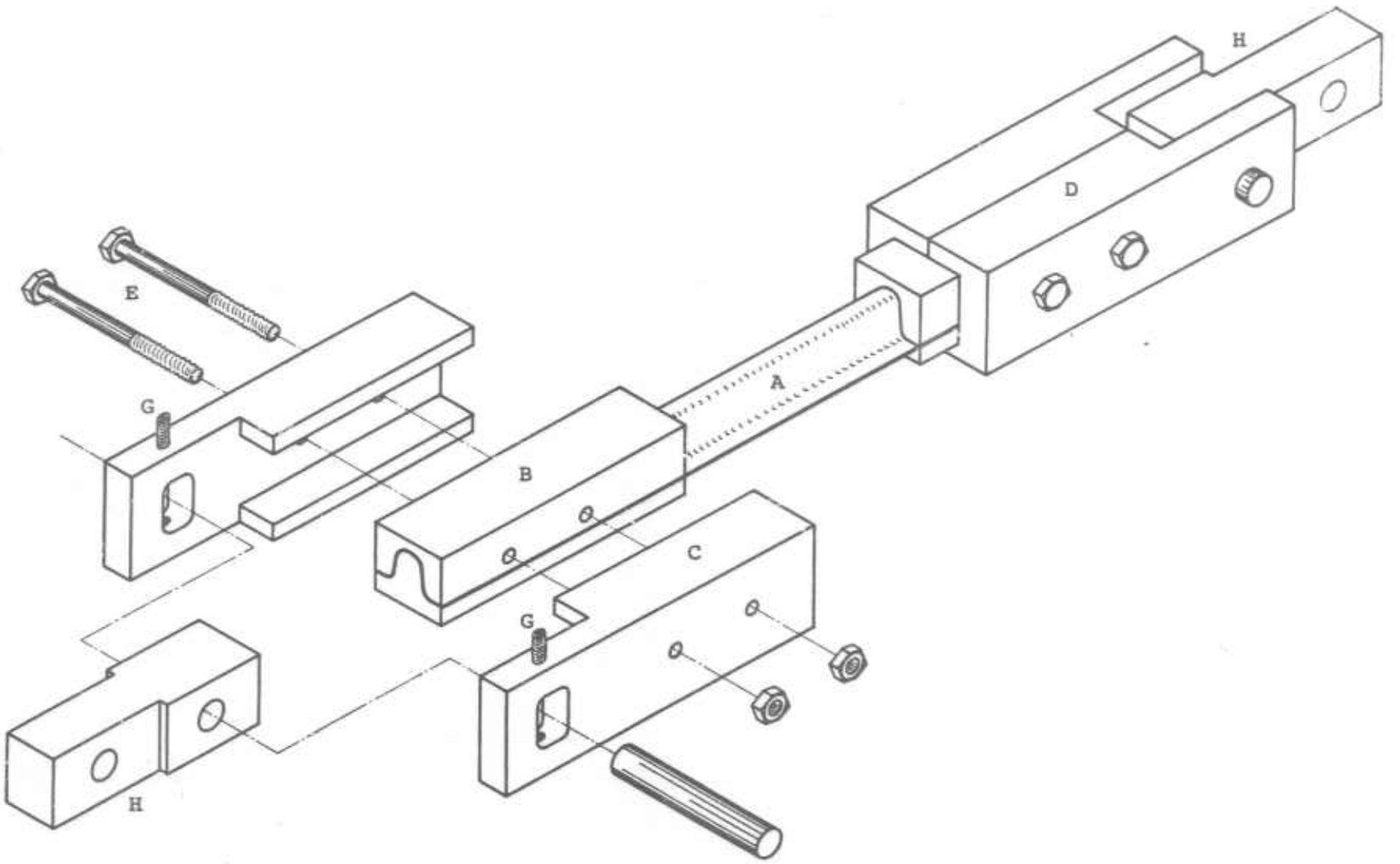

Figure 37. Stringer Specimen Assembly for Tensile Test.

N-23342

TABLE XI

TENSILE TEST RESULTS ON HAT-SHAPED STRINGERS

Specimen	Cross-Sectional Area ($in.^2$)	Young's Modulus (10^6 psi)	Yield Strength (psi)	Tensile Strength (psi)	Tensile Strain (10^{-6} in./in.)
H50-223-1	.096	17.9	39,200	50,500	2630
H50-223-2*	.097	17.9	43,700	>54,500	>2770
H50-223-3	.100	16.6	30,300	54,500	2860
H50-233-1	.067	23.5	20,500	52,200	2050

*Not tested to failure

The measured values of Young's modulus were in good agreement with those measured sonically on the 44-inch long stringer (Section IV D of Reference 6). The tensile strength values were very close to the compression strengths previously measured on the same stringers and exceeded the value of 45,000 psi used by Bell in the shell analysis (Table IV of this report). The tensile strains of Stringer H50-223 were higher than the predicted values of 2250 μ inch/inch, but below the average skin ultimate tensile strain measured by Bell (Table X of this report). Thus, Bell's conclusion that the stringer tensile strain was the limiting factor in the component performance remains valid. The tensile strain of Stringer H50-233 was exceptionally low. However, the Young's modulus of this stringer was higher than that of any stringer used for the component.

The test of H50-223-2 was terminated just prior to the point at which fracture was expected to occur so that optical examinations on crack formation in the specimen could be made. Figures 38, 39, and 40 show photomicrographs of this stringer. Small cracks running parallel to the sidewalls, shown in Figure 38, were observed in the straight web sections of the stringer. The cracks generally occurred within plies rather than between plies. A photomicrograph of the cap section is shown in Figure 39. Fewer cracks were found in the cap section than in the other areas of the stringer. Figure 40 shows large cracks which were observed in the cap-web and web-flange bend sections. Most of these cracks are believed to have initiated from the external surface, and seldom propagated inward beyond the outermost layer.

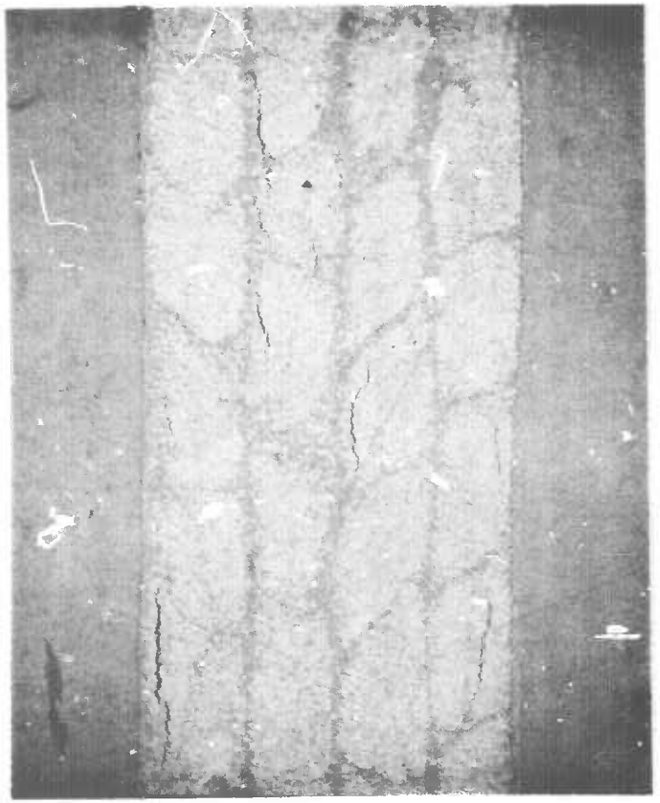

Figure 38. Photomicrograph of Web Section on Hat-Shaped Stringer Tensile Specimen, H50-223-2. 50X Magnification.

N-23522

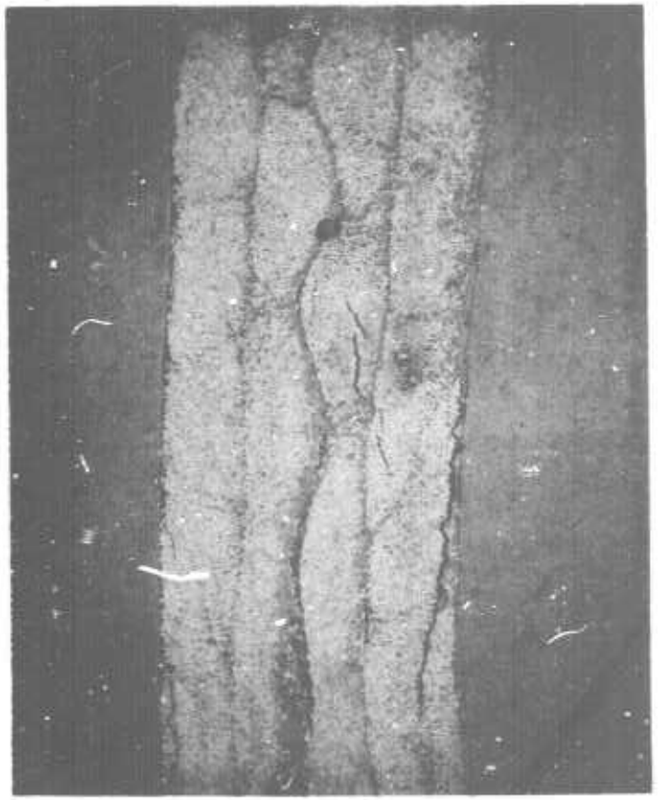

Figure 39. Photomicrograph of Cap Section on Hat-Shaped Stringer Tensile Specimen, H50-223-2. 50X Magnification.

N-23523

Figure 40. Photomicrograph of Web-Flange Section of Hat-Shaped Stringer Tensile Specimen, H50-223-2. 50X Magnification.

N-23524

E. Tests on Skin-Stringer Combinations
(T. Weng, Union Carbide Corporation)

Three stringer-skin combination specimens were cut from the fuselage component and tested to failure in tension. Ten-inch long specimens containing stringers No. 1, 2, and 3 were cut from the component in the vicinity of the failure area; these stringers were selected because of the evidence that failure initiated at stringer No. 1. The width of the skin remaining on the stringers was the same as that of the stringer flanges. The test fixture was identical to that used in testing of the stringers alone.

The results of these tensile tests are given in Table XII.

TABLE XII

TENSILE TEST RESULT ON STRINGER-SKIN COMBINATION SPECIMENS

Specimen Stringer Number	Stringer Area ($in.^2$)	Stringer E_{son} (10^6 psi)	Skin Area ($in.^2$)	Yield Load (lbs)	Yield Strain Stringer (10^{-6} in./in.)	Yield Strain Skin (10^{-6} in./in.)	Fracture Load (lbs)	Fracture Strain Stringer (10^{-6} in./in.)	Fracture Strain Skin (10^{-6} in./in.)
1	.073	19.7	.058	3,100	1,460	1,530	4,730	2,230	2,250
2	.074	21.6	.057	3,200	1,370	1,550	3,570	1,700	1,650
31	.083	18.7	.057	4,200	1,980	2,200	5,250	2,540	2,660

The specimens containing stringers No. 1 and 2 failed within the grips of the fixture; these failures appeared to initiate at the pin holes in the grip fixture and involved a delamination of stringers and skin. The fracture load and strain to failure of these specimens were lower than those measured on stringers alone. Table XIII lists the stresses in the stringers and skin at the yield point (i.e., the load at which an initial crack was observed) and at failure; these stresses were calculated from the expression

$$\sigma = E_{son}\ \varepsilon.$$

TABLE XIII

STRESSES IN STRINGER-SKIN COMBINATION SPECIMENS

Specimen Stringer Number	Yield Stress Stringer (10^3 psi)	Yield Stress Skin (10^3 psi)	Fracture Stress Stringer (10^3 psi)	Fracture Stress Skin (10^3 psi)
1	28.7	13.0	44.0	19.1
2	29.6	13.2	36.7	14.0
3	37.0	18.7	47.5	22.5

These results could indicate that the strength of the stringers and skin were not fully utilized at failure. A more likely explanation, however, is that the material was already damaged during the destruct test of the component and that stress concentrations at the pins of the test fixture contributed to the premature failure.

F. Fracture Surface Studies
(Professor Kicher and Mr. T. C. Esselman, Case)

The fracture surface of the fuselage component was investigated as part of the post test evaluation. For this purpose, a two-inch band on each side of the fracture surface was removed with a jewelers saw, and the balance of the specimen was returned to Union Carbide Corporation.

Visual and optical observations indicated no evidence of failure away from the final fracture surface and no stringer debonding even at the edge of the fracture. The fuselage component maintained its gross structural integrity up to the point of failure.

The first general observation of the fracture surface was the anti-symmetry of the side portions of the fracture surface. Figure 41 is a sketch of the general orientation of the fracture surface relative to the structure axes. A segment of the fracture surface (B to C) was generally perpendicular to the cylinder axis. The side portions of the fracture surface (A to B) and (C to D) were in parallel planes, tilted to the axis of the cylinder. This general orientation was probably caused by a lateral shift of the load after a crack propagated through the region B to C. This perpendicular region (B to C) was subjected to the maximum tensile stress under the combined loading of bending and shear with predicted negative margins of safety near points B and C.

Next, a 15x photographic map of both fracture surfaces in the vicinity of the bottom five stringers (30, 31, 1, 2 and 3) was prepared. Variations in the general character of these fracture surfaces were observed. For example, relatively flat regions of a granular nature were observed across the cap of stringer No. 1 which was located at the extreme bottom during the test as shown in Figure 41. Figure 42 is a scanning electron microscope (SEM) micrograph at 50x of the cap of stringer No. 1. Note the flat, granular character of a major portion through the thickness. This same characteristic surface was observed over the entire cap of stringer No. 1. Figure 43 is a SEM photograph of the flat region at 500x. Note the absence of fiber pull-out. Figure 44 shows another portion of this same region with an apparent irregularity of "Thornel" fiber orientation. Similar regions of misaligned fibers were noted at other locations on this stringer cap. The consequences of the presence of such flaws (in terms of critical flaw size) in the fracture region were not determined because of time and equipment limitations.

At other locations on the fracture surface, significant amounts of fiber pull-out were observed. Figure 45 is a SEM photograph of the root (curved region between stringer wall and flange) showing fibers in bundles. Because of the variation of thickness due to the stringer molding process, these bundles were originally interpreted as strands of yarn in a matrix rich

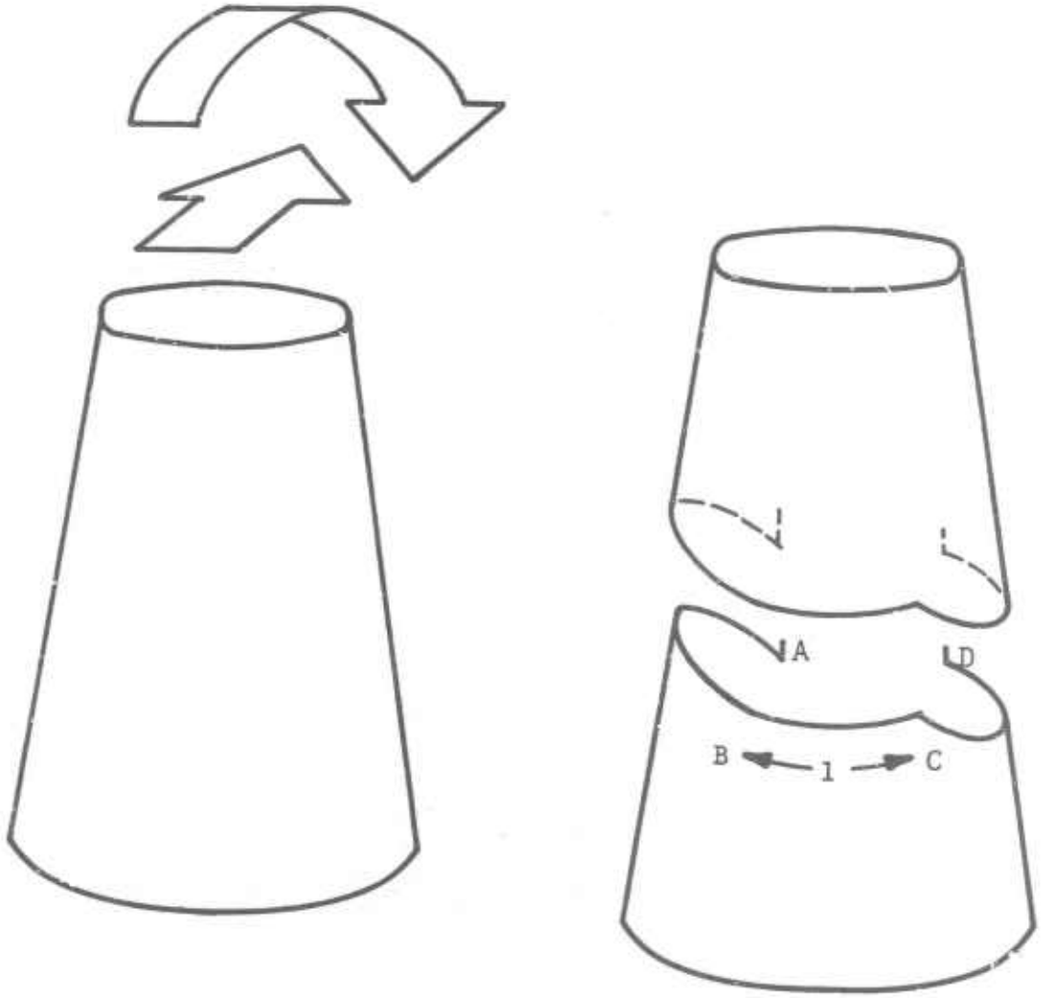

Figure 41. General Orientation of the Fuselage Fracture Surface

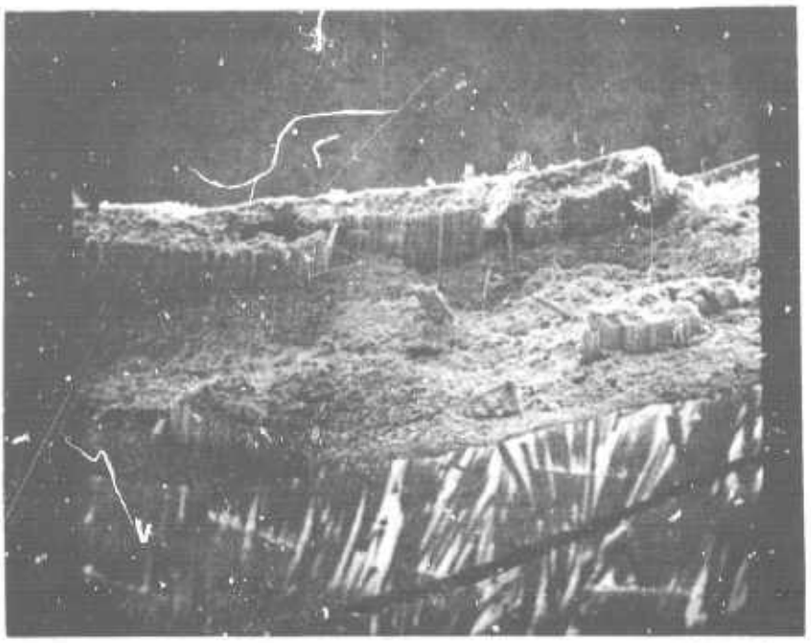

P700077

Figure 42. Scanning Electron Microscope Photograph of the Cap of Stringer No. 1

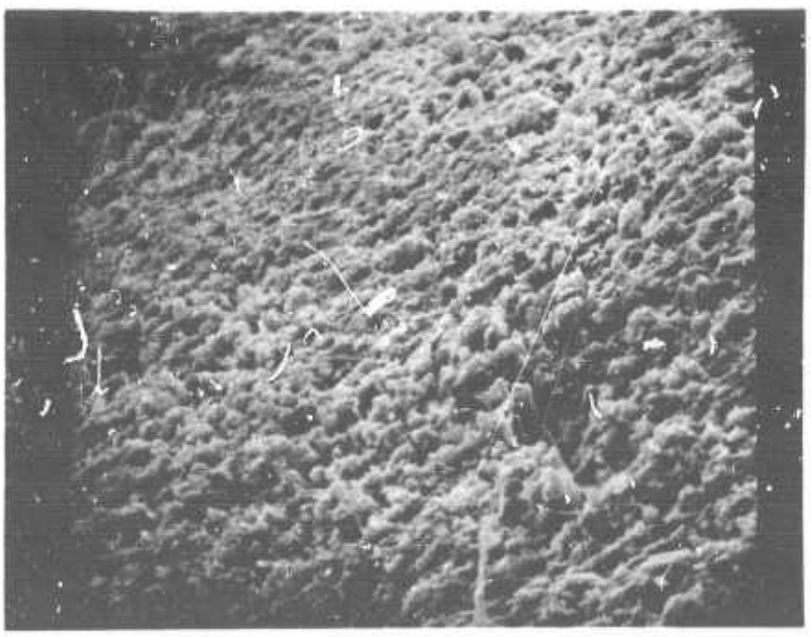

P700078

Figure 43. SEM Photograph of Flat Region of Cap of Stringer No. 1. 500X Magnification.

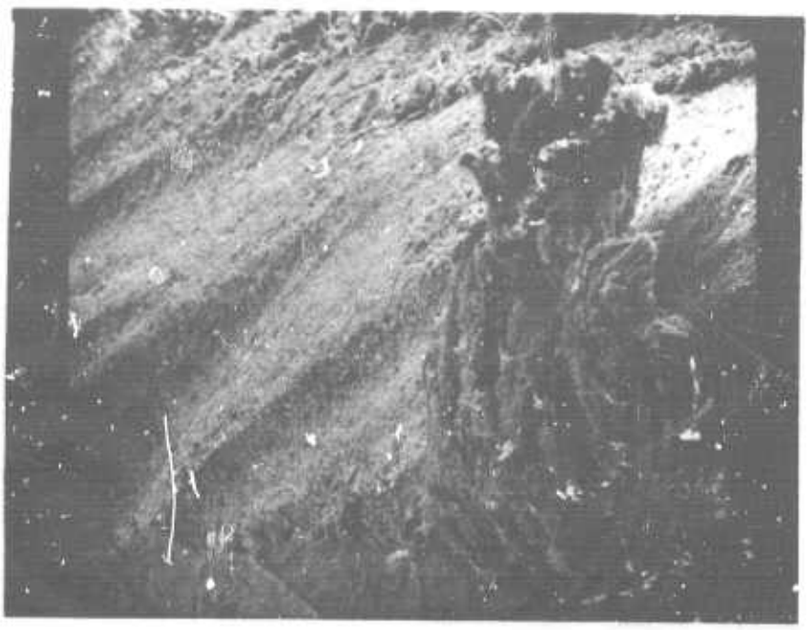

P700079

Figure 44. SEM Photograph of the Cap of Stringer No. 1 Showing a Region of Irregularly Oriented "Thornel" Fibers.

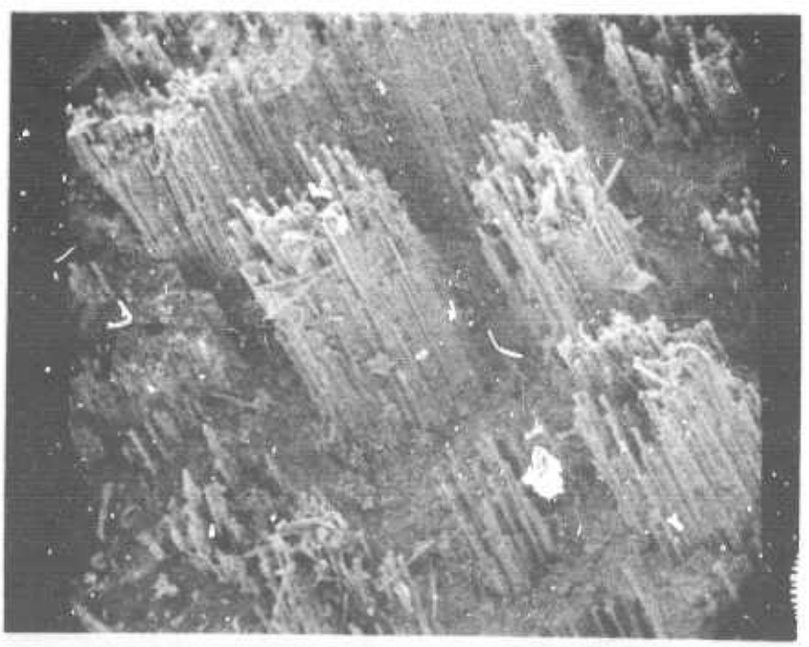

P700080

Figure 45. SEM Photograph of the Root of Stringer No. 1. 100X Magnification.

region. However the photographs reveal a variation in the number of fibers in each bundle and the presence of many fibers between the bundles (Figure 46). Therefore the fibers did not fail in their original bundles but failed sequentially in groups until the remaining region could no longer carry the applied load. Because of the mismatch of elastic modulus in the axial direction between the skin and the stringers, the region of the stringers adjacent to the skin carried a higher tensile stress. This observation is substantiated by the presence of local bending in the strain gage data. Strains observed in the skin were higher than those in the stringer cap (gages 5 and 6) near the fracture region. Furthermore a close examination of the fracture surface at the base of the bundles indicates a higher velocity crack than the granular region of the cap of stringer No. 1. The higher velocity crack confirms the existence of a higher stress intensity.

Similar regions of high fiber pull out were noted throughout the fracture surface. Figure 47 is a SEM photograph of the cap of stringer No. 31. Note the contrast to the cap of stringer No. 1 where virtually no fiber pull-out was observed. This difference indicates that the cap of stringer No. 31 was in a higher state of stress at the time of failure; consequently more fibers were broken in an irregular pattern. The strain gage data (gage 75) again substantiates the occurrence of the higher strains.

The exact causes for the variations in stresses were not determined. The strain patterns are similar to what might be produced by local bending effects; however, the gross loading conditions preclude the existence of local bending. Ovaling of the open bay regions between the ring stiffeners was not detected by the dial indicators.

A failure at 76% of the ultimate load was heard and recorded on the strain gages during the destruct test. This initial failure was probably confined to a segment of the perpendicular fracture region (B to C) of Figure 41. Since no failure was visually detected during the test, only a portion of this region must have failed. Finally, the fracture surface asymmetry in the side regions (A to B) and (C to D) indicate another phase of the fracture, namely a shifting of the load. This failure was sequential in nature but occurring over a rather short time span. Movie coverage indicated that fracture occurred over a time span of three frames or three twenty-fourths of a second.

A closer examination of the fracture surface in the perpendicular region gave a further indication of the direction of crack propagation. When the stringers were bonded to the skin with a room temperature curing adhesive, excess resin collected at the skin-stringer bond region. A close examination of these regions of excess resin revealed fracture origins, mirror and feather markings of a crack propagating through each skin-stringer bond. From the location of the fracture origin and the orientation of the feather markings, the crack appeared to have propagated from the center (stringer No. 1) out to points B and C of Figure 41. Figure 48 shows the fracture surface characteristics of the excess resin of stringer No. 31. The crack appears to have initiated at the right (nearest to stringer No. 1) and propagated to the left. This observation is substantiated by the high speed

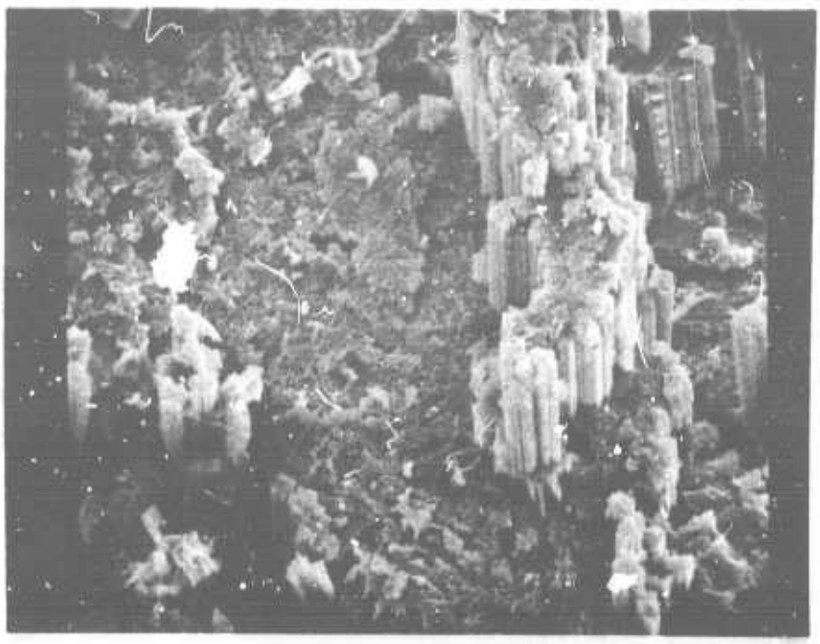

P700081

Figure 46. SEM Photograph of the Root of Stringer No. 1. 500X Magnification.

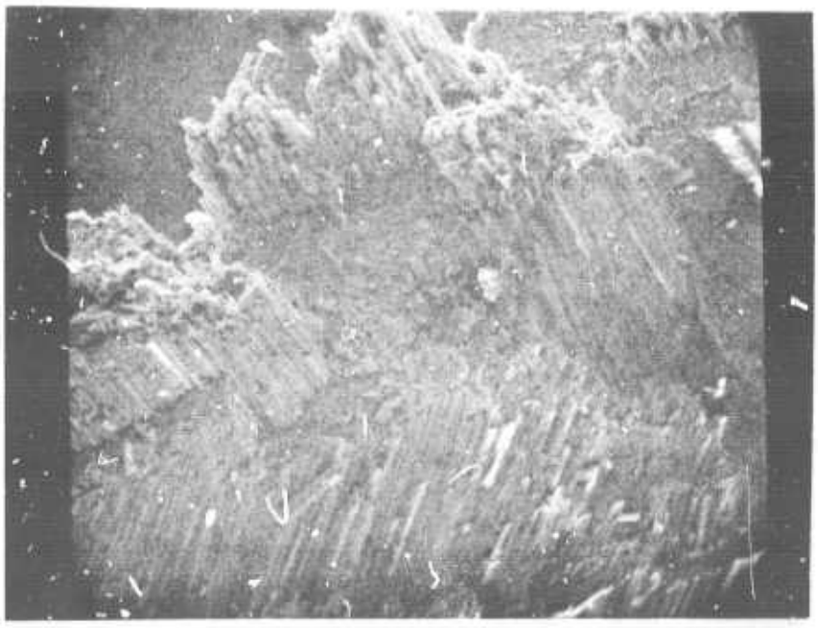

P700082

Figure 47. SEM Photograph of the Cap of Stringer No. 31. 100X Magnification.

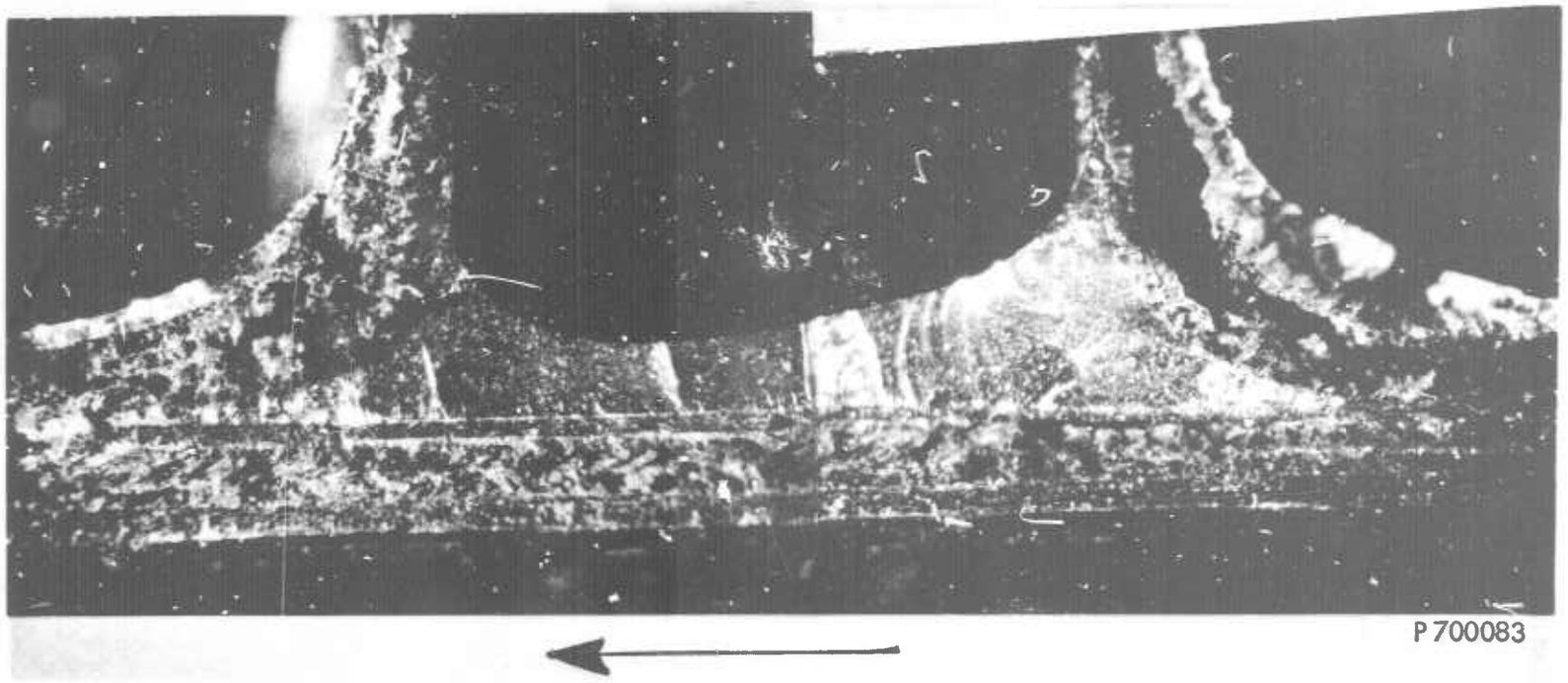

Figure 48. Photomicrograph of Excess Resin of Stringer No. 31 Showing Crack Initiation and Propagation. ∿20X Magnification.

motion picture taken during the destruct test.

In conclusion, the failure initiated at or near stringer No. 1 and propagated circumferentially to points B and C. At this point, an apparent load shift caused the fracture to occur in a plane tilted to the axis of the cylinder. The regions of high fiber pull-out are associated with high stress levels prior to the crack propagation. The regions of small amounts of fiber pull-out also displayed severe surface roughness and consequently were interpreted as regions of low stress level prior to fracture.

REFERENCES

1. Union Carbide Corporation, Carbon Products Division, in Association with Case Western Reserve University and Bell Aerospace Company, a Division of Textron, Integrated Research on Carbon Composite Materials, AFML-TR-66-310, Part I (October 1966) (AF 33(615)-3110, Air Force Materials Laboratory, Wright-Patterson Air Force Base, Ohio).

2. Union Carbide Corporation, Carbon Products Division, in Association with Case Western Reserve University and Bell Aerospace Company, a Division of Textron, Integrated Research on Carbon Composite Materials, AFML-TR-66-310, Part II (December 1967) (AF 33(615)-3110, Air Force Materials Laboratory, Wright-Patterson Air Force Base, Ohio).

3. Union Carbide Corporation, Carbon Products Division, in Association with Case Western Reserve University and Bell Aerospace Company, a Division of Textron, Integrated Research on Carbon Composite Materials, AFML-TR-66-310, Part III (January 1969) (AF 33(615)-3110, Air Force Materials Laboratory, Wright-Patterson Air Force Base, Ohio).

4. Union Carbide Corporation, Carbon Products Division, in Association with Case Western Reserve University and Bell Aerospace Company, a Division of Textron, Integrated Research on Carbon Composite Materials, AFML-TR-66-310, Part IV, Volume I (September 1969) (F33615-68-C-1077, Air Force Materials Laboratory, Wright-Patterson Air Force Base, Ohio).

5. Union Carbide Corporation, Carbon Products Division, in Association with Case Western Reserve University and Bell Aerospace Company, a Division of Textron, Integrated Research on Carbon Composite Materials, AFML-TR-66-310 Part IV, Volume II (April 1970) (F33615-68-C-1077, Air Force Materials Laboratory, Wright-Patterson Air Force Base, Ohio).

6. Union Carbide Corporation, Carbon Products Division, in Association with Case Western Reserve University and Bell Aerospace Company, a Division of Textron, Integrated Research on Carbon Composite Materials, AFML-TR-66-310, Part IV, Volume III (July 1970) (F33615-68-C-1077, Air Force Materials Laboratory, Wright-Patterson Air Force Base, Ohio).

7. P. H. Pettit, "Ultimate Strength of Laminated Composites," General Dynamics Report FZM-4977, Contract AF 33(615)-5257, December 1, 1967.

8. J. E. Ashton, "Anisotropic Plate Analysis," General Dynamics Report FSM-4899, Contract 33(615)-4899, October 12, 1967.

9. D. L. Block, "Buckling of Eccentrically Stiffened Orthotropic Cylinders Under Pure Bending," NASA TN D-3351, March 1966.

UNCLASSIFIED

Security Classification

DOCUMENT CONTROL DATA - R & D

(Security classification of title, body of abstract and indexing annotation must be entered when the overall report is classified)

1. ORIGINATING ACTIVITY (Corporate author)

Union Carbide Corporation
Case Western Reserve University
Bell Aerospace Company

2a. REPORT SECURITY CLASSIFICATION

Unclassified

2b. GROUP

3. REPORT TITLE

INTEGRATED RESEARCH ON CARBON COMPOSITE MATERIALS, Part V
Volume III - Structural Component Development

4. DESCRIPTIVE NOTES (Type of report and inclusive dates)

Summary Technical Report July 1969 to September 1970

5. AUTHOR(S) (First name, middle initial, last name)

Union Carbide Corporation, Carbon Products Division, in Association with Case Western Reserve University and Bell Aerospace Company, a Division of Textron

6. REPORT DATE	7a. TOTAL NO. OF PAGES	7b. NO. OF REFS
January 1971	92	9

8a. CONTRACT OR GRANT NO.	9a. ORIGINATOR'S REPORT NUMBER(S)
F-33615-68-C-1077	
b. PROJECT NO. ARPA Order No. 719	
c. Program Code 7D10	9b. OTHER REPORT NO(S) (Any other numbers that may be assigned this report) AFML-TR-66-310, Part V, Volume III
d.	

10. DISTRIBUTION STATEMENT This document is subject to special export controls and each transmittal to foreign governments or foreign nationals may be made only with prior approval of the Nonmetallic Materials Division, AFML/LN, Air Force Materials Laboratory, Wright-Patterson AFB, Ohio 45433.

11. SUPPLEMENTARY NOTES	12. SPONSORING MILITARY ACTIVITY
	Air Force Materials Laboratory Wright-Patterson AFB, Ohio

13. ABSTRACT

The work presented in this volume is concerned with the performance prediction, testing, and post-test evaluation of a representative graphite-fiber, resin-matrix aircraft fuselage component. Additional material properties were determined and structural margins of safety defined by discrete element analysis. After seven response tests under various load combinations, the component was tested to destruction under combined bending and shear loads. Failure occurred at 110 percent of the target design load but below the failure load predicted from tests on flat panels. A weight saving of 27 percent over an aluminum structure of equivalent strength was demonstrated. The component was also three times stiffer than an aluminum structure of the same weight. Performance projections indicate that the same component built with presently available "Thornel" 50S fibers would offer a weight saving of 49 percent. Post-test evaluations included tensile and compression tests on curved skin panels, on stringers, and on stringer-skin combinations. Optical and electron microscopic examination of the fracture surfaces provided further insight into the failure mechanism.

DD FORM 1 NOV 68 1473 (PAGE 1)

S/N 0101-807-8811

UNCLASSIFIED

Security Classification

A-31408

14. KEY WORDS	LINK A		LINK B		LINK C	
	ROLE	WT	ROLE	WT	ROLE	WT
Carbon						
Graphite						
Fibers						
Graphite Fibers						
Composites						
Plastic Matrix						
Metal Matrix						
Properties						
Analysis						
Synthesis						
Mechanical Properties						